UNIVERSIDAD DE CÓRDOBA

Junta de Andalucía
Consejería de Agricultura, Ganadería, Pesca y Desarrollo Sostenible
Instituto Andaluz de Investigación y Formación Agraria, Pesquera, Alimentaria y de la Producción Ecológica

Programa de doctorado

Dinámica de Flujos Biogeoquímicos y sus Aplicaciones

PhD Dissertation

Use of remote sensing in the monitoring of *dehesa* vegetation and its influence on the hydrological balance at basin scale

Uso de sensores remotos en el seguimiento de la vegetación de dehesa y su influencia en el balance hidrológico a escala de cuenca

Elisabet Carpintero García

Supervisors:

María Patrocinio González Dugo

Ana Andreu Méndez

Octubre 2021

TITULO: *Use of remote sensing in the monitoring of dehesa vegetation and its influence on the hydrological balance at basin scale*

AUTOR: *Elisabet Carpintero García*

Campus de Rabanales
Ctra. Nacional IV, Km. 396 A
14071 Córdoba

https://www.uco.es/ucopress/index.php/es/
ucopress@uco.es

TÍTULO DE LA TESIS: Use of remote sensing in the monitoring of *dehesa* vegetation and its influence on the hydrological balance at basin scale

DOCTORANDO/A: Elisabet Carpintero García

INFORME RAZONADO DEL/DE LOS DIRECTOR/ES DE LA TESIS

(se hará mención a la evolución y desarrollo de la tesis, así como a trabajos y publicaciones derivados de la misma).

María Patrocinio González-Dugo, Investigadora Titular del Instituto de Investigación y Formación Agraria y Pesquera de Andalucía, y Ana Andreu Méndez, doctora en Dinámica de Flujos Biogeoquímicos y sus Aplicaciones, como directoras de la tesis doctoral de la alumna del Programa de Doctorado "Dinámica de Flujos Biogeoquímicos y sus Aplicaciones" Elisabet Carpintero García.

INFORMAN

Que la doctoranda ha cubierto los objetivos presentados en la tesis, que ha avanzado el conocimiento disponible sobre la dinámica de la evapotranspiración en cubiertas de vegetación Mediterránea heterogénea, con especial atención al complejo sistema de dehesa. Asimismo, este trabajo ha profundizado en la estimación de la evapotranspiración a escala local y de cuenca, adaptando y mejorando las aproximaciones que integran sensores remotos para tal fin. Como conclusión de la tesis se han desarrollado y evaluado metodologías de estimación de la evapotranspiración a diferentes escalas, basadas en modelos de balance de agua y energía integrando datos remotos de diferentes fuentes y escalas.

Además la doctoranda ha demostrado una gran capacidad de trabajo, tanto autónomo como en equipo, y ha perfeccionado su conocimiento sobre el modelado del consumo de agua por la vegetación Mediterránea. Ha realizando el trabajo de campo requerido para la validación de estas herramientas, con una gran carga de procesamiento de datos provenientes de diversa instrumentación instalada en las zonas experimentales. Asimismo ha participado en campañas de campo dirigidas a la recolección de información sobre las cubiertas vegetales estudiadas, necesaria para la evaluación y análisis del funcionamiento de ecosistemas complejos, como son las dehesas típicas del sudeste de la Península Ibérica y la montaña mediterránea. Ha gestionado y analizado dichos datos, junto con aquellos procedentes de sensores remotos.

A lo largo de su doctorado ha presentado los resultados obtenidos en diversos foros científicos, nacionales e internacionales, a la vez que ha participado como docente en

la Universidad de Córdoba, en las asignaturas de Hidrología y Riegos, y Gestión Integral de Cuencas, cumpliendo con los objetivos de la beca de Formación de Profesorado Universitario. Muestra de la calidad internacional de la tesis es la estancia en el USDA-Agricultural Research Service, Beltsville Agricultural Research Center, Hydrology and Remote Sensing Laboratory (HRSL), en Estados Unidos, donde la doctoranda investigó sobre la aplicación del modelo de balance de energía ALEXI/DisALEXI y técnicas de fusión de datos, resultando en uno de los artículos presentados en la tesis.

Cuatro de los capítulos de este trabajo se han plasmado en publicaciones en revistas indexadas en el JCR, además de en dos aportaciones a congresos indexados con revisión por pares como primera autora, lo que avala la calidad del trabajo realizado.

Las publicaciones concretas que derivan de esta tesis son:

Carpintero, E., Anderson, M.C., Andreu, A., Hain, C., Gao, F., Kustas, W.P., González-Dugo, M.P., 2021. Estimating Evapotranspiration of Mediterranean Oak Savanna at Multiple Temporal and Spatial Resolutions. Implications for Water Resources Management. Remote Sens. 13 (18), 3701. https://doi.org/10.3390/rs13183701

Carpintero, E., Andreu, A., Gómez-Giráldez, P.J., Blázquez, Á., González-Dugo, M.P., 2020. Remote-Sensing-Based Water Balance for Monitoring of Evapotranspiration and Water Stress of a Mediterranean Oak-Grass Savanna. Water 12, 1418. https://doi.org/10.3390/w12051418

Carpintero, E., Mateos, L., Andreu, A., González-Dugo, M.P., 2020. Effect of the differences in spectral response of Mediterranean tree canopies on the estimation of evapotranspiration using vegetation index-based crop coefficients. Agric. Water Manag. 238, 106201. https://doi.org/10.1016/j.agwat.2020.106201

Jódar, J., **Carpintero, E.**, Martos-Rosillo, S., Ruiz-Constán, A., Marín-Lechado, C., Cabrera-Arrabal, J.A., Navarrete-Mazariegos, E., González-Ramón, A., Lambán, L.J., Herrera, C., González-Dugo, M.P., 2018. Combination of lumped hydrological and remote-sensing models to evaluate water resources in a semi-arid high altitude ungauged watershed of Sierra Nevada (Southern Spain). Sci. Total Environ. 625, 285–300. https://doi.org/10.1016/j.scitotenv.2017.12.300.

<u>Congresos:</u>

Carpintero, E., Andreu, A., Gómez-Giráldez, P.J., González-Dugo, M.P., 2020. Monitoring evapotranspiration and water stress of Mediterranean oak savannas using optical and thermal remote sensing-based approaches. EGU2020-21742, 2020. EGU General Assembly 2020. Online.

Carpintero, E., Mateos, L., Andreu, A., González-Dugo, M.P., 2019. Respuesta espectral de dos cultivos leñosos mediterráneos (olivo y naranjo) en condiciones de cobertura completa del suelo. Influencia en la estimación de la evapotranspiración utilizando coeficientes de cultivo. XVIII Congreso de la AET. 24- 27 Septiembre 2019. Valladolid, España.

Carpintero, E., Gómez-Giráldez, P.J., Andreu, A.; González-Dugo, M.P., 2018. Estimation of evapotranspiration over a dehesa ecosystem using satellite data and a simplified soil water balance model. Remote Sensing and Hydrology Symposium 2018. 8-10 May 2018. Córdoba, Spain.

Carpintero, E., González-Dugo, M.P., Jódar, J., Martos-Rosillo, S., 2018. Use of canopy coefficients obtained from satellite data to estimate evapotranspiration over high mountain Mediterranean watersheds. Remote Sensing and Hydrology Symposium 2018. 8-10 May 2018. Córdoba, Spain. In: Proceeding of the IAHS. 380, pp. 23 – 28.

Carpintero, E., Gómez-Giráldez, P.J., Andreu, A., González-Dugo. M.P., 2018. Application of canopy coefficients obtained from remote-sensing data to monitor the evapotranspiration of Mediterranean oak savanna. Geophysical Research Abstracts, Vol. 20, EGU2018-18314, 2018. EGU General Assembly 2018. Vienna, Austria.

Carpintero, E., González-Dugo, M.P., Polo, M.J., Hain, C., Nieto, H., Gao, F., Andreu, A., Kustas, W.P., Anderson, M.C., 2017. Scale effects on the evapotranspiration estimation over a water-controlled Mediterranean ecosystem and its influence on hydrological modeling. Geophysical Research Abstracts, Vol. 19, EGU2017-18955, 2017. EGU General Assembly 2017. Vienna, Austria.

Carpintero, E., González-Dugo, M.P., Hain, C., Nieto, H., Gao, F., Andreu, A., Kustas, W.P., Anderson, M.C., 2016. Continuous evapotranspiration monitoring and water stress at watershed scale in a Mediterranean oak savanna. SPIE Remote Sensing 2016. in: Proc. of SPIE. Remote Sensing for Agriculture, Ecosystems, and Hydrology XVIII. 9998, ISBN 9781510604001.

Carpintero, E., González-Dugo, M.P., Semmens, K., Anderson, M.C., Andreu, A., Gao, F., Kustas, W.P., 2015. Aplicación de un modelo de balance de energía y técnicas de fusión de datos para el seguimiento continuo de la evapotranspiración de un ecosistema de dehesa. XVI Congreso de la AET. 21-23 Octubre 2015. Sevilla, España.

Carpintero, E., Andreu, A., González-Dugo, M.P., 2015. Vegetation monitoring and estimation of evapotranspiration using remote sensing-based models in heterogeneous areas with patchy natural vegetation and crops. Geophysical Research Abstracts, Vol. 17, EGU2015-945, 2015. EGU General Assembly 2015. Vienna, Austria.

Carpintero, E., Semmens, K., Anderson, M.C., Andreu, A., Gao, F., Kustas W.P., González-Dugo, M.P., 2014. Use of remote sensing data fusion for daily evapotranspiration monitoring at watershed scale over a dehesa ecosystem. Fourth International Symposium on Recent Advances in Quantitative Remote Sensing. 23-26 September 2014. Valencia, España.

Carpintero, E., González-Dugo, M.P., Polo, M.J.. Dynamic characterization of vegetation using remote sensing for hydrological modelling at basin scale. Remote Sensing for Agriculture, Ecosystems, and Hydrology XV. 8887, Proceeding of SPIE, 2013. ISSN 0277-786X, ISBN 9780819497567

Por todo ello, se autoriza la presentación de la tesis doctoral.

Córdoba, 29 de Septiembre de 2021

Firma del/de los Director/es

Firmado por GONZALEZ DUGO MARIA PATROCINIO - 30509431T el día 01/10/2021 con un certificado emitido por AC FNMT Usuarios

Fdo.: María P. González Dugo

Firmado por ANDREU MENDEZ ANA - 74246249H el día 30/09/2021 con un certificado emitido por AC FNMT Usuarios

Fdo.: Ana Andreu Méndez

TÍTULO DE LA TESIS: Use of remote sensing in the monitoring of *dehesa* vegetation and its influence on the hydrological balance at basin scale

DOCTORANDO/A: Elisabet Carpintero García

INFORME RAZONADO DEL TUTOR

(Ratificando el informe favorable del director. Sólo cuando el director no pertenezca a la Universidad de Córdoba).

La doctoranda ha desarrollado satisfactoriamente los objetivos de su tesis y ha alcanzado las competencias esperables en un grado de doctor. Además, su producción científica es muy adecuada y cumple los requisitos de la Universidad de Córdoba, por lo que ratifico el informe de sus directoras e informo favorablemente para la presentación de su tesis doctoral.

Por todo ello, se autoriza la presentación de la tesis doctoral.

Córdoba, 28 de septiembre de 2021

POLO GOMEZ MARIA JOSE - 30534116Y

Firmado digitalmente por POLO GOMEZ MARIA JOSE - 30534116Y
Nombre de reconocimiento (DN): c=ES, serialNumber=IDCES-30534116Y, givenName=MARIA JOSE, sn=POLO GOMEZ, cn=POLO GOMEZ MARIA JOSE - 30534116Y
Fecha: 2021.09.28 17:21:37 +02'00'

Fdo.: María José Polo Gómez

Firma del responsable de línea de investigación

AGUILAR PORRO CRISTINA - 30956348G

Firmado digitalmente por AGUILAR PORRO CRISTINA - 30956348G
Nombre de reconocimiento (DN): c=ES, serialNumber=IDCES-30956348G, givenName=CRISTINA, sn=AGUILAR PORRO, cn=AGUILAR PORRO CRISTINA - 30956348G
Fecha: 2021.09.28 17:21:58 +02'00'

Fdo.: María Cristina Aguilar Porro

Tesis por compendio de publicaciones

Esta tesis cumple el requisito establecido por la Universidad de Córdoba para su presentación por compendio de publicaciones, con 3 artículos publicados en revistas incluidas en los 3 primeros cuartiles de la relación de revistas del ámbito de la especialidad, donde la doctoranda es la primera autora.

1. **Carpintero, E**., Anderson, M.C., Andreu, A., Hain, C., Gao, F., Kustas, W.P., González-Dugo, M.P., 2021. Estimating Evapotranspiration of Mediterranean Oak Savanna at Multiple Temporal and Spatial Resolutions. Implications for Water Resources Management. Remote Sens. 13 (18), 3701. https://doi.org/10.3390/rs13183701

Datos de 2020 (JCR): índice de impacto 4.848, posición 76/274 (Q2) del área temática *Environmental sciences*.

2. **Carpintero, E.**, Andreu, A., Gómez-Giráldez, P.J., Blázquez, Á., González-Dugo, M.P., 2020. Remote-Sensing-Based Water Balance for Monitoring of Evapotranspiration and Water Stress of a Mediterranean Oak-Grass Savanna. Water 12, 1418. https://doi.org/10.3390/w12051418

Datos de 2020 (JCR): índice de impacto 3.103, posición 39/98 (Q2) del área temática *Water Resources*.

3. **Carpintero, E.**, Mateos, L., Andreu, A., González-Dugo, M.P., 2020. Effect of the differences in spectral response of Mediterranean tree canopies on the estimation of evapotranspiration using vegetation index-based crop coefficients. Agric. Water Manag. 238, 106201. https://doi.org/10.1016/j.agwat.2020.106201

Datos de 2020 (JCR): índice de impacto 4.516, posición 16/98 (Q1) del área temática *Water Resources*.

La doctoranda:

Firmado por CARPINTERO GARCIA ELISABET - 54097795R el dï¿½a 29/09/2021 con un certificado emitido por AC FNMT Usuarios

Fdo: Elisabet Carpintero García

Agradecimientos

A mis directoras de tesis, Mª Pat y Ana, por su ayuda y dedicación a lo largo de todo este tiempo en el que a veces flaquean las fuerzas.

A mi tutora, María José, por su sabiduría y su buen hacer.

A mis compañeros del IFAPA, por los buenos momentos que me han hecho pasar en estos años y lo mucho que he aprendido de ellos.

A mi familia, porque siempre está ahí cuando la necesito.

A Damián, por entender mi trabajo y apoyarme incondicionalmente.

Y por supuesto a mis padres, hermana y abuela, por los momentos que no les he dedicado y porque lo que soy es gracias a ellos.

Table of Contents

List of Figures

List of Tables

List of Acronyms

ALEXI: Atmosphere-Land Exchange Inverse

CAI: Cellulose Absorption Index

CFSR: Climate Forecast System Reanalysis

DisALEXI: Associated flux disaggregation technique

DMS: Data Mining Sharpener

DOY: day-of-year

EC: Eddy Covariance

ECT: Eddy Covariance Tower

EO: Earth Observation

ERDF: European Regional Development Fund

ESA: European Space Agency

ET: Evapotranspiration

ET_o: Reference Evapotranspiration

ETM+: Enhanced Thematic Mapper Plus

FLAASH: Fast Line-of-Sight Atmospheric Analysis of Spectral Hypercube

FLUXNET: Flux Networks

FPAR: Fraction of Photosynthetically Active Radiation

FOV: Field Of View

G: Soil heat flux

H: Sensible heat flux

HBV: Hydrologiska Byråns Vattenbalansavdelning

HSD: Honestly Significant Difference

IDW: Inverse Distance model

LAI: Leaf Area Index

LE: Latent heat flux

LST: Land Surface Temperature

MAE: Mean Absolute Error

MBE: Mean Bias Error

METRIC: Mapping EvapoTranspiration at high Resolution Internalized with Calibration

MODIS: Moderate Resolution Imaging Spectroradiometer

MSI: MultiSpectral Instrument

NIR: Near Infrared

OLI: Operational Land Imager

NVDI: Normalized Difference Vegetation Index

P: Precipitation

PET: Potential Evapotranspiration

PUB: Predictions in ―Ungauged Basins

RAIF: Phytosanitary Alert and Information Network of Andalusia

RE: Relative Error

RIA: Agroclimatic Information Network of Andalusia

RMSE: Root Mean Square Error

RMSD: Root Mean Square Deviation

Rn: Net radiation flux

SAPFLUXNET: Plant-level sap flow measurement

SAVI: Soil Adjusted Vegetation Index

SEBAL: Surface Energy Balance Algorithm for Land

SEB: Surface Energy Balance

SEBS: Surface Energy Balance System

SR CDR: Surface Reflectance Climate Data Record

STARFM: Spatial and Temporal Adaptive Reflectance Fusion Model

SWB: Soil Water Balance

SWIR: Short Wave Infrared

T: Temperature

TDD: Tenez-Degrre Day

TIR: Thermal Infrared

TIRS: Thermal Infrared Sensors

TSEB: Two Source Energy Balance

VI: Vegetation Index

VIS: Visible

Abstract

The Mediterranean region is characterized by hot summers with long dry periods, a situation that may be exacerbated by the progressive global warming. In these water-limited environments where productivity of the ecosystems depends mainly on water availability, the reduction of freshwater resources can have severe consequences. An increase in aridity may lead to low productivity, land degradation and unwanted changes in land use. To reduce the vulnerability of Mediterranean landscapes it is important to improve our knowledge of the hydrological processes conditioning the water exchanges, with evapotranspiration (ET) being a key indicator of the state of ecosystems and playing a crucial role in the basin's water and energy balances. The goal of this dissertation is to improve our understanding of the evapotranspiration dynamics over Mediterranean heterogeneous and complex vegetation covers, with a focus on the *dehesa* ecosystem. The final aim is to contribute to the conservation of the water resources in these regions in the medium to long term, supporting the decision-making processes with quantitative, distributed, and high-quality information.

To reach this goal, in this research the evaluation of remote sensing-based soil water balance (SWB) and surface energy balance (SEB) models was proposed to monitor the water consumption and water stress of typical Mediterranean vegetation at different spatial and temporal scales. In particular, the VI-ETo methodology (SWB) and the ALEXI/DisALEXI approach (SEB) have been adapted and applied. ET modeling using the VI-ETo scheme has been improved through the assessment of the vegetation layers' effective parameters. A data fusion algorithm was applied to the ET maps produced by the SEB model over the *dehesa* ecosystem, and we analyzed the opportunities that this high-resolution ET product in time and space can provide for water and vegetation resource management. The results have demonstrated the feasibility of both approaches (SWB and SEB models) to accurately monitor ET dynamics over the *dehesa* landscape, adequately reproducing the annual bimodal behavior and the response of the vegetation in periods of water deficit.

The error obtained using the SWB approach (the VI-ETo method) was RMSE = 0.47 mm day^{-1} over the whole *dehesa* system (grass + trees) and over an open grassland. The monitoring of water stress for both systems with different canopy structure, using as a proxy the ET/ETo ratio, and the stress coefficient (Ks), was successful. Improvements on the specific spectral properties of oak trees and layer-specific parameters were included into the modeling. We also analyzed the influence of the spectral properties of oak trees and another typical Mediterranean tree canopy, the olive orchard, in the VI-ETo model. We found that the use of appropriate values of the parameter $SAVI_{max}$ (0.51 for oak trees and 0.57 for olive trees) had notable implications in the computation of ET and water stress, in

contrast to using a generic value for Mediterranean crops ($SAVI_{max}$= 0.75). The accuracy of this water balance-based approach was also evaluated over two heterogeneous Mediterranean basins, with a mosaic of holm oaks and grasslands, shrubs, coniferous plantations, and irrigated horticultural crops. The annual discharge flows of both watersheds, which were determined from the modeled ET data and using a simple surface water balance, were very similar to those obtained with the HBV hydrological model, and to the values measured at the outlet of one of the basins, corroborating the usefulness of the VI-ETo methodology on these vegetation types.

On the other hand, the resulting ET series (30 m, daily) derived with the SEB approach (ALEXI/DisALEXI method) and the STARFM fusion algorithm provided an RMSE value of 0.67 mm day^{-1}, which was considered an acceptable error for management purposes. This error was slightly lower compared to using simpler interpolation methods, probably due to the high temporal frequency and better spatial representation of the flux tower footprint of the fused time series. The analysis of ET patterns over small heterogeneous vegetated patches that form the *dehesa* structure revealed the importance of having fine resolution information at field scale to distinguish the water consumed by the different vegetation components, which influences the provision of many ecosystem services. For example, it was key for identifying phenology dates of grasslands, or understanding the hydrological functioning of riverside dense evergreen vegetation with high ET rates during the whole year, in contrast with the herbaceous areas. Accurately modeling these different behaviors of *dehesa* microclimates is useful to support farmers' management and provide recommendations tailored for each structural component and requirements.

Resumen

La región mediterránea se caracteriza por veranos calurosos con largos períodos sin precipitaciones, situación que puede agravarse con el progresivo calentamiento global. En estos ambientes donde la productividad de los ecosistemas depende principalmente de la disponibilidad de agua, la reducción de los recursos hídricos puede tener graves consecuencias. Un aumento de la aridez puede conducir a una baja productividad, degradación de la tierra y cambios no deseados en el uso del suelo. Para reducir la vulnerabilidad de las zonas mediterráneas es importante profundizar en el estudio de los procesos hidrológicos que condicionan los intercambios de agua, siendo la evapotranspiración (ET) un indicador clave del estado de los ecosistemas y jugando un papel crucial en los balances hídricos y energéticos de la cuenca. El objetivo de esta tesis es mejorar nuestro conocimiento sobre la dinámica de la evapotranspiración en cubiertas mediterráneas heterogéneas y complejas, con el foco en el ecosistema de dehesa. El objetivo final es contribuir a la conservación de los recursos hídricos de estas regiones en el medio-largo plazo, apoyando en los procesos de toma de decisiones con información cuantitativa, distribuida y de calidad.

Para alcanzar este objetivo, en esta investigación se propuso evaluar modelos de balance de agua en el suelo (SWB) y balance de energía en superficie (SEB) basados en el uso de sensores remotos, para el seguimiento del consumo de agua y el estrés hídrico de la vegetación mediterránea a diferentes escalas espaciales y temporales. En particular, se ha adaptado y aplicado la metodología VI-ET_o (SWB) y el enfoque ALEXI/DisALEXI (SEB). Se ha mejorado el modelado de ET utilizando el esquema VI-ET_o mediante la evaluación de los parámetros efectivos de las capas de vegetación. Se aplicó un algoritmo de fusión de datos remotos a los mapas de ET generados por el modelo SEB sobre el ecosistema de dehesa, y estudiamos las oportunidades que este producto de ET con alta resolución espacial y temporal puede aportar en la gestión de los recursos hídricos y de los ecosistemas. Los resultados han demostrado la viabilidad de ambos enfoques (modelos SWB y SEB) para monitorear con precisión la dinámica de la ET sobre el ecosistema de dehesa, reproduciendo adecuadamente el comportamiento bimodal anual y la respuesta de la vegetación en períodos de déficit hídrico.

El error obtenido usando el enfoque SWB (el método VI-ET_o) fue RMSE = 0.47 mm $día^{-1}$, tanto para el sistema dehesa (pasto + árboles) como para una zona de pastizal. El seguimiento del estrés hídrico para ambos sistemas con diferente estructura de vegetación, utilizando la relación ET/ET_o y el coeficiente de estrés (K_s), fue satisfactorio. Se incluyeron en el modelado mejoras sobre las propiedades espectrales específicas de las encinas y los parámetros específicos de los diferentes estratos de vegetación. También analizamos la influencia de las propiedades espectrales de las encinas y otra cubierta mediterránea, el olivar, en el modelo VI-ET_o. Encontramos que el uso de valores apropiados del parámetro

$SAVI_{max}$ (0,51 para robles y 0,57 para olivos) tuvo un efecto significativo en la determinación del consumo de agua y estrés hídrico, en comparación con usar un valor genérico para cultivos mediterráneos ($SAVI_{max}$ = 0,75). La precisión de este enfoque basado en el balance hídrico también se evaluó en dos cuencas mediterráneas heterogéneas, con un mosaico de encinas y pastizales, arbustos, plantaciones de coníferas y cultivos hortícolas de regadío. Los caudales de descarga anual de ambas cuencas, determinados a partir de los datos de ET modelados y utilizando un balance hídrico superficial muy simple, fueron muy similares a los obtenidos con el modelo hidrológico HBV, y a los valores medidos en la salida de una de las cuencas, corroborando la utilidad de la metodología VI-ET_o sobre estas formaciones vegetales.

Por otra parte, la serie final de ET (30 m, diaria) derivada del enfoque SEB (método ALEXI/DisALEXI) y del algoritmo de fusión STARFM proporcionó un valor de RMSE de 0,67 mm $día^{-1}$, considerado un error aceptable para fines de manejo. Este error fue ligeramente inferior a los obtenidos usando métodos de interpolación más simples, debido probablemente a la alta frecuencia temporal y una mejor representación espacial del *footprint* de la torre de medida de flujos en la serie temporal fusionada. El análisis de los patrones de la ET sobre pequeñas manchas de vegetación heterogéneas, que forman la estructura de la dehesa, reveló la importancia de tener información con alta resolución a escala de campo para distinguir el agua consumida por los diferentes componentes de la vegetación, que tienen influencia en el aprovisionamiento de muchos servicios ecosistémicos. Por ejemplo, fue clave para identificar ciertas fechas fenológicas de los pastizales, o entender el funcionamiento hidrológico de la vegetación densa de hoja perenne en zonas de ribera con altas tasas de ET durante todo el año, en comparación con zonas de especies herbáceas. Modelar con precisión estos comportamientos diferentes de los microclimas de la dehesa es útil para apoyar la gestión de los agricultores y ofrecer recomendaciones adaptadas a cada componente y necesidades estructurales.

Chapter 1

Introduction and objectives

1.1. Water scarcity in Mediterranean basins. Research motivation

The Mediterranean climate, located between latitudes 30° and 40° on the west side of continents, is characterized by mild wet winters and warm to hot, dry summers (Peel et al., 2007). This climate prevails in the lands around the Mediterranean Sea but it is also found in other parts of the world, including California, Central Chile, Southwestern South Africa, Central Asia, and Western and Southern Australia (Strahler and Strahler, 1989). The average temperature in warm months is around 22°C, with mild temperatures in the cold ones (Peel et al., 2007). Near the coast, due to the moderating influence of the sea, the average winter temperature does not exceed 10ºC. Rainfall is low and irregular, with a marked seasonality (Martín-Vide and Olcina, 2001), ranging from 400 to 600 mm per year, although there are areas where it exceeds 1000 mm, and distributed mainly in autumn and spring.

Climate models suggest that these regions are especially vulnerable to global warming, with higher occurrence of heat waves (Jacob et al., 2014; Lionello and Scarascia, 2018) and an increase in the frequency and severity of droughts (Schleussner et al., 2016; Thiébault et al., 2016). The higher variability in climate patterns, coupled with an increase in water demand is expected to reduce the quality and quantity of available freshwater resources, intensifying these basins' recurrent water scarcity problems (Figure 1.1.) (Milano et al., 2013; Cramer et al., 2020).

Under these conditions, a general increase in aridity is expected, and the subsequent desertification may affect many Mediterranean ecosystems (Cramer et al., 2020), for which water availability is the main climate factor controlling vegetation growth and productivity. It may lead to the abandonment of farmland and grazing areas and cause land-use changes (García-Ruíz et al., 2011; Turco et al., 2014; Cramer et al., 2018).

Figure 1.1. The situation of a reservoir in a Mediterranean basin after the summer season.

The soil moisture dynamics play a crucial role in the ecosystems of these semiarid regions, conditioning the existence and spatial distribution of the different vegetation functional types (Rodríguez-Iturbe et al., 2001; Rundel et al., 2016). The discontinuities in the functioning of these environments are related to an alternation in the dry and wet periods (Gauquelin et al., 2016). A feedback relationship is observed in these environments, where the vegetation water consumption strongly conditions the hydrological balance of the system, while plants are impacted by water stress situations.

In this context, it is essential to improve our knowledge about the hydrological processes that control the functioning of these systems at the field and the basin scales, and about the role of the vegetation in them, in order to reinforce ecosystem water resource management and planning, reducing their vulnerability to global warming. Evapotranspiration (ET), i.e. the water transferred to the atmosphere by evaporation from the soil and by transpiration from vegetation, is considered a useful indicator of ecosystem health (Moran et al., 2004), linking the soil-atmosphere-vegetation interactions. The global land surface ET represents about 60% of the terrestrial precipitation (Zhang et al., 2016), becoming greater than 80% in some desert places (Glenn et al., 2007). The use of models that estimate ET, integrating remotely sensed data as inputs, enables extending their application from local to large scale, and provides water demand information at different spatial and temporal scales. To offer accurate and reliable estimations, these models need to be validated with *in-situ* observations, and they also require an adequate characterization of the specific properties and the complex structure of Mediterranean vegetation. A regular and accurate estimation of the vegetation water consumption is a key tool for hydrological planning, watershed management, and drought impact evaluations in semi-arid ecosystems.

1.2. Mediterranean vegetation: the *dehesa* ecosystem

The vegetation that dominates the Mediterranean areas is adapted to the seasonal variability, and has developed control mechanisms to face the frequent droughts and the high atmospheric evapotranspiration rates. For example, we find evergreen sclerophyll trees and bushes with deep roots that reach groundwater, small coriaceous or needle-like leaves for stomatal regulation, annual grasses dead in the dry season and deciduous tree formations that reduce the time period when the vegetation transpires (Ehleringer and Mooney, 1983; Baldocchi and Xu, 2007, Cubera and Moreno, 2007; David et al., 2007; Baldocchi et al., 2010). Understanding how these ecosystems cope with water scarcity is extremely useful in the current context of global warming.

A representative ecosystem of Mediterranean vegetation is the oak savanna or *dehesa*, a system with a great natural, economic, and social value. It is a man-made landscape that covers 3.5 million hectares in the Southwest of the Iberian Peninsula. It has a complex canopy structure composed of sparse clumped trees (mostly evergreen *Quercus Ilex* L. and *Quercus Suber* L.) with grassland, scrubs, and/or crops understory (Figure 1.2). The main

economic activity is extensive livestock production fed with acorns and pastures, but the system also provide other uses (e.g. cork, cereal production, hunting, mushroom harvesting, and beekeeping), playing a key role in the economy of rural areas (Moreno and Cáceres, 2016). *Dehesas* offer multiple environmental services such as biodiversity hotspots, water provisioning, CO_2 fixation, and high diversity of habitats (Campos et al., 2013; Moreno and Cáceres, 2016). It is listed in the EU directive as a habitat with community-wide interest (Díaz et al., 2013). Despite its relevance, in the last decades numerous threats, such as the lack of natural regeneration of tree species (Plieninger et al., 2010), profitability problems, or soil degradation, mainly caused by the intensification of agricultural and livestock activities (Coelho et al., 2004; Moreno and Pulido, 2009), are endangering the conservation of the *dehesa* ecosystem.

Figure 1.2. *Dehesa* landscape (left) and Mediterranean high mountain ecosystem (right).

Other Mediterranean canopies have developed similar strategies to improve their tolerance to water stress, and their study in comparison with oak trees is also addressed in this dissertation. Some Mediterranean tree crops, for instance olive orchards, one of the major crops of the Guadalquivir River Basin, present leaf morphological characteristics that favor a high water use efficiency (e.g. thickness and size), as well as extensive roots to extract water from deeper layers during the dry season (Barranco et al., 2005; Santos et al., 2007). Another example of a typically Mediterranean landscape with sclerophyllous vegetation is the high-altitude ecosystem of *Sierra Nevada* Mountains (Figure 1.2). It is considered one of the most important biodiversity hotspots in the Mediterranean region (Blanca et al., 2001). The main vegetation types of this landscape are: sclerophyllous natural formations of olm oak forests, Pyrenean oak forests (*Quercus ilex* and *Quercus pyrenaica*) and coniferous forests, pine plantations (Pinus sylvestris, Pinus nigra, Pinus halepensis, and Pinus pinaster), evergreen sclerophyll shrubs (great variety of species, highlighting *Juniper*, *Genista*, *Cytisus*, *Rosmarinus* and *Thymus*), high mountains grasslands, river vegetation, and extensive mountain crops (Moreno et al., 2011).

1.3. Evapotranspiration: measurements and modeling

Evapotranspiration is a key ecological process that stems from the interaction between climate, soil, and vegetation, and connects the water and energy cycles (Jin et al., 2017). ET is defined as the water loss by a vegetated surface in the form of vapor, through transpiration from plants and by evaporation from the soil; and it is normally expressed in mm. The change of phase from liquid to vapor water requires an amount of energy called latent heat flux (LE) measured as energy flux density (W m^{-2}). This is a different way to express and measure the same process, with ET being the single most important mechanism of mass and energy exchange between the hydrosphere, biosphere and atmosphere (Sellers et al., 1996). Both exchanges can be described by balance equations.

The water balance equation is based on the principle of mass conservation, and applied to the soil root zone is expressed as:

$$R + I + \Delta S + CR = ET + RO + DP \quad (1.1)$$

where R is rainfall, I represents the incoming water by irrigation, ΔS is the change in soil water content, CR is the water transported upward by capillary rise, whereas RO is the loss by surface runoff and DP by deep percolation, all terms expressed in mm. Some fluxes such as DP and CR are difficult to assess and short periods cannot always be considered (Allen et al., 1998).

The energy conservation balance equation in the surface is expressed in a simplified way as:

$$R_n = LE + H + G \quad (1.2)$$

where Rn is the net radiation or incoming energy that reaches the surface (sum of incident downward and upward shortwave and longwave radiation), H is the heat exchange by convection in the air (sensible heat flux), and G (soil heat flux) represents the heat exchange by conduction into the soil, all variables expressed in W m^{-2}. According to the estimates of some models, LE uses between 48% to 88% of Rn (Wang & Dickinson, 2012).

ET can be measured in the field with different instruments described below. However, its application is limited to points or small areas, and models are used to estimate ET at large scale and under different vegetation and soil moisture conditions. The parametrization of these models is often derived using Earth Observation (EO) technologies.

1.3.1. In-situ measurements methods

The measurement of ET is not simple. In addition to specific and expensive instrumentation, complex physical principles and techniques are needed (Allen et al., 2011). The main disadvantage of most techniques is that they are limited to points or small

experimental fields. *In-situ* measurements are thus generally used with validation purposes, as the ground truth data used to evaluate models feasibility. The methods for determining ET, directly or indirectly, are divided in different categories according to the approach used: hydrological, micrometeorological, and plant physiology, each one suitable for a given space and time scales, and applications (Rana and Katerji, 2000). In this section, the most commonly used methods in each category are briefly reviewed.

1.3.1.1. Lysimetry

Weighing lysimeters were developed to give a measurement of ET through the water budget. They are tanks (Figure 1.3) containing soil cultivated with the same vegetation as around them, with an electronic sensor, for example, a load cell to weight variations of the tank content. The losses or gains of weight in the lysimeter determine changes in soil water storage. This system also measures rainfall and drainage directly for obtaining ET by mass balance (Wang and Dickinson, 2012). It is considered a suitable tool that provides accurate water requirements, commonly used as a standard for the comparison with other procedures (Jensen et al, 1990). On the other hand, non-weighing lysimeters determine ET indirectly by volume balance (Howell et al., 1991). Although they have a lower cost, they are only suitable for long term measurements, while the weighting equipment is more reliable for short-term values (Wang and Dickinson, 2012).

Lysimeters take point measurements, representing ET observations from areas generally ranging from 0.05-40 m^2 (Allen et al., 2011). Other disadvantages of this system that can severely affect ET observations might be the differences in height and vegetation density inside and outside the lysimeter, the tank rims, or the presence of cracks on the edges in contact with the soil (Rana and Katerji, 2000).

Figure 1.3. Weighing lysimeter system installed in a crop field of IFAPA Alameda del Obispo experimental farm: load cell connected to datalogger (left) and counterbalanced platform (right).

1.3.1.2. Eddy covariance system

The eddy covariance (EC) technique is a micrometeorological approach designed to measure carbon, water and energy exchanges, depending on the equipment configuration (Allen et al., 2011). This measurement method was used in this dissertation to test the performance of the models employed. It assumes that the air turbulence behaves as a horizontal flow of numerous rotating eddies, each one with tridimensional components, including the vertical movement of the air (Figure 1.4) (Burba and Anderson, 2010). The energy fluxes from the surface can be measured correlating (with statistical covariance) the vertical wind fluctuations from the mean with the fluctuations from the mean in the concentration of the transported admixture (e.g. water vapor or temperature) (Rana and Katerji, 2000). Because fluctuations happen very quickly, and changes in concentration, density or temperature are small, it is required to take high speed measurements, usually at frequencies of 5-20 Hz, using quick response sensors of high cost (Burba and Anderson, 2010; Allen et al., 2011).

In this way, the eddy flux is approximately equal to the product of mean air density (ρ_a; Kg m^{-3}) and the covariance between deviations in instantaneous vertical wind speed (w'; m s^{-1}), and the mixing ratio of the gas of interest (s'), with some assumptions such as: (1) the density fluctuations are assumed to be negligible and (2) the mean vertical flow is assumed to be negligible for horizontal homogeneous terrain (Burba and Anderson, 2010). The generic flux is therefore expressed with the following equation:

$$F \approx \rho_a \overline{w' s'} \tag{1.3}$$

Figure 1.4. Representation of air turbulence as a horizontal flow of numerous rotating eddies (Source: Andreu et al., 2017).

Particularizing for the case of the latent and sensible heat turbulent fluxes (LE and H), they can be computed with Equations 1.4 and 1.5:

$$LE = L\rho_a \overline{w' q'} \quad (1.4)$$

$$H = C_p \rho_a \overline{w' T'} \quad (1.5)$$

where the instantaneous fluctuations of vapor density and temperature are represented with q' (g m^{-3}) and T', and Cp is the air specific heat (J Kg^{-1} C^{-1}).

Three-dimensional sonic anemometers collect observations of sonic temperature and wind speed, while the water vapor can be measured using a quick response hygrometer or, together with carbon dioxide and/or methane, N_20, or other gases, using gas analyzers (Figure 1.5) (Fekete et al., 2021). LE flux can also be computed as a residual of the energy balance (Equation 1.2), for which it is necessary to accurately measure the convective fluxes Rn and G.

Figure 1.5. Equipment of eddy covariance systems installed over a *dehesa* ecosystem in *Sta. Clotilde* farm (Córdoba).

The EC system is a reliable technique with good results at hourly and daily scales, also over semi-arid landscapes (Rana and Katerji, 2000), with the fluxes being representative of medium sized areas (or footprint). Water vapor and air density corrections are an important aspect to be considered (Webb et al., 1980), particularly relevant in semiarid ecosystems (Rana and Katerji, 2000). This method presents the disadvantage that the sum of turbulent fluxes measured (H+LE) is generally less than the available energy (Rn-G), obtaining a "closure error" of around 5-30% (Twine et al., 2000; Foken, 2008). Several networks of eddy covariance measurements, such as FLUXNET with more than 900 tower sites around the world (Chu et al., 2017; Baldocchi, 2020), have been established.

1.3.1.3. Sap flow method

It is a plant physiology approach, being the heat balance method the most popular. The plant transpiration is determined by estimating the sap mass flow using gauges attached or inserted in the plant stem. In the heat balance method, the stem is heated electrically, and the difference between that supplied heat and the conducted one is assumed to be related with the sap flow and the plant transpiration (Rana and Katerji, 2000; Wang and Dickinson, 2012).

The scaling up of the transpiration rate measurements from plant level to field scale is only possible if we know the vegetation structure and their spatial variability. Another limitation is that the sap flow method only measures transpiration, neglecting soil evaporation. Nevertheless, in Mediterranean areas, evaporation from the soil is a very important fraction (up to 20% of total evapotranspiration) (Rana and Katerji, 2000). A first global database of plant-level sap flow measurements (SAPFLUXNET) has been built (Poyatos et al., 2016).

1.3.2. ET modeling

The difficulties to collect the ET observations in the field, besides the high cost and maintenance of instrumentation, and the short spatial representation, have promoted significant research efforts to estimate ET by using models. These models can be broadly classified into analytical and empirical approaches (Rana and Katerji, 2000). The Penman-Monteith combination equation (Penman, 1948; Monteith, 1973) for estimating the latent heat flux is the most widely used analytical method. It recognizes that this flux is due both to net radiation and to "mass transfer" and takes into consideration the meteorological variables and the canopy properties.

Within the empirical approaches, the crop coefficient method recommended by FAO (Doorenbos and Pruit, 1992; Allen et al., 1998) to compute the crop water requirements is the most extended. The ET is computed as the product of a crop coefficient (K_c) characterized through the growth cycle and a reference evapotranspiration (ET_o). The FAO Penman-Monteith method is recommended for determining ET_o, and Allen et al. (1998) compiled a set of K_c for different conditions and management practices.

For applications at large scale, the parametrization of most currently used models to estimate ET is derived using remotely sensed data. The integration of this distributed information into models allows for ET mapping, scales expanding from local to regional and continental areas. Moreover, mosaic-type Mediterranean areas' hydrological regime strongly relies on the local environmental conditions; EO data provides a representation of that vegetation and climate heterogeneity. There are currently two general types of approaches to model ET using EO data: methods based on a soil water balance, and those based on a surface energy balance, described in Section 1.5.

1.4. Remotely sensed-based data to estimate ET

Nowadays, EO techniques have become an essential tool to support management and planning in many areas, such as agriculture, forestry, hydrology, meteorology, or ecology, and in many other sectors not related to Earth sciences, such as the humanitarian or the military. The images are acquired using sensors mounted on aircraft or spacecraft platforms, or from field equipment. EO technology can provide real-time distributed data, with a sufficient temporal frequency, digital format, and with a global coverage. Moreover, many space agencies offer the images free of charge.

The characteristics of each sensor are defined according to the combination of the following types of resolution: (1) spatial resolution or capability to distinguish the smallest object; (2) spectral resolution or bandwidth in which the data is collected; (3) temporal resolution or frequency of image acquisition on the same area; and (4) radiometric resolution or sensor ability to discriminate different radiation intensities (Joseph, 2005). Figure 1.6 shows an example of some images acquired by airborne and satellite-borne sensors over a farm with a *dehesa* ecosystem, which present different spatial resolutions from higher resolution of less than 1 m (left) to moderate resolution (right). The spatial resolution influences the type and scale of environmental applications. While the finer resolution (<1 m) is more appropriate for local or experimental applications, as we approach moderate resolution images, applications have a regional or global scale. In the case of the *dehesa* landscape, with a complex structure of sparse trees and scrubs, and an understory of grasses and soil, all influencing the microclimate variables and radiative/turbulent exchanges differently, the information availability at high spatial resolution is relevant to study each vegetation layer and their distribution in a separate manner.

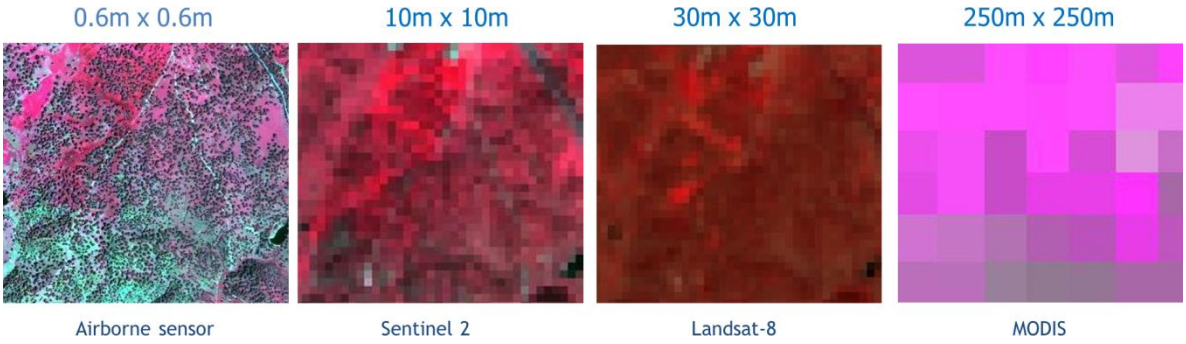

Figure 1.6. Images over a *dehesa* landscape farm (*Santa Clotilde*, in *Sierra de Cardeña y Montoro* Natural Park) with different spatial resolutions.

In this dissertation a set of satellite images, listed below following a decreasing order of spatial resolution, has been used. All of them are provided by passive sensors:

- Sentinel 2A and 2B satellite images are acquired by the MSI (MultiSpectral Instrument) sensor, with a temporal frequency of 10 days (5 days when both satellites are combined). They have a spectral resolution of 13 bands, ranging from 0.44 to 22 μm, a spatial resolution of 10 m (bands 2 to 4 and 8), 20 m (bands 5 to 7, 8a, 11 and 12), and 60 m (bands 1, 9 and 10), and a radiometric resolution of 12 bits. These images are supplied by the European Space Agency (ESA) (https://scihub.copernicus.eu/).
- Landsat 7 and 8 satellite images are acquired by the ETM+ (Enhanced Thematic Mapper Plus) and OLI/TIRS (Operational Land Imager/Thermal Infrared) sensors. They have an overpass frequency of 16 days, with a spectral resolution of 8 bands in Landsat-7 (0.45-12.50 μm) and 11 bands in Landsat-8 (0.43-12.51 μm). The spatial resolution is 60 and 100 m in the thermal region (band 6 in Landsat 7 and bands 10-11 in Landsat-8), 15 m in the panchromatic region (band 8), and 30 m in the rest. The radiometric resolution of these images is 8 bits and 12 bits respectively, and they are provided by the North American Geological Survey (http://espa.cr.usgs.gov).
- Aqua and Terra satellite images were acquired by the MODIS (Moderate Resolution Imaging Spectroradiometer) sensor. They have a daily temporal resolution, a spectral resolution of 36 bands ranging from 0.4 to 14 μm, a spatial resolution of 250 m (bands 1 and 2), 500 m (bands 3 to 7), 1 km (bands 8 to 36), and a radiometric resolution of 12 bits (https://modis.gsfc.nasa.gov).

Field equipment, such as the spectroradiometers used in this research, determinate the curve of spectral reflectance along different regions of the electromagnetic spectrum, which is characteristic of each surface and state; and could be utilized for recognizing and mapping all kinds of surface features (Rajendran et al., 2009). Figure 1.7 shows some examples of spectral signatures in the regions VIS/NIR/SWIR of bare soil and photosynthetic and non-photosynthetic natural grass on a *dehesa* farm in Cardeña (Córdoba), measured with a field spectroradiometer. The typical spectral behavior of vigorous vegetation makes certain bandwidths to be frequently used in environmental monitoring applications.

Spectral data in the VIS and NIR regions are used to characterize the vegetation canopies state through an algebraic relationship between bands, which forms the vegetation indices (VI). The most commonly employed indices as descriptors of the vigor and density of vegetation are the normalized difference vegetation index, NDVI (Rouse et al., 1974), and the soil adjusted vegetation index, SAVI (Huete, 1988). From these indices, certain properties and parameters of the vegetation, such as the leaf area index, the soil cover fraction, or the fraction of photosynthetically active radiation intercepted are derived (Choudhury et al., 1994; Carlson and Ripley, 1997). These indices are, thus, useful in monitoring processes related to photosynthesis or canopy transpiration (Glenn et al., 2008).

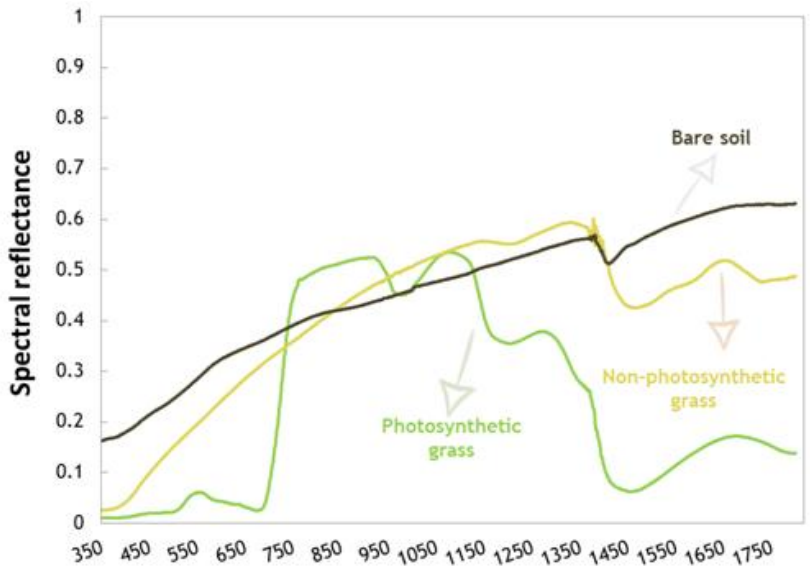

Figure 1.7. Spectral signature (measured with the spectroradiometer ASD FieldSpec3) of bare soil, photosynthetic and non-photosynthetic grass under full vegetation conditions.

On the other hand, the thermal infrared region is useful in assessing and detecting vegetation water stress, due to the direct relationship between the transpiration process and the canopy temperature (Sobrino et al., 2016). When transpired water is evaporated, the leaves get cold below the air temperature around them. Similarly, in situations with limited water availability that reduce plant transpiration, the temperature of the leaves increases (Jackson, 1982; Moran, 2003). This relationship provides thermal measurements with great potential for monitoring and managing plant ecosystem health (Moran, 2003).

In this dissertation, the information provided by remote sensors in the VIS/NIR and thermal regions has been used for ET modeling by using the approaches described below.

1.5. Remote sensing-based approaches to estimate ET

The integration of remotely sensed data into models to estimate water consumption provides maps of vegetation water use with different spatial and temporal resolutions, defined by the characteristics of the sensors used (Glenn et al., 2007). In this dissertation, we used two types of approaches to estimate water consumption using remote data, based either on the soil water balance (section 1.5.1), or on the surface energy balance (section 1.5.2). Figure 1.8 schematically shows the different processes involved in the water and energy cycles, as well as their balance equations, where ET is the nexus between both budgets. The figure also picks the remote information needed for the ET modeling, where each scheme uses reflectance data from a different spectral bandwidth.

The first modeling scheme (soil water balance, SWB) uses the canopy reflectance in

the VIS and NIR regions of the spectrum to characterize the vegetation and its role in this process through the computation of vegetation indices (Neale et al. 1989; González-Dugo and Mateos, 2008; Poças et al., 2020). On the other hand, those models based on the surface energy balance use the radiometric temperature registered by the sensors in the thermal band as the primary input to derive the ET, which is computed as the residual of the energy balance (Kustas and Norman, 1997; Bastiaanssen et al., 1998).

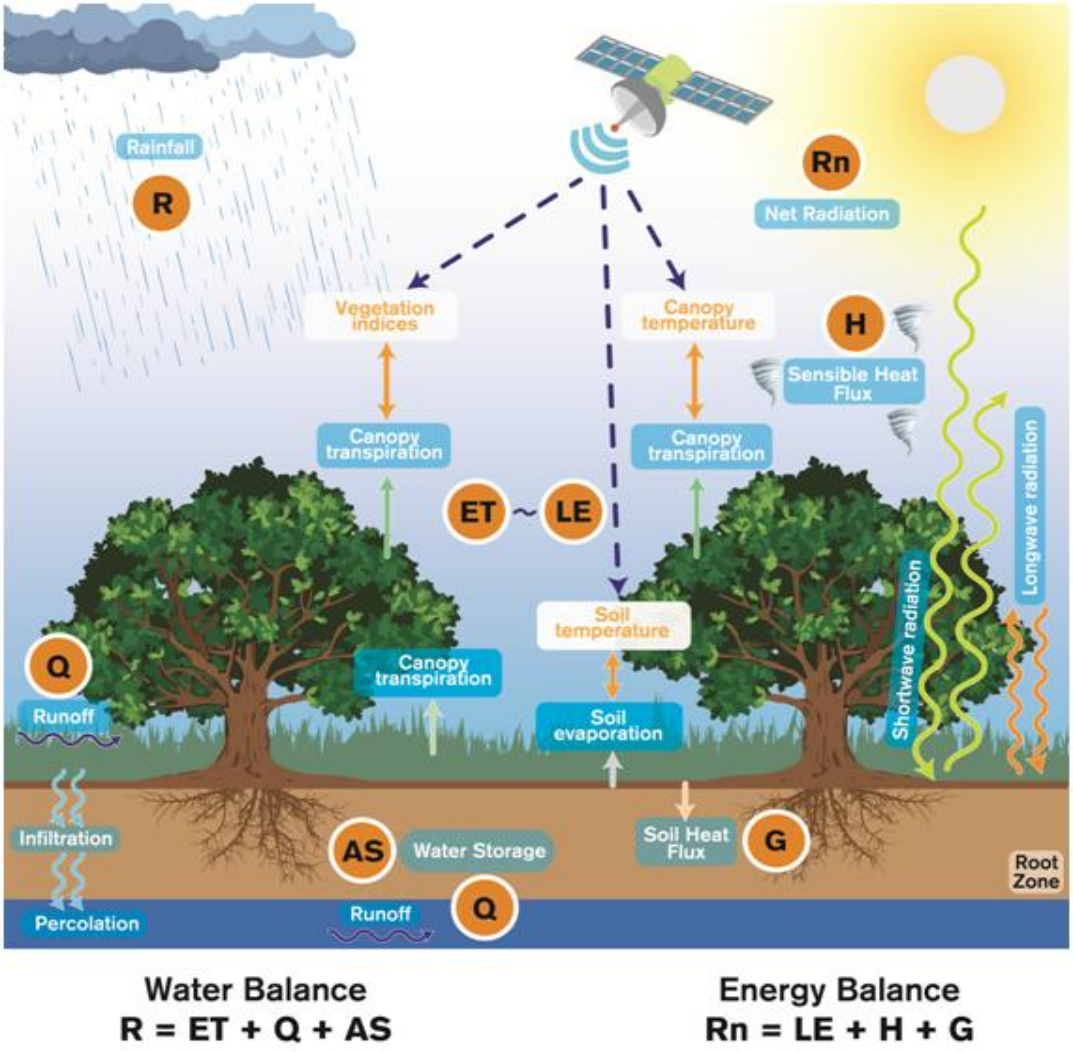

Figure 1.8. Components of the water and energy budgets.

1.5.1. Remote sensing-based soil water balance models

The model proposed in FAO-56 guidelines to determine crop water requirements estimates the canopy ET as a product of reference ET (ET_o), representing the atmospheric evaporative demand, and a crop coefficient (K_c) used to account for crop factors, applying a

surface and root zone soil water balance (Allen et al., 1998). This approach can be combined with the computation of vegetation indices (VI-ET_o method), to provide a distributed basal crop coefficient, K_{cb}, that determines the transpiration of the plant, and takes advantage of the spatial and temporal resolutions of remote data. There are numerous VI-K_{cb} empirical relationships for different crops, besides multiple applications that validate this proposal with good results over agricultural areas (Bausch and Neale, 1987; Padilla et al., 2011; Mateos et al., 2013; Calera et al, 2017). Applications over natural ecosystems are substantially fewer than over crops, with the difficulties derived from the higher heterogeneity of the vegetation properties. Some studies over Mediterranean and African savannas were conducted by Campos et al., (2013) and Andreu et al. (2019), and highlighted the difficulty of taking into account the complexity of the system in the estimation of effective model parameters.

An advantage of this approach is that information on optical regions is available with higher spatial resolution than thermal bands and they have a relatively simpler formulation. As disadvantages, local meteorological and soil data are required, and it does not account for the reduction of transpiration due to stomatal closure under water stress conditions, nor changes in ET at time scale of hours (Glenn et al., 2007; González-Dugo et al., 2009).

1.5.2. Remote sensing-based energy balance models

As described before, the radiometric temperature (T_{RAD}) is the input information provided by the remote sensors, although it differs from the aerodynamic temperature (T_0), necessary to estimate the sensible heat flux (Kustas, 1990). The way to deal with this temperature difference characterizes the various types of energy balance models, which are generally classified into one-source, two-source, and multi-layer models (Kalma et al, 2008).

The one source models are characterized by considering the surface as a single layer, without separating the vegetation and soil components. Some examples are the Surface Energy Balance Algorithm for Land (SEBAL; Bastiaanssen et al., 1998), the Mapping EvapoTranspiration at high Resolution Internalized with Calibration (METRIC; Allen et al., 2007) or the Surface Energy Balance System (SEBS; Su, 2002).

Mediterranean landscapes can not be considered as a single spatially uniform layer for ecosystem exchanges, and we should include their characteristics into the models, developing methodologies to account for the non-homogeneous canopy covers. Therefore, dual source models which make the partition into vegetation and soil fluxes, have shown its utility in partially covered canopies (Timmermans et al., 2007; González-Dugo et al., 2009). However, one-source models have also presented satisfactory results at coarse scale (Gonzalez-Dugo et al., 2021).

An example of a dual source scheme is the Two Source Energy Balance model (TSEB; Norman et al, 1995; Kustas and Norman, 1999). The TSEB gives a physical representation of the evapotranspiration process by means of distinguishing between soil and vegetation contribution to the satellite-derived temperature and to the exchange of superficial energy fluxes. Anderson et al. (1997) proposed an improvement to the two-source scheme by incorporating a simple description of the dynamics of the atmospheric boundary layer. The result was the Atmosphere-Land Exchange Inverse (ALEXI) model and an associated flux disaggregation technique (DisALEXI). This approach uses thermal data from multiple sensors to estimate ET, without the need for local observations as input data, and minimizing the effect of deviations in the temperature recorded by the sensor due to the use of data obtained twice in the morning hours (Anderson et al., 2007).

These models have the advantage that they are capable of capturing plant stress without the need for precipitation data or soil properties (Anderson et al., 2007). Among the disadvantages of these models are the complexity of their formulation, the accuracy of T_{RAD} observations due to atmospheric factors and surface emissivity (Kalma et al., 2008), and the limitations of thermal observations coverage. Normally, satellites that provide high-frequency surface temperature data have a coarse spatial resolution, and vice versa.

1.6. Remote data fusion techniques and coupling models

Satellites have capabilities and limitations for providing the necessary data, hampered by cloud coverage, sensor failures, and the sensor's own characteristics. However, many ecosystem management applications often require high resolution in both time and space. To address this issue, some procedures such as gap filling methods, flux disaggregation (Anderson et al., 1997), thermal sharpening (Gao et al., 2012), or multiple satellite data combinations (Gao et al., 2006; Renzullo et al., 2008; Guzinski and Nieto, 2019) have been developed.

The direct fusion of remote data from multiple sensors is an interesting approach for downscaling ET maps, and has been addressed in this dissertation. In this context, the Spatial and Temporal Adaptive Reflectance Fusion Model (STARFM) developed by Gao et al. (2006) stands out. STARFM was developed for the integration of surface reflectance data from Landsat and MODIS platforms (Singh, 2012; Walker et al., 2012), and has been later extended to fusing multisensory ET retrievals with satisfactory results in agricultural (Cammalleri et al., 2014; Semmens et al., 2016) and heterogeneous areas (Yang et al., 2017; Anderson et al., 2018). The working scheme of this method (reflected in Figure 1.9) is based on generating "predicted images" between Landsat overpasses at 30 m spatial resolution. To do that, it used the spatial differences in Landsat-MODIS on known dates and temporal differences from MODIS images.

Another alternative is the coupling of models based on different remote sensed input data (of different temporal and spatial scales), which can be carried out because the

schemes are physically coupled through ET. Some works have been developed using one of the modeling approaches as the central nucleus and the other as support to solve specific problems. In this sense, Tasumi et al. (2005) calculated the crop coefficients from real ET values derived from the METRIC energy balance model. Similarly, Andreu et al. (2019) integrated two different ET-estimation approaches: the Kc-FAO56 model and the TSEB methodology.

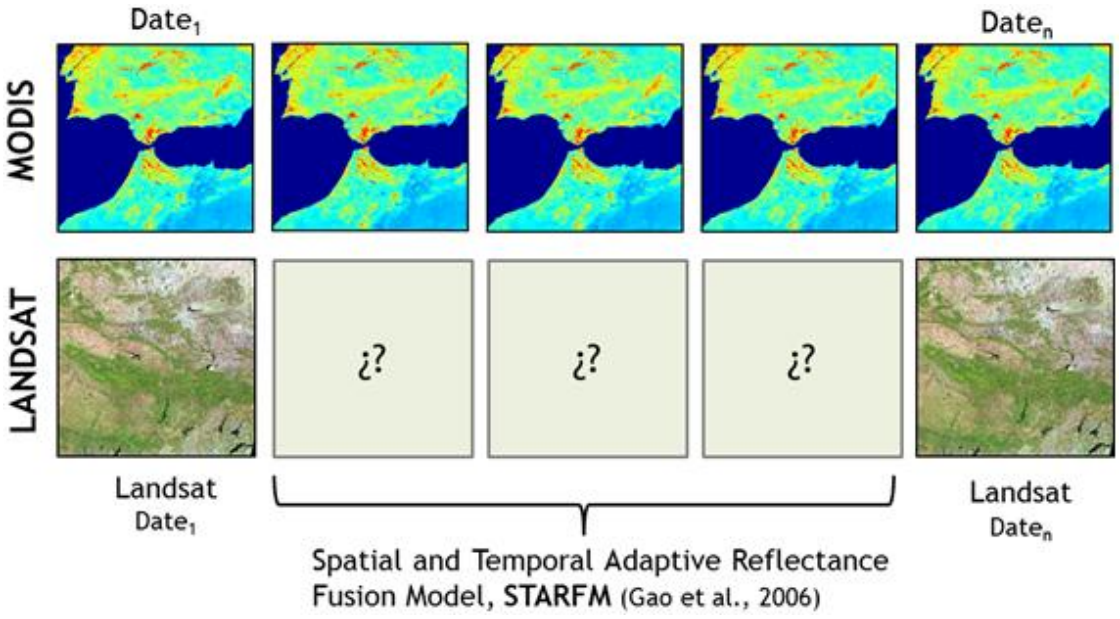

Figure 1.9. Working scheme of the Spatial and Temporal Adaptive Reflectance Fusion Model STARFM (Gao et al., 2006).

1.7. Objectives and thesis structure

The general objective of this dissertation was to advance in the knowledge of the evapotranspiration estimation processes at the field and basin scales over heterogeneous vegetation covers, with special attention paid to *dehesa* ecosystems and their response to water stress conditions. To fulfil this goal, this research has focused on the evaluation of remote sensing-based soil water balance (SWB) and surface energy balance (SEB) models, to monitor the water consumption by the Mediterranean vegetation at different spatial and temporal scales. In order to achieve this goal, the following specific objectives were proposed:

1. Evaluate the suitability of a remote sensing-based SWB approach, the VI-ET_o method, for monitoring the evapotranspiration dynamics of Mediterranean vegetation canopies. This objective was divided into three sub-objectives:

1.1. Improve the knowledge of the spectral response of Mediterranean tree species, both natural and cultivated, and improve their modeling by providing effective vegetation parameters that influence the VI-ET_o method.

1.2. Explore the capability of this model to quantify water resources over Mediterranean watersheds with mosaic and complex vegetation canopies, with a special focus on *dehesa* ecosystems.

1.3. Improve our understanding of the varying role of the two main vegetation components of *dehesa* ecosystems (oak-grass) in the system hydrology and the ability of VI-ET_o methodology to model them separately.

2. Assess the use of a SEB model, in particular, the combination of the ALEXI/DisALEXI approach, to reproduce the temporal dynamics of ET over the *dehesa* landscape, analyzing the effects of spatial and temporal resolutions of estimated water consumptions.
3. Increase the spatial and temporal resolution of water monitoring with a data fusion algorithm, and analyze the opportunities that a high-resolution ET product in time and space (daily, 30 m) can provide for water and vegetation resource management at field scale.
4. Explore the potential for monitoring the water stress of the vegetation canopy, through the ratio between the real ET and the reference ET.

The main body of this document consists of four chapters where the objectives proposed were addressed. These chapters are the result of the publication of four research papers in peer-reviewed journals. The PhD candidate is the first author in three of them (Chapters Two, Three and Five), while she collaborated as a co-author in Chapter Four. A final chapter (Chapter Six) is included with the general conclusions obtained from this research.

Chapter Two evaluated the differences in spectral response of holm oak trees and olive trees compared to other plant species under full cover conditions. A canopy-specific parameter, used as input in the VI-ET_o model (SAVI for full-cover), was determined in each case, assessing the effect of this parameterization in estimating water consumption and water stress monitoring (objective 1.1).

Chapter Three estimated ET and analyzed dynamics over a *dehesa* ecosystem located in Southern Spain, by using the SWB approach known as VI-ET_o model, and validating the modeled water use values with *in-situ* flux measurements. The two main canopy system components (tree + grass) were studied separately by estimating ET at different spatial scales, in order to characterize the differential contribution of each one to the system's hydrology (objectives 1.2 and 1.3). Moreover, some effective vegetation parameters to

model the water balance were provided (objective 1.1), and water stress was monitored with the ET/ET_o ratio (objective 4).

Chapter Four contains the publication by Jódar et al. (2018), in which the PhD candidate collaborated as a co-author. This research focused on assessing water resources in Mediterranean high altitude watersheds of the *Sierra Nevada* Mountains, by combining a lumped hydrological model (HBV model) and the VI-ET_o approach. The PhD candidate participated in this publication by generating spatially distributed daily ET at watershed scale estimated with the VI-ET_o model, and annual flow of discharge considering a simple surface water balance (objective 1.2).

Table 1.1. Titles of the papers related to the chapters of the dissertation and the corresponding journal.

Chapter	Article Title	Journal
2	**Carpintero, E.**, Mateos, L., Andreu, A., González-Dugo, M.P., 2020. Effect of the differences in spectral response of Mediterranean tree canopies on the estimation of evapotranspiration using vegetation index-based crop coefficients. Agric. Water Manag. 238, 106201. https://doi.org/10.1016/j.agwat.2020.106201	Published in *Agricultural Water Management*
3	**Carpintero, E.**, Andreu, A., Gómez-Giráldez, P.J., Blázquez, Á., González-Dugo, M.P., 2020. Remote-Sensing-Based Water Balance for Monitoring of Evapotranspiration and Water Stress of a Mediterranean Oak-Grass Savanna. Water 12, 1418. https://doi.org/10.3390/w12051418	Published in *Water*
4	Jódar, J., **Carpintero, E.**, Martos-Rosillo, S., Ruiz-Constán, A., Marín-Lechado, C., Cabrera-Arrabal, J.A., Navarrete-Mazariegos, E., González-Ramón, A., Lambán, L.J., Herrera, C., González-Dugo, M.P., 2018. Combination of lumped hydrological and remote-sensing models to evaluate water resources in a semi-arid high altitude ungauged watershed of Sierra Nevada (Southern Spain). Sci. Total Environ. 625, 285–300. https://doi.org/10.1016/j.scitotenv.2017.12.300	Published in *Science of the Total Environment*
5	**Carpintero, E**., Anderson, M.C., Andreu, A., Hain, C., Gao, F., Kustas, W.P., González-Dugo, M.P., 2021. Estimating Evapotranspiration of Mediterranean Oak Savanna at Multiple Temporal and Spatial Resolutions. Implications for Water Resources Management. Remote Sens. 13 (18), 3701. https://doi.org/10.3390/rs13183701	Published in *Remote Sensing*

Chapter Five monitored ET over the oak-grass savanna landscape by using a SEB model (the combination of ALEXI/DisALEXI approach) at field and watershed scale, vaidalting the results with flux tower measurements (objective 2). In addition, the STARFM data fusion technique was applied and the effects of the different spatial and temporal resolutions were assessed at field scale, analyzing the opportunities offered by these high resolution ET maps to provide information that is useful to improve water and vegetation management (objective 3).

Chapter Six presents the main findings and general conclusions of this dissertation.

1.8. References

Allen, R.G., Pereira, L.S., Howell, T.A., Jensen, M.E., 2011. Evapotranspiration information reporting: I. Factors governing measurement accuracy. Agric. Water Manag. 98, 899–920. https://doi.org/10.1016/j.agwat.2010.12.015.

Allen, R.G., Pereira, L.S., Raes, D., Smith, M., 1998. FAO Irrigation and Drainage Paper No. 56 -Crop Evapotranspiration, Rome, Italy.

Allen, R.G., Tasumi, M., Trezza, R., 2007. Satellite-based energy balance for mapping evapotranspiration with internalized calibration (METRIC)—model. J. Irrig. Drain. Eng. ASCE 133 (4), 380–394. https://doi.org/10.1061/(ASCE)0733-9437(2007)133:4(380).

Anderson, M., Gao, F., Knipper, K., Hain, C., Dulaney, W., Baldocchi, D., Eichelmann, E., Hemes, K., Yang, Y., Medellin-Azuara, J., Kustas, W.P., 2018. Field-scale assessment of land and water use change over the California delta using remote sensing. Remote Sens. 10. https://doi.org/10.3390/rs10060889.

Anderson, M.C., Norman, J.M., Diak, G.R., Kustas, W.P., Mecikalski, J.R., 1997. A two-source time-integrated model for estimating surface fluxes using thermal infrared remote sensing. Remote Sens. Environ. 60, 195–216. https://doi.org/10.1016/S0034-4257(96)00215-5.

Anderson, M.C., Norman, J.M., Mecikalski, J.R., Otkin, J.A., Kustas, W.P., 2007. A climatological study of evapotranspiration and moisture stress across the continental United States based on thermal remote sensing: 2. Surface moisture climatology. J. Geophys. Res. Atmos. 112, 1–13. https://doi.org/10.1029/2006JD007507.

Andreu, A., Dube, T., Nieto, H., Mudau, A.E., González-Dugo, M.P., Guzinski, R., Hülsmann, S., 2019. Remote sensing of water use and water stress in the African savanna ecosystem at local scale – Development and validation of a monitoring tool. Phys. Chem. Earth 112, 154–164. https://doi.org/10.1016/j.pce.2019.02.004.

Baldocchi, D.D., 2020. How eddy covariance flux measurements have contributed to our understanding of Global Change Biology. Glob. Chang. Biol. 26, 242–260. https://doi.org/10.1111/gcb.14807.

Baldocchi, D., Ma, S.Y., Rambal, S., Misson, L., Ourcival, J.M., Limousin, J., Pereira, J., Papale, D., 2010. On the differential advantages of evergreenness and deciduousness in mediterranean oak woodlands: A flux perspective. Ecological applications: a publication of the Ecological Society of America. 20, 1583-97. https://doi.org/10.1890/08-2047.1.

Baldocchi, D.D., Xu, L., 2007. What limits evaporation from Mediterranean oak woodlands - The supply of moisture in the soil, physiological control by plants or the demand by the atmosphere? Adv. Water Resour. 30, 2113–2122. https://doi.org/10.1016/j.advwatres.2006.06.013.

Barranco, D., Rallo, L., Trujillo, I. 2005. Elaiografía Hispánica, in: Rallo, L., Barranco, D., Caballero, J.M., del Río, C., Martín, A., Tous, J., Trujillo, I. (Eds), Variedades de olivo en España, Junta de Andalucía, MAPA. Ediciones Mundiprensa, Madrid, pp. 80-231.

Bastiaanssen, W.G.M., Menenti, M., Feddes, R.A., Holtslag, A. A. M., 1998. A remote sensing surface energy balance algorithm for land (SEBAL). 1 Formulation. J. Hydrol. 212–213, 198–212. https://doi.org/10.1016/S0022-1694(98)00254-6.

Bausch, W.C., Neale, C.M.U., 1987. Crop Coefficients Derived From Reflected Canopy Radiation: a Concept. Trans. Am. Soc. Agric. Eng. 30, 703–709. https://doi.org/10.13031/2013.30463.

Blanca López, G., López Onieva, M., Lorite, J., Martínez Lirola, M. J., Molero Mesa, J., Quintas, S., Ruíz Girela, M., Varo, M.A., Vidal, S., 2001. Flora amenazada y endémica de Sierra Nevada. Universidad de Granada. Consejería de Medio Ambiente, Junta de Andalucía, Granada.

Burba, G., Anderson, D., 2010. A Brief Practical Guide to Eddy Covariance Flux Measurements: Principles and Workflow Examples for Scientific and Industrial Applications. https://doi.org/10.13140/RG.2.1.1626.4161.

Calera, A., Campos, I., Osann, A., D'Urso, G., Menenti, M., 2017. Remote sensing for crop water management: From ET modelling to services for the end users. Sensors (Switzerland) 17, 1–25. https://doi.org/10.3390/s17051104.

Cammalleri, C., Anderson, M.C., Gao, F., Hain, C.R., Kustas, W.P., 2014. Mapping daily evapotranspiration at field scales over rainfed and irrigated agricultural areas using remote sensing data fusion. Agric. For. Meteorol. 186, 1–11. https://doi.org/10.1016/j.agrformet.2013.11.001.

Campos, P., Huntsinger, L., Oviedo, J., Díaz, M., Starrs, P., Standiford, R., Montero, G., 2013. Mediterranean Oak Woodland Working Landscapes: Dehesas of Spain and Ranchlands of California, Springer: Dordrecht, The Netherlands.

Campos, I., Villodre, J., Carrara, A., Calera, A., 2013. Remote sensing-based soil water balance to estimate Mediterranean holm oak savanna (dehesa) evapotranspiration under water stress conditions. J. Hydrol. 494, 1–9. https://doi.org/10.1016/j.jhydrol.2013.04.033.

Carlson, T.N., Ripley, D.A., 1997. On the relation between NDVI, fractional vegetation cover, and leaf area index. Remote Sens. Environ. 62, 241–252. https://doi.org/10.1016/S0034-4257(97)00104-1.

Choudhury, B.J., Ahmed, N.U., Idso, S.B., Reginato, R.J., Daughtry, C.S.T., 1994. Relations between evaporation coefficients and vegetation indices studied by model simulations. Remote Sens. Environ. 50, 1–17. https://doi.org/10.1016/0034-4257(94)90090-6.

Chu, H., Baldocchi, D.D., John, R., Wolf, S., Reichstein, M., 2017. Fluxes all of the time? A primer on the temporal representativeness of FLUXNET. J. Geophys. Res. Biogeosciences 122, 289–307. https://doi.org/10.1002/2016JG003576.

Coelho, C.; Ferreira, A.J.D., Laouina, A., Hamza, A., Chaker, M., Naafa, R., Regaya, K., Boulet, A. K., Keizer, J.J., Carvalho, T.M.M., 2004. Changes in Land Use and Land Management Practices Affecting Land Degradation within Forest and Grazing Ecosystems in the Western Mediterranean, in: Schnabel, S., Ferreira, A. (Eds.), Sustainability of Agrosylvopastoral Systems, Dehesas, Montados, Schweizerbart Science Publishers: Stuttgart, Germany, pp. 137–154.

Cramer, W., Guiot, J., Fader, M., Garrabou, J., Gattuso, J.P., Iglesias, A., Lange, M.A., Lionello, P., Llasat, M.C., Paz, S., Peñuelas, J., Snoussi, M., Toreti, A., Tsimplis, M.N., Xoplaki, E., 2018. Climate change and interconnected risks to sustainable development in the Mediterranean. Nat. Clim. Chang. 8, 972–980. https://doi.org/10.1038/s41558-018-0299-2.

Cramer, W., Guiot, J., Marini, K, 2020. Climate and Environmental Change in the Mediterranean Basin – Current Situation and Risks for the Future. First Mediterranean Assessment Report. MedECC (Mediterranean Experts on Climate and Environmental Change). Union for the Mediterranean, Plan Bleu, UNEP/MAP, Marseille, France.

Cubera, E., Moreno, G., 2007. Effect of single Quercus ilex trees upon spatial and seasonal changes in soil water content in dehesas of central western Spain. Ann. For. Sci. 64, 355–364. https://doi.org/10.1051/forest:2007012.

David, T.S., Henriques, M.O., Kurz-Besson, C., Nunes, J., Valente, F., Vaz, M., Pereira, J.S., Siegwolf, R., Chaves, M.M., Gazarini, L.C., David, J.S., 2007. Water-use strategies in two co-occurring Mediterranean evergreen oaks: Surviving the summer drought. Tree Physiol. 27, 793–803. https://doi.org/10.1093/treephys/27.6.793.

Díaz, M., Tietje, W.D., Barrett, R.H., 2013. Effects of Management on Biological Diversity and Endangered Species, in: Campos, P., Huntsinger. L., Oviedo, J.L., Starrs, P.F., Díaz, M., Standiford, R.B, Montero, G. (Eds.), Mediterranean Oak Woodland Working Landscapes. Landscape Series, 16, Springer, Dordrecht, The Netherlands, pp. 213-243.

Doorenbos, J., Pruitt, W.O., 1977. Guidelines for predicting crop water requirements. FAO Irrig. Drain. Pap. 24, 144, Rome, Italy.

Ehleringer, J., Mooney, H.A., 1983. Productivity of dessert and Mediterranean-climate plants, Springer-Berlag, Berlin, Germany.

Fekete, B. M., Andreu, A., Argent, R., Avellán, T., Birkett, C., Caucci, S., Cohen, S., Dube, T., Kirschke, S., Looser, U., 2021. Observations, Monitoring and Data Management, in: Bogardi, J. J., Gupta, J., Nandalal, K.D.W., Salamé, L., van Nooijen, R. R. P., Kumar, N., Tingsanchali, T., Bhaduri, A., Kolechkina, A.G. (Eds), Handbook of Water Resources Management: Discourses, Concepts and Examples, Switzerland: Springer Nature, Switzerland, pp. 385-442.

Foken, T., 2008. The energy balance closure problem: An overview. Ecol. Appl. 18(6), 1351–1367. https://doi.org/10.1890/06-0922.1.

Gao, F., Kustas, W.P., Anderson, M.C., 2012. A data mining approach for sharpening thermal satellite imagery over land.*Remote Sens.* 4, 3287–3319. https://doi.org/10.3390/rs4113287.

Gao, F., Masek, J., Schwaller, M., Hall, F., 2006. On the blending of the landsat and MODIS surface reflectance: Predicting daily landsat surface reflectance. IEEE Trans. Geosci. Remote Sens. 44, 2207–2218. https://doi.org/10.1109/TGRS.2006.872081.

García-Ruiz, J.M., López-Moreno, I.I., Vicente-Serrano, S.M., Lasanta-Martínez, T., Beguería, S., 2011. Mediterranean water resources in a global change scenario. Earth-Science Rev. 105, 121–139. https://doi.org/10.1016/j.earscirev.2011.01.006.

Gauquelin, T., Michon, G., Joffre, R., Duponnois, R., Génin, D., Fady, B., Bou Dagher-Kharrat, M., Derridj, A., Slimani, S., Badri, W., Alifriqui, M., Auclair, L., Simenel, R., Aderghal, M., Baudoin, E., Galiana, A., Prin, Y., Sanguin, H., Fernandez, C., Baldy, V., 2016. Mediterranean forests, land use and climate change: a social-ecological perspective. Reg. Environ. Chang. 18, 623–636. https://doi.org/10.1007/s10113-016-0994-3.

Glenn, E.P., Huete, A.R., Nagler, P.L., Hirschboeck, K.K., Brown, P., 2007. Integrating remote sensing and

ground methods to estimate evapotranspiration. CRC. Crit. Rev. Plant Sci. 26, 139–168. https://doi.org/10.1080/07352680701402503.

Glenn, E.P., Huete, A.R., Nagler, P.L., Nelson, S.G., 2008. Relationship between remotely-sensed vegetation indices, canopy attributes and plant physiological processes: What vegetation indices can and cannot tell us about the landscape. Sensors 8, 2136–2160. https://doi.org/10.3390/s8042136.

González-Dugo, M., Chen, X., Andreu, A., Carpintero, E., Gómez-Giraldez, P., Carrara, A., Su, Z., 2021. Long-term water stress and drought monitoring of Mediterranean oak savanna vegetation using thermal remote sensing. Hydrol. Earth Syst. Sci. 25, 755–768. https://doi.org/10.5194/hess-25-755-2021.

González-Dugo, M.P., Mateos, L., 2008. Spectral vegetation indices for benchmarking water productivity of irrigated cotton and sugarbeet crops. Agric. Water Manag. 95, 48–58. https://doi.org/10.1016/j.agwat.2007.09.001.

Gonzalez-Dugo, M.P., Neale, C.M.U., Mateos, L., Kustas, W.P., Prueger, J.H., Anderson, M.C., Li, F., 2009. A comparison of operational remote sensing-based models for estimating crop evapotranspiration. Agric. For. Meteorol. 149, 1843–1853. https://doi.org/10.1016/j.agrformet.2009.06.012.

Guzinski, R., Nieto, H., 2019. Evaluating the feasibility of using Sentinel-2 and Sentinel-3 satellites for high-resolution evapotranspiration estimations. Remote Sens. Environ. 221, 157–172. https://doi.org/10.1016/j.rse.2018.11.019.

Howell, T.A., Schneider, A.D., Jensen, M.E., 1991. History of lysimeter design and use for evapotranspiration measurements. in: Allen, R.G., Howell, T.A., Pruitt, W.O., Walter, I.A., Jensen, M.E. (Eds.), Proceeding of the International Symposium on Lysimetry, July 23–25, Honolulu, HI, pp. 1–9.

Huete, A. R., 1988. A soil-adjusted vegetation index (SAVI). Remote Sens. Environ. 25, 295-309.

Jackson, R.D., 1982. Canopy temperature and crop water stress, Adv. Irrig. 1, 43–85. https://doi.org/10.1016/B978-0-12-024301-3.50009-5.

Jacob, D., Petersen, J., Eggert, B., Alias, A., Christensen, O.B., Bouwer, L.M., Braun, A., Colette, A., Déqué, M., Georgievski, G., Georgopoulou, E., Gobiet, A., Menut, L., Nikulin, G., Haensler, A., Hempelmann, N., Jones, C., Keuler, K., Kovats, S., Kröner, N., Kotlarski, S., Kriegsmann, A., Martin, E., van Meijgaard, E., Moseley, C., Pfeifer, S., Preuschmann, S., Radermacher, C., Radtke, K., Rechid, D., Rounsevell, M., Samuelsson, P., Somot, S., Soussana, J.F., Teichmann, C., Valentini, R., Vautard, R., Weber, B., Yiou, P., 2014. EURO-CORDEX: New high-resolution climate change projections for European impact research. Reg. Environ. Chang. 14, 563–578. https://doi.org/10.1007/s10113-013-0499-2.

Jensen, M.E., Burman, R.D., Allen, R.G., 1990. Evapotranspiration and irrigation water requirements. ASCE Manuals No. 70. Amer Society of Civil Engineers, Reston, Virginia, U.S.A.

Jin, Z., Liang, W., Yang, Y., Zhang, W., Yan, J., Chen, X., Li, S., Mo, X., 2017. Separating Vegetation Greening and Climate Change Controls on Evapotranspiration trend over the Loess Plateau. Sci. Rep. 7, 1–15. https://doi.org/10.1038/s41598-017-08477-x.

Joseph, G., 2005. Fundamentals of Remote Sensing. Second Edition. Universities Press Private Limited, India.

Kalma, J.D., McVicar, T.R., McCabe, M.F., 2008. Estimating land surface evaporation: A review of methods using remotely sensed surface temperature data. Surv. Geophys. 29, 421–469. https://doi.org/10.1007/s10712-008-9037-z.

Kustas, W.P., 1990. Estimates of evapotranspiration with a one- and two-layer model of heat transfer over partial cover. J. Appl. Met. 29, 704–715. https://doi.org/10.1175/15200450(1990)029<0704:EOEWAO>2.0.CO;2.

Kustas, W.P., Norman, J.M., 1997. A two-source approach for estimating turbulent fluxes using multiple angle thermal infrared observations. Water Resour. Res. 33, 1495-1508.

Kustas, W.P., Norman, J.M., 1999. Evaluation of soil and vegetation heat flux predictions using a simple two-source model with radiometric temperatures for partial canopy cover. Agric. For. Meteorol. 94, 13–29. https://doi.org/10.1016/S0168-1923(99)00005-2.

Lionello, P., Scarascia, L., 2018. The relation between climate change in the Mediterranean region and global warming. Reg. Environ. Chang. 18, 1481–1493. https://doi.org/10.1007/s10113-018-1290-1.

Martín-Vide, J., Olcina, J., 2001. Climas y tiempos de España, Alianza Editorial, Madrid.

Mateos, L., González-Dugo, M.P., Testi, L., Villalobos, F.J., 2013. Monitoring evapotranspiration of irrigated crops using crop coefficients derived from time series of satellite images. I. Method validation. Agric. Water Manag. 125, 81-91. https://doi.org/10.1016/j.agwat.2012.11.005.

Milano, M., Ruelland, D., Fernandez, S., Dezetter, A., Fabre, J., Servat, E., Fritsch, J.M., Ardoin-Bardin, S., Thivet, G., 2013. Current state of Mediterranean water resources and future trends under climatic and anthropogenic changes. Hydrol. Sci. J. 58, 498–518. https://doi.org/10.1080/02626667.2013.774458.

Monteith, J.L., 1973. Principles of Environmental Physics. Edward Arnold, London, UK.

Moran, M.S., 2003. Thermal infrared measurement as an indicator of plant ecosystem health, in: D.A.Q.a.J. Luvall (Ed.), Thermal Remote Sensing in Land Surface Processes, Pa: Taylor and Francis, Philadelphia, pp. 257-282.

Moran, M.S., Peters-Lidard, C.D., Watts, J.M., McElroy, S., 2004. Estimating soil moisture at the watershed scale with satellite-based radar and land surface models. Can. J. Remote Sens. 30, 805-826. https://doi.org/10.5589/m04-043.

Moreno, G., Cáceres, Y., 2016. System report: Iberian Dehesas, Spain. AGFORWARD. Agroforestry for Europe, Plasencia.

Moreno G., Pulido F.J., 2009. The Functioning, Management and Persistence of Dehesas, in: Rigueiro-Rodríguez A., McAdam J., Mosquera-Losada M.R. (Eds.), Agroforestry in Europe. Advances in Agroforestry, vol 6, Springer, Dordrecht.

Moreno Llorca, R.A., González Moreno, P., Navarro González, I., Bonet García, F.J., Pérez Luque, A.J., Zamora Rodríguez, R. III. 9. Montaña Mediterránea. En: Evaluación de los ecosistemas del milenio de España. Conservación de los servicios de los ecosistemas y la biodiversidad para el bienestar humano. Infome final. http://www.ecomilenio.es/wp-content/uploads/2012/03/09-Monta%C3%B1a-mediterr%C3%A1nea-web.pdf (accessed 30 May 2021).

Neale, C.M.U., Bausch, W.C., Heermann, D.F., 1989. Development of reflectance-based crop coefficients for corn. Trans. Am. Soc. Agric. Eng. 32, 1891–1899. https://doi.org/10.13031/2013.31240.

Norman, J.M., Kustas, W.P., Humes, K.S., 1995. Source approach for estimating soil and vegetation energy fluxes in observations of directional radiometric surface temperature. Agric. For. Meteorol. 77, 263–293. https://doi.org/10.1016/0168-1923(95)02265-Y.

Padilla, F.L.M., González-Dugo, M.P., Gavilán, P., Domínguez, J., 2011. Integration of vegetation indices into a water balance model to estimate evapotranspiration of wheat and corn. Hydrol. Earth Syst. Sci. 15, 1213–1225. https://doi.org/10.5194/hess-15-1213-2011.

Peel, M. C., Finlayson, B. L., McMahon, T. A., 2007. Updated world map of the Köppen-Geiger climate classification. Hydrol. Earth Syst. Sci. 11, 1633–1644. https://doi.org/10.5194/hess-11-1633-2007.

Penman, H.L., 1948. Natural evaporation from open water, bare soil and grass. Proc. Roy. Soc. A. 193, 120–146. https://doi.org/10.1098/rspa.1948.0037.

Plieninger, T., Rolo, V., Moreno, G., 2010. Large-scale patterns of Quercus ilex, Quercus suber, and Quercus pyrenaica regeneration in central-western Spain. Ecosystems *13*, 644–660. https://doi.org/10.1007/s10021-010-9345-2.

Pôças, I., Calera, A., Campos, I., Cunha, M., 2020. Remote sensing for estimating and mapping single and basal crop coefficientes: A review on spectral vegetation indices approaches. Agric. Water Manag. 233, 106081. https://doi.org/10.1016/j.agwat.2020.106081.

Poyatos, R., Granda, V., Molowny-Horas, R., Mencuccini, M., Steppe, K., Martínez-Vilalta, J., 2016. SAPFLUXNET: Towards a global database of sap flow measurements. Tree Physiol. 36, 1449–1455. https://doi.org/10.1093/treephys/tpw110.

Rajendran, S., Aravindan, S., Rajakumar, T.J., Sivakumar, R., Mohan, K.R., 2009. Hyperspectral Remote Sensing and Spectral Signature Applications. New India Publishing Agency, India.

Rana, G., Katerji, N., 2000. Measurement and estimation of actual evapotranspiration in the field under Mediterranean climate: A review. Eur. J. Agron. 13, 125–153. https://doi.org/10.1016/S1161-0301(00)00070-8.

Renzullo, L.J., Barrett, D.J., Marks, A.S., Hill, M.J., Guerschman, J.P., Mu, Q., Running, S.W., 2008. Multi-sensor model-data fusion for estimation of hydrologic and energy flux parameters. Remote Sens. Environ. 112, 1306–1319. https://doi.org/10.1016/j.rse.2007.06.022.

Rodriguez-Iturbe, I., Porporato, A., Laio, F., Ridolfi, L., 2001. Plants in water-controlled ecosystems: Active role in hydrologic processes and responce to water stress I. Scope and general outline. Adv. Water Resour. 24, 695–705. https://doi.org/10.1016/S0309-1708(01)00004-5.

Rouse, J.W., Haas, R.H., Schell, J.A., Deering, D.W., 1974. Monitoring vegetation systems in the Great Plains with ERTS. In: Proceeding of the 3rd Earth Resource Technology Satellite (ERTS) Symposium, vol. 1, 48–62.

Rundel, P.W., Arroyo, M.T.K., Cowling, R.M., Keeley, J.E., Lamont, B.B., Vargas, P., 2016. Mediterranean Biomes: Evolution of Their Vegetation, Floras, and Climate. Annu. Rev. Ecol. Evol. Syst. 47, 383–407. https://doi.org/10.1146/annurev-ecolsys-121415-032330.

Santos, F.L., Valverde, P.C., Ramos, A.F., Reis, J.L., Castanheira, N.L., 2007. Water use and response of a dry-farmed olive orchard recently converted to irrigation. Biosyst. Eng. 98, 102–114. https://doi.org/10.1016/j.biosystemseng.2007.03.027.

Schleussner, C.F., Lissner, T.K., Fischer, E.M., Wohland, J., Perrette, M., Golly, A., Rogelj, J., Childers, K., Schewe, J., Frieler, K., Mengel, M., Hare, W., Schaeffer, M., 2016. Differential climate impacts for policy-relevant limits to global warming: The case of 1.5 °c and 2 °c. Earth Syst. Dyn. 7, 327–351. https://doi.org/10.5194/esd-7-327-2016.

Sellers, P.J, Bounoua, L., Collatz, G.J., Randall, D.A., Dazlich, D.A., Los, S.O., Berry, J.A., Fung, I., Tucker, C.J., Field, C.B., Jensen, T.G., 1996. Comparison of radiative and physiological effects of doubled atmospheric CO_2 on climate. Science 271, 1402-1406. https://doi.org/10.1126/science.271.5254.1402.

Semmens, K.A., Anderson, M.C., Kustas, W.P., Gao, F., Alfieri, J.G., McKee, L., Prueger, J.H., Hain, C.R., Cammalleri, C., Yang, Y., Xia, T., Sanchez, L., Alsina, M.M., Vélez, M., 2016. Monitoring daily evapotranspiration over two California vineyards using Landsat 8 in a multi-sensor data fusion approach. Remote Sens. Environ. 185, 155–170. https://doi.org/10.1016/j.rse.2015.10.025.

Singh, D., 2012. Evaluation of long-term NDVI time series derived from landsat data through blending with MODIS data. Atmosfera 25, 43–63.

Sobrino, J.A., Del Frate, F., Drusch, M., Jiménez-Muñoz, J.C., Manunta, P., Regan, A., 2016. Review of thermal infrared applications and requirements for future high-resolution sensors. IEEE Trans. Geosci. Remote Sens. 54, 2963–2972. https://doi.org/10.1109/TGRS.2015.2509179.

Strahler, A.N., Strahler, A.H., 1989. Geografía física, Ed. Omega, Barcelona.

Su, Z., 2002. The Surface Energy Balance System (SEBS) for estimation of turbulent heat fluxes. Hydrol. Earth Syst. Sci. 6, 85–100. https://doi.org/10.5194/hess-6-85-2002.

Tasumi, M., Allen, R.G., Trezza, R., Wright, J.L., 2005. Satellite-Based Energy Balance to Assess Within-Population Variance of Crop Coefficient Curves. J. Irrig. Drain. Eng. 131, 94–109. https://doi.org/10.1061/(asce)0733-9437(2005)131:1(94).

Thiébault, S., Moatti, J., Ducrocq, V., Gaume, E., Dulac, F., Hamonou, E., Shin, Y., Joel, G., Boulet, G., Guégan, J., et al., 2016. The Mediterranean Region Under Climate Change: A Scientific Update, IRD Éditions, Marseille, France.

Timmermans, W.J., Kustas, W.P., Anderson, M.C., French, A.N., 2007. An intercomparison of the Surface Energy Balance Algorithm for Land (SEBAL) and the Two-Source Energy Balance (TSEB) modeling schemes. Remote Sens. Environ. 108, 369–384. https://doi.org/10.1016/j.rse.2006.11.028.

Twine, T.E., Kustas, W.P., Norman, J.M., Cook, D.R., Houser, P.R., Meyers, T.P., Prueger, J.H., Starks, P.J., Wesely, M.L., 2000. Correcting eddy-covariance flux underestimates over a grassland. Agric. For. Meteorol. 103, 279–300. https://doi.org/10.1016/S0168-1923(00)00123-4.

Walker, J.J., De Beurs, K.M., Wynne, R.H., Gao, F., 2012. Evaluation of Landsat and MODIS data fusion products for analysis of dryland forest phenology. Remote Sens. Environ. 117, 381–393, https://doi.org/10.1016/j.rse.2011.10.014.

Wang, K., Dickinson, R.E., 2012. A review of global terrestrial evapotranspiration: Observation, modeling, climatology, and climatic variability. Rev. Geophys. 50. https://doi.org/10.1029/2011RG000373.

Webb, E.K., Pearman, G.I., Leuning, R., 1980. Correction of flux measurements for density effects due to heat and water vapour transfer. Q. J. R. Meteorol. Soc. 106, 85–100. https://doi.org/10.1002/qj.49710644707.

Yang, Y., Anderson, M.C., Gao, F., Hain, C.R., Semmens, K.A., Kustas, W.P., Noormets, A., Wynne, R.H., Thomas, V.A., Sun, G., 2017. Daily Landsat-scale evapotranspiration estimation over a forested landscape in North Carolina, USA, using multi-satellite data fusion. Hydrol. Earth Syst. Sci. 21, 1017–1037. https://doi.org/10.5194/hess-21-1017-2017.

Zhang, Y., Peña-Arancibia, J.L., McVicar, T.R., Chiew, F.H.S., Vaze, J., Liu, C., Lu, X., Zheng, H., Wang, Y., Liu, Y.Y., Miralles, D.G., Pan, M., 2016. Multi-decadal trends in global terrestrial evapotranspiration and its components. Sci. Rep. 6, 1–12. https://doi.org/10.1038/srep19124.

Chapter 2

Effect of the differences in spectral response of Mediterranean tree canopies on the estimation of evapotranspiration using vegetation index-based crop coefficients

Carpintero, E., Mateos, L., Andreu, A., González-Dugo, M.P., 2020. Effect of the differences in spectral response of Mediterranean tree canopies on the estimation of evapotranspiration using vegetation index-based crop coefficients. Agric. Water Manag. 238, 106201. https://doi.org/10.1016/j.agwat.2020.106201.

Abstract

The vegetation index (VI)-reference evapotranspiration (ET_o) method incorporates the estimation of basal crop coefficients from spectral VIs into the FAO56 guidelines for computing crop evapotranspiration (ET). Previous research pointed to the possibility of the differential spectral response of some Mediterranean crops, specifically olive trees. To evaluate this hypothesis and the potential related effects on the VI-ET_o method, this work studied the spectral response of four Mediterranean canopies under full vegetation coverage: three fruit trees (olive, orange and almond trees), and the holm oak trees of the *dehesas* ecosystem. Spectral measurements were taken on dense vegetation placed on a workbench and over dense treetops, avoiding in both cases the effect of soil background. The results showed that the soil adjusted vegetation index (SAVI) for full-cover olive trees was significantly lower than for other fruit trees (0.57 for olive trees *vs.* 0.71 for orange tree and 0.70 for almond tree). SAVI of olive vegetation measured on the workbench was lower than that measured over treetops, probably due to the effects of canopy architecture and shadowing. SAVI obtained on oak treetops (0.51) was even lower than that on olive treetops. This differential spectral response of olive and oak trees influenced the estimation of ET (and water stress). The validation using ET measurements obtained with the eddy covariance method in the olive orchards showed a reduction of root mean square deviation (RMSD) from 0.73 to 0.6 mm day^{-1} when daily ET was estimated assuming $SAVI_{max}$ = 0.57 in comparison with a generic value for Mediterranean crops.

Chapter 3

Remote-Sensing-Based Water Balance for Monitoring of Evapotranspiration and Water Stress of a Mediterranean Oak-Grass Savanna

Carpintero, E., Andreu, A., Gómez-Giráldez, P.J., Blázquez, Á., González-Dugo, M.P., 2020. Remote-Sensing-Based Water Balance for Monitoring of Evapotranspiration and Water Stress of a Mediterranean Oak-Grass Savanna. Water 12, 1418. https://doi.org/10.3390/w12051418

Abstract

Mediterranean oak savannas (known as *dehesas* in Spain) are exposed to numerous threats from natural and economic causes. A close monitoring of the use of water resources and the status of the vegetation in these ecosystems can be useful tools for maintaining the production of ecological services. This study explores the estimation of evapotranspiration (*ET*) and water stress over a *dehesa* by integrating remotely sensed data into a water balance using the FAO-56 approach (*VI-ET$_o$* model). Special attention is paid to the different phenology and contribution to the system's hydrology of the two main canopy layers of the system (tree + grass). The results showed that the model accurately reproduced the dynamics of the water consumed by the vegetation, with RMSE of 0.47 mm day^{-1} and low biases for both, the whole system and the grass layer, when compared with flux tower measurements. The *ET/ET$_o$* ratio helped to identify periods of water stress, confirmed for the grassland by measured soil water content. The modeling scheme and Sentinel-2 temporal resolution allowed the reproduction of fast and isolated *ET* pulses, important for understanding the hydrologic behavior of the system, confirming the adequacy of this sensor for monitoring grasslands water dynamics.

3.1. Introduction

Water availability is the main climate factor limiting the primary production of Mediterranean agroforestry systems. Recurrent water scarcity conditions are likely to worsen, with a decrease in the quality, quantity, and resilience of freshwater resources predicted for the Mediterranean region under the current global change scenario (Birot et al., 2011; Milano et al., 2013). In this context of increased variability, improved knowledge of hydrological process dynamics and its impact on vegetation is essential to reinforce ecosystem water resource management and planning, which may contribute to reducing vulnerability to climate change. Metrics describing the ecosystem's status regarding water consumption and vegetation growth, as well as its general stability, can facilitate regular monitoring and the implementation of conservation strategies at different scales (regional, national, or European policies), while maintaining the productivity required to support the rural economy. Earth observation technologies provide timely and quantitative open data to assist in the calculation of these metrics at different resolutions.

Oak savannas growing in the Mediterranean region, known as *dehesa* in Spain and *montado* in Portugal, are structurally and physiologically adapted to survive under extreme seasonal water scarcity conditions, including high temperatures and soil dryness levels for several months every summer (Baldocchi and Xu, 2007; David et al., 2007). This landscape is a complex mosaic of widely-spaced oak trees (mostly *Quercus Ilex* L. and *Quercus Suber* L.), combined with pastures, shrubs, and crops. The low ground fractional coverage of the oak trees constrains the leaf area index (LAI) of the ecosystem and enables light to enter the

understory, meaning that grass production can be maintained in these soils, usually with a low fertility (Moreno and Pulido, 2009). In addition, scattered tree roots can explore a large volume of soil (Moreno et al., 2005; Cubera and Moreno, 2007), with pasture tapping shallow water supplies. This structure imposes a marked spatial heterogeneity on the functioning of the ecosystem, with additional differences in the water use below and outside the tree canopy (Joffre and Rambal, 1993; Gauquelin et a., 2016).

This human-induced ecosystem has historically offered a compromise between production and conservation, satisfying the population's economic needs while providing multiple environmental services, such as biodiversity hotspots, landscape, water provisioning, or CO2 fixation (Campos et al., 2013). However, it is currently being exposed to numerous threats, such as the lack of the natural regeneration of tree species (Plieninger et al., 2010), its low profitability, the intensification of agricultural and livestock activities, and changes in soil properties and hydrological processes, increasing soil erosion (Coelho et al., 2004; Moreno and Pulido, 2009). The situation might worsen due to climate change, with prediction models forecasting warmer and drier summers, a growing occurrence of extreme high-temperature events and heatwaves (Giorgi and Lionello, 2008; Jacob et al., 2014), and increased drought frequency and intensity (Mishra and Singh, 2010; Milano et al., 2011; Polade et al., 2014; Schleussner et al., 2016). The abandonment of farmland and grazing areas due to the aforementioned processes will also trigger changes in land use and management (García-Ruíz et al., 2011; Seneviratne et al., 2018), leading to an additional risk to *dehesa* conservation.

Remote sensing is widely used in agricultural areas to assist in the computation of crop water requirements, using an adaptation of the Food and Agriculture Organization (FAO) Irrigation and drainage paper-56 approach (Allen et al., 1998, 2005). This model estimates crop evapotranspiration (*ET*) as being the product of reference evapotranspiration (ET_o), representing the atmospheric evaporative demand, and a crop coefficient (K_c) used to account for crop factors, such as crop type, developmental stage, ground cover, or soil water content. The integration of vegetation indices (*VI*s) derived from remote sensing into this model (herein called *VI*-ET_o) improves the estimation of canopy transpiration (Bausch, 1995; Jayanthi and Neale, 2001; Er-Raki et al., 2007; González-Dugo and Mateos, 2008; Consoli and Vanella, 2014; Odi-Lara et al., 2016) and takes advantage of the spatial and temporal resolutions (daily, weekly, monthly) of remotely sensed data. Different approaches and applications of this method have been reviewed by Glenn et al. (2011), Calera et al. (2017), and Pôças et al. (2020). Applications over natural ecosystems are substantially fewer than over crops, and present additional difficulties due to the higher heterogeneity in plant properties. The adjustments proposed by Allen et al. (1998) for using this method in native vegetation under water deficit conditions, and the good estimations of the vegetation ground cover fraction (f_c) and LAI produced by remote sensing over mixed vegetation types and natural ecosystems (Glenn et al., 2010), are the basis for applications in non-cropped areas.

Previous studies have given good results in the application of *VI*-ET_o over savanna landscapes in Mediterranean and African semi-arid areas (Campos et al., 2013; Andreu et al., 2019). However, these studies highlighted the difficulty of taking into account the heterogeneity of the system in the estimation of effective model parameters. Another factor that needs to be considered in the use of this method over *dehesas* is the differential spectral response of holm oak trees (similar to olive trees) compared to other plant species under full cover conditions, which may condition *ET* and water stress monitoring when *VI*-based techniques are used (Carpintero et al., 2020). On the other hand, Mateos et al. (2013) underlined the importance of the accurate computation of f_c for incomplete canopies when applying this method. In this case, the frequent presence of a senescent or dead grass layer during the summer and the low tree cover, as the only photosynthetic vegetation during this season, might reduce the ability of broadband *VIs* to accurately estimate f_c in the dry period. Depending on the sensor and the spectra of the soils, the non-photosynthetic vegetation may be spectrally indistinguishable from the soil (Roberts et al., 1993). Xu et al. (2014) found a linear relationship between Normalized Difference Vegetation Index (*NDVI)* and dead cover in grasslands, with a variable contribution to *NDVI* depending on the dead cover fraction. This study uses both measurements and models to explore the factors influencing the estimation of *ET* and water stress over a *dehesa* ecosystem in an attempt to provide effective vegetation parameters to model the water balance with the assistance of remote sensing. Special attention is paid to the different behavior and phenology of the two main canopy layers of the ecosystem (tree + grass) and to the varying contribution to the system's hydrology. The use of layer-specific parameters and the effect of the non-photosynthetic vegetation on the modeling scheme are evaluated.

3.2. Materials and Methods

3.2.1. Study Site

The study was conducted over a *dehesa* farm (Santa Clotilde, 38°12′ N; 4°17′ W, 736 m a.s.l.; Figure 3.1a) located in the Natural Park of the *Sierra de Cardeña y Montoro*, in Southern Spain. It is a homogeneous landscape with gentle slopes and multiple uses (agriculture, extensive livestock grazing, and hunting). The continental Mediterranean climate of the area is characterized by a strong seasonality, with moderately cold winters alternating with long, hot, and dry summers. The rainfall presents intra- and interyear variability, with an annual average of 895 mm (from 1990 to 2015), concentrated during spring and fall.

The study site vegetation consists of widely-spaced oak trees (mostly *Quercus ilex* L., with a scattering of *Quercus faginea* Lam. and *Quercus pyrenaica* Willd. individuals) combined with a subcanopy composed of annual grassland. The layer of annual species emerges after the first rainfall in autumn and dries out in late spring. The majority of the herbaceous species belong to the *Stellarieteamediae* class, and more specifically to the

Bromo scoparii-Hordeetumleporini association (Rivas Martínez, 1988), according to field visual identification based on the work of Melendo (Melendo, 1998). This grass cover corresponds to annual ephemeral, ruderal, and nitrophilous weed communities as a result ofmoderately intense continuous grazing. The predominant species are: *Bromus hordeaceus*, *Hordeum leporinum*, *Bromus diandrus*, *Echium plantagineum*, *Lolium rigidum*, *Anthemis arvensis*, *Plantago lagopus*, *Raphanus raphanistrum*, *Sisymbrium officinale*, and *Avena barbata*.

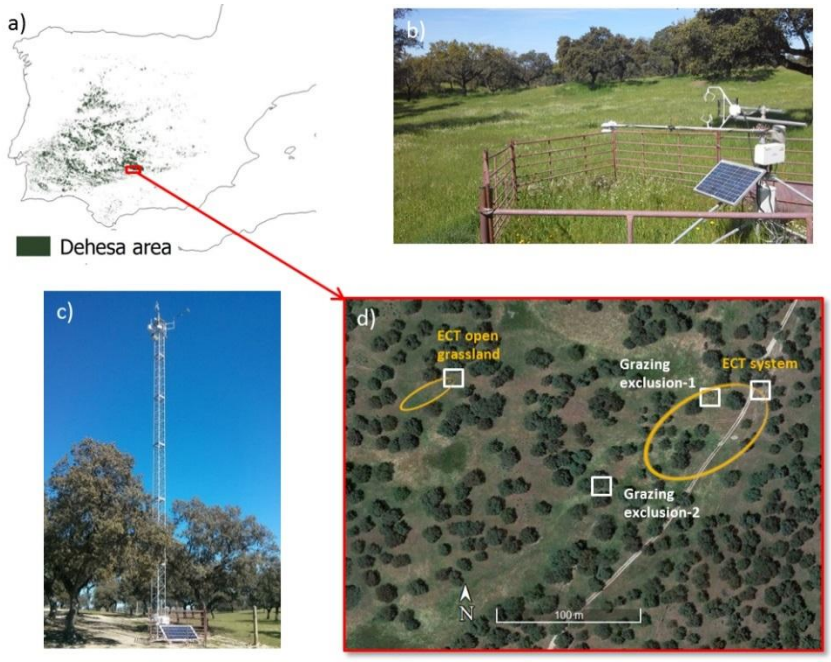

Figure 3.1. (**a**) Distribution of the *dehesa* ecosystem in the Iberian Peninsula (in green) and the study area location (**b**) Eddy covariance tower (ECT) over open grassland. (**c**) ECT over the combined tree + grassland system; (**d**) Aerial photograph showing the locations of validation sites.

In relation to the soil's properties, the prevailing textural class in the area is sandy loam, with variations in soil depths generally ranging between 0.5 and 2.40 m. The bulk density increases linearly with depth, from a mean value of 1.3 Mg m^{-3} at the surface to 1.6 Mg m^{-3} at around 25-30 cm. This increase with depth is commonly linked to a lower C content and higher compaction, but in this area it is also related to the increase in stoniness (Román-Sánchez et al., 2018).

3.2.2. Ground Validation Measurements

Ground validation measurements were taken at the study area using two eddy covariance towers (ECT), one over the combined tree + grassland system and another over open grassland (Figure 3.1b,c,d). Measurement sites to complement the flux towers data

were located on two grazing exclusion enclosures, over open grassland and under a holm oak tree, to assess the heterogeneity of the study area. The setup encompasses all the instruments required for continuous measurement of all energy balance components, including the turbulent fluxes of sensible (H) and latent heat (LE), the net radiation (Rn), and the soil heat flux (G).

The ECT system over the *dehesa* was installed on a tower at a height of 18 m in April 2012, registering the ecosystem response as a whole (Figure 3.1c). A 3D sonic anemometer (model CSAT3 Campbell Scientific Inc., Logan, UT, USA) measuring horizontal and vertical fluctuations of temperature and wind speed, and a hygrometer (model KH20, Campbell Scientific Inc., Logan, UT,USA) used to estimate water vapor fluctuations were installed at the beginning, with the latter being replaced in 2015 by a LICOR-7500 open path CO2/H2O gas analyzer (IRGA; model LI-7500A, Li-Cor, Lincoln, NE, USA), taking simultaneous measurements of carbon dioxide and water vapor in turbulent air structures. These measurements were recorded with high frequency (10 Hz), and half-hourly averages were computed after applying corrections of density effects due to heat and water vapor transfer (Webb et al., 1980). The net radiation was first obtained with a net radiometer (model NR-Lite,Kipp and Zonen, Delft, Netherlands), which was also replaced by a four-component net-radiometer (model NR01, Hukseflux Thermal Sensors, Delft, The Netherlands) in 2015. The relative humidity and air temperature were also measured with a probe (model HMP155, Vaisala, Helsinki, Finland). More information on the study area and the equipment can be found in the work of Andreu et al. (2018).

The soil heat flux was measured by soil heat flux plates (model HFP01, Huseflux Thermal Sensors, Delft, Netherlands) buried in the two grazing exclusion areas together with soil thermocouples, which were used to calculate the temporal variation of the soil temperature above the plates. The data were corrected with the soil moisture obtained with five humidity soil probes (model EnviroSCAN, Sentek Pty. Ltd., Stepney, Australia) located in grazing exclusion areas 1 and 2 (Figure 3.1d), which were continuously measured at depths of 10, 30, and 50 cm. The ground cover fraction of trees and pasture was integrated into a weighted average to estimate the ecosystem G value.

The quality of the measurements was tested by Andreu et al. (2018) for the 2012 summer season, resulting in an average closure balance ($Rn - G = LE + H$) of 86%. For the period 2014-2015, the closure balance was 91%. The energy balance closure method used in this study preserves the Bowen ratio (the residual of the available energy is allocated to H and LE, depending on their relative proportions), and the corrector factor is subsequently estimated on a daily basis (Mauder et al., 2018).

The second ECT over the open grassland was installed in February 2015, taking measurements at 1.5 m of surface energy exchanges (Figure 3.1b). This tower had a CSAT three-dimensional (3D) sonic anemometer, a KH20 hygrometer, and a NR-1 four-component net radiometer (all from Campbell Sci. Inc., Logan, UT, USA). A humidity and temperature probe (Vaisala model HMP45A, Helsinki, Finland) was also installed, and soil

heat flux plates and soil thermocouples were buried to determine the G flux. The ECT measurements were recorded with high frequency (20 Hz), and half-hourly averages were computed after applying the corrections regarding density effects due to heat and water vapor transfer (Webb et al., 1980). Two soil water content probes were installed under this grass eddy tower in 2017; no data were available for the study period. For the period when all the probes located over open grassland were measuring, a correlation between the grazing exclusion 1 probes and the grass ECT probes was computed, finding an $R^2 = 0.92$. The humidity values shown in the Results section were computed using the correlation equation.

A footprint analysis was performed over both ECT by estimating the contribution areas to daily fluxes for the years studied, as described by Hsieh et al. (2000). From the analysis, it was observed that 100% of the system ECT fluxes were collected from an area within 130 m upwind in 78% of the cases, with the maximum contribution to the energy fluxes measured being approximately found at 33 m upwind over the period analyzed. According to these results, average values of a 3 × 3 grid cell (with 30 × 30 m cell and oriented towards the predominant south-west footprint direction of the ECT) of the modeled fluxes were evaluated. At the open grass ECT, the peak contribution was 8.5 m, with 76% of the fluxes being measured within the first 10 m. A grid cell with 2 × 1 pixels (with a 10 × 10 m cell) was selected; due to the characteristics of the installation, all the fluxes recorded at the tower came from the herbaceous vegetation area.

3.2.3. Remote-Sensing-Based Soil-Water Balance Model

The *VI-*ET_o approach applied in this work to assess vegetation water requirements is based on the concepts of ET_o, calculated using the Penman-Monteith equation, and the crop and vegetation coefficients (K_c), which are partly derived from satellite *VIs*. ET_o takes into account the atmospheric evaporative demand, while the K_c accounts for the influence of the plant properties on the *ET*, considering the growth of the canopy and the related changes in its biophysical properties. K_c is estimated daily by means of the FAO-56 dual method, which separates crop transpiration from soil surface evaporation (Wright, 1982; Allen et al., 1998):

$$ET = (K_{cb} K_s + K_e) ET_o \quad (3.1)$$

Where K_{cb} is the basal canopy coefficient determining canopy transpiration; K_s is the water stress coefficient, quantifying the reduction in transpiration due to soil water deficit; and K_e is the soil evaporation coefficient.

The K_{cb} of the whole system and that of the grass were derived from satellite spectral information provided by *VIs*, combining bands in the near-infrared and red domains. Numerous *VI-*K_{cb} empirical relationships can be found in the literature for different crops (Hunsaker et al., 2003; González-Piqueras et al., 2004; Hunsaker et al., 2005; Jayanthi et

al., 2007; Campos et al., 2010). This work used the generalized linear equation proposed by González-Dugo et al. (2009) through the soil adjusted vegetation index (*SAVI*, (Huete, 1988)), as follows:

$$K_{cb} = \frac{K_{cbfull}}{f_{ceff-full}}\left(\frac{SAVI - SAVI_{min}}{SAVI_{max} - SAVI_{min}}\right) \; if \quad f_c < f_{ceff-full} \tag{3.2}$$

$$K_{cb} = K_{cbfull} \qquad if \quad f_c \geq f_{ceff-full} \tag{3.3}$$

Where $f_{c\ eff\text{-}full}$ is the ground cover fraction at which K_{cb} is at its maximum ($K_{cb\ full}$), and the subscripts max and min refer to the values of *SAVI* for high LAI and bare soil, respectively. The K_{cb} values distributed over the study area were linearly interpolated between satellite overpasses in order to obtain a daily K_{cb} image throughout the study period.

The energy available at the topsoil was calculated to compute K_e with Equation (3.4):

$$K_e = K_r(K_{cmax} - K_{cb}) \tag{3.4}$$

Here, K_r is a dimensionless evaporation reduction coefficient that depends on topsoil water depletion (Allen et al., 1998) and $K_{c\ max}$ is the maximum value of K_c following a rainfall or irrigation event. K_e should be lower than $f_{ew} \times K_{c\ max}$, with f_{ew} being equal to the fraction of the soil surface that is both exposed and wetted.

A daily soil root zone water balance test was carried out in order to determine the vegetation water stress coefficient (K_s). The variation in the root zone water content, ΔS_w, was computed as the balance between water inflows and outflows:

$$\Delta S_w = S_{wf} - S_{wi} = R - ET - D \tag{3.5}$$

Where S_{wi} and S_{wf} (mm) are the root zone water contents at the beginning and end of the water balance period, R is infiltrated rainfall, and D is deep drainage during the balance period.

The root zone water daily deficit can be expressed with Equation (3.6), as below:

$$RZWD_i = RZWD_{i-1} + ET_i + D_i - R_i \tag{3.6}$$

where the subscript i indicates the balance day, and $RZWD_i$ and $RZWD_{i\text{-}1}$ are the root zone water deficits on days i and i-1, respectively. The water depth between the soil field capacity and wilting point extremes is called the root zone water holding capacity (*RZWHC*).

Equation (3.7 and 3.8) calculates the stress coefficient, K_s, based on the relative root zone water deficit:

$$K_s = \frac{RZWHC - RZWD_i}{(1-p)RZWHC} \quad if \quad RZWD_i < (1-p)RZWHC \tag{3.7}$$

$$K_s = 1 \quad if \quad RZWD_i \geq (1-p)RZWHC \tag{3.8}$$

Where p is the fraction of the *RZWHC* that can be reduced before water stress occurs (depletion fraction). This stress coefficient is equal to 1 for non-stress conditions and less than 1 when a shortage of water is found in the root zone (Allen et al., 1998). A complete description of the model can be found in the work by Allen et al. (1998, 2005).

This approach was applied at a daily time step (1) over the whole *dehesa* ecosystem (integrating the tree cover layer and the herbaceous understory) at the farm scale over the Santa Clotilde area and (2) over the open grassland area, in order to exclusively model the water balance of the herbaceous layer to improve our understanding of the function of each canopy component separately. The water balance calculation over the combined tree + grassland system was initiated in September 2012 at the end of a dry summer and ended in August 2017. For the initiation of the balance and due to a longtime without rainfall events, the soil was considered to be completely dry and the root zone water deficit was assumed to be equal to the soil water holding capacity. Over grass, the *VI-ET$_o$* model was applied during the hydrological years 2015-2016 and 2016-2017. The starting-out soil water deficit was taken as the value estimated for the *dehesa* for that exact period but related to its root zone water holding capacity. To model the water balance in the soil, the strategies have to be assessed, followed by each of the vegetation clusters, trees, and grass, and later implemented into the balance, using tabulated and calibrated input parameters to reproduce the behavior of the different components.

To quantify the impact of water stress over the whole ecosystem, the ratio of *ET* to reference *ET* (*ET/ET$_o$*) was computed at a daily time step for the period 2013-2017. This ratio is a widely used drought indicator (Anderson et al., 2016).

3.2.4. Tree-Grass Cover Fraction during the Dry Season

The evidence shows a medium to high coverage of senescent or dead grass in this ecosystem during the summer. This coverage is highly variable and depends on the annual climatology and farm management strategies. This could challenge the application of the *VI-ET$_o$* methodology in the *dehesa*, given the high sensitivity of this model to the estimation of f_c, with significant *ET* inaccuracies when this variable is poorly determined, as Mateos et al. (2013) concluded over an olive orchard.

The main spectral differences between non-photosynthetic grass and bare soil are located in shortwave infrared regions, and spectral mixture analysis is normally used to

discriminate both covers from hyperspectral data (Roberts et al., 1993). Bare soil and dead grass are not easily discriminated by only using visible (VIS) and near infrared (NIR) (Nagler et al., 2003) due to neither of them having a unique spectral feature in that region, and due to the fact that the reflectance of the dead grass can be higher or lower than that of the soil (Aase and Tanaka, 1991). The absorption of senescent grass at 2.1 μm in the spectra is associated with its cellulose and lignin contents. Thus, the shortwave infrared region ranging from 2.0-2.2 μm is used to discriminate plant litter from soil, defining a spectral variable called cellulose absorption index (CAI, (Nagler et al., 2000), which describes the depth of the lignocellulose absorption. However, Xu et al. (2014) found a linear relationship between *NDVI* and dead cover in grasslands, having a variable contribution to *NDVI* depending on the dead cover fraction. It can be hypothesized that the effect of the non-photosynthetic grass layer on summer *VIs* might produce a slight deviation in tree f_c estimation in using these *VIs*, leading to an overestimation of the transpiration rates during this season.

To evaluate this effect, ground spectral measurements over the non-photosynthetic grass (100% of ground cover) were conducted at the Santa Clotilde farm with a spectroradiometer (model ASD FieldSpec 3, ASD Inc., Boulder, CO, USA). This instrument provides uniform VIS/NIR/SWIR data collection, with a spectral range from 350 to 2500 nm (the sampling interval is 1.4 nm from 350 to 1050 nm, and 2 nm from 1000 to 2500 nm). The spectral measurements were referenced with regular ones over a white Spectralon panel (Labsphere, North Sutton, NH, USA) with 100% reflectance across the entire spectrum. The spectral data were taken on 7 July 2015 over 20 sampling points, and this information was later integrated into the Landsat Operational Land imager (OLI) sensor bandwidths, using the spectral response function for those wavelengths in order to compute the broadband *VIs*.

In addition, in order to accurately compute the fractional cover of the multiple ecosystem layers (grass, tree), digital classification was performed during the dry season using an airborne hyperspectral image (39 bands ranging from 400.8 to 680.8 nm) with a high spatial resolution (1 m). The image was acquired on 27 August 2015 at 12:00 pm with the Micro-Hyperspec visible/near infrared VNIR model sensor (Headwall Photonics, MA, USA). This high-resolution image was classified (using a trained maximum likelihood classification algorithm) into the different components (shadow, tree, and grass + soil). To validate this image, 70 ground truth points for each component were used. To choose the classification training vectors, the spectra of the different components were analyzed, with bare soil + plant litter, green canopy, and dark shadows being clearly identified. On the other hand, some mixed pixel spectra located in between the tree spectrum and nearby shadows were more difficult to isolate, and a new class was derived (mixed tree-shadow). For the final assessment, the pure shadow class was added to the soil-dry grass fraction and the mixed pixels were added to the tree fraction. The results were then compared with the

estimation of the tree and dead grass + soil ground coverage fractions using summer satellite *VIs*.

3.2.5. Satellite Remote Sensing Dataset

A set of 84 cloud-free images provided by Landsat-8, Sentinel-2, and MODIS satellites, collected between September 2012 and September 2017, were employed for the application of the *VI-*ET_o model over the system. The frequency of images was variable between seasons due to cloudiness. Most of the images were Landsat-8 images (46 images), with 30 m spatial resolution in the visible and NIR spectral bands, which were provided geometrically and atmospherically corrected by the Landsat surface reflectance climate data record (SR CDR) (http://espa.cr.usgs.gov). MODIS (product MOD09GQ, 12 images) was used at the beginning of the study period to complete the data series, due to the lack of Landsat images and Sentinel-2A (subsequently resampled at 30 m for the analysis). Georeferenced surface reflectance from Sentinel-2A (17 images) was generated with the Sen2cor processor, which performs the atmospheric, terrain, and cirrus correction of top-of-atmosphere input data (Mueller-Wilm et al., 2017). In addition, the Spatial and Temporal Adaptive Reflectance Fusion Model (STARFM) (Gao et al., 2006) data fusion technique was applied on nine dates to fill a long period without cloudless images. This approach compares one pair of observed Landsat or MODIS images acquired on the same day to predict maps at the Landsat spatial scale on other MODIS observation dates. In order to apply the method over grassland, a set of 99 Sentinel-2 images (10 m spatial resolution), collected between August 2015 and September 2017, was used for the two hydrological years. The processing was by using a Google Engine processor.

3.2.6. Meteorological Information and Soil Properties

Meteorological data and spatially distributed soil properties are required to apply the soil-water balance model. Daily meteorological data, including rainfall, solar radiation, air temperature, humidity, and wind speed, were provided by two ground stations operated by the Spanish Meteorological Agency (AEMET) near the study area (~3 km).

Soil parameters were supplied by Rodríguez et al. (2008), who offer distributed information at 250-m spatial resolution. Maps of soil texture (sand, clay, and silt), water content at field capacity, and water content at the wilting point were used. The saturation point was also determined by performing a daily analysis of the soil moisture content for several years. From this information, and using the expressions proposed by Mbah (2012), we computed the water content at field capacity and at the wilting point, adjusting the values provided by the distributed map. Finally, the employed land cover map was based on the Information and Soil Uses System of Spain (SIOSE 2013), which groups classes with similar characteristics and spectral responses.

3.2.7. Obtaining Soil and Vegetation Parameters

3.2.7.1. Tabulated and Measured Soil and Vegetation Parameters

The vegetation root depth determines the control volume of soil for water balance. Grass roots are found mostly in the upper 30 cm, with the root length density decreasing exponentially until 100 cm depth, while the oak root density is lower in the first 10 cm of the soil, remaining almost uniform with depth at a given distance from the tree (Moreno et al., 2005). Pulido-Fernández et al. (2013) showed the low dependence of oak trees on water in the uppermost soil layer. A high dependence on the water located below a depth of 3 m during summer, when the herbaceous layer is dry, was shown by Cubera and Moreno (2007). These limited vertical overlaps of grass and oak root profiles suggest that the competitive effects of the understory are unimportant for tree water uptake in *dehesa* landscapes (Moreno and Cáceres, 2016). In this work, to account for the whole system, the average root depth of oak trees was considered as being equal to 4 m (Moreno et al., 2005), while that of grasslands was considered as being equal to 1 m (Canadell et al., 1996; Moreno et al., 2005; Rolo et al., 2012; Pierret et al., 2016). These values were linearly combined, considering the area covered by each component to estimate the maximum effective root depth over the tree + grassland system of 2 m. The average coverage fraction in the study area of 0.25 for oak trees (estimated from the classification of the high-resolution image) was increased by 50% to account for the fact that tree roots explore a larger area than that occupied by their treetops (Moreno et al., 2005). For the modeling of the grassland area, a constant effective depth equal to 1 m was used (Canadell et al., 1996; Moreno et al., 2005; Rolo et al., 2012; Pierret et al., 2016).

The minimum *SAVI* was assumed to be 0.09 for bare soil (González-Dugo and Mateos, 2008), while *SAVI* under full vegetation cover conditions ($SAVI_{max}$) was determined from ground radiometric measurements at the site, measured over the tree and herbaceous canopies, using aspectroradiometer (model ASD FieldSpec3, ASD Inc., Boulder, CO, USA). A $SAVI_{max}$ value equal to 0.51 was measured for oak trees (Carpintero et al., 2020). For pasture, a $SAVI_{max}$ value equal to 0.70 was determined from field measurements on 29 April 2015, when full vegetation conditions were reached. Finally, a value of 0.65 for the combined system (weighted with the coverage fraction of each vegetation type) was used.

3.2.7.2. Calibration of Vegetation Parameters

Due to the lack of information on the value of some vegetation parameters in this ecosystem, such as K_{cb} under full vegetation conditions ($K_{cb\ full}$), as well as the depletion fraction (p), a calibration process was followed to determine the optimal values for the best model's performance. The $f_{c\ eff\text{-}full}$ was assumed to be equal to 0.8, as the average f_c at the beginning of the effective full cover is supposed to be reached at about 0.7-0.8 in most crops (Stegman et al., 1980; Allen et al., 1998). The model was run in multiple simulations, with a wide range of $K_{cb\ full}$ varying between 0.7 and 1.1 (the minimum corresponds to the

value for pastures with extensive grazing, while the maximum corresponds to the tabulated annual herbaceous crops in FAO-56 guidelines) in increments of 0.05; *p* varied between 0.3 and 0.7 (interval taken from the same guidelines and Campos et al. (2013)) in increments of 0.1.

In this work, we used the cross-validation method to evaluate the performance of the different water balance simulations (Browne, 2000). Cross-validation is a model validation technique that assesses how the performance of a model will generalize to an independent dataset. Various methods of cross-validation are available to partition a set of data and to validate a model, including the *k*-fold cross-validation used here (Arlot and Celisse, 2010; Lee et al., 2019). In *k*-fold cross-validation, the data is divided into *k* subsets. Then, the holdout method is repeated *k* times, so that each time one of the *k* subsets is used as the validation set and the other *k*-1 subsets are put together to form a training set. The error estimation is averaged over all *k* trials to obtain the total effectiveness of the model (Browne, 2000). This method has been applied to evaluate the accuracy of some hydrologic models (Schoups et al., 2008; Tegegne et al., 2017). In this case, the cross-validation method was preferred to a conventional one (partitioning the dataset into two sets for training and testing) due to the existing inter- and intra-annual differences, which may result in the pool data selected for calibration not being able to encompass all the different scenarios and climate variability, meaning the calibrated model would end up being a biased framework. We used the *k*-fold cross-validation with $k = 4$ folds, 3 hydrological years for calibration, and 1 year for validation. The performance indicator used in this study was the root mean square error (RMSE). The $K_{cb\ full}$ and *p* parameters with the minimum validation error were selected as the optimal values.

In the grassland area modeling, a similar analysis as for the whole system (trees + grass) was performed to determine the best model performance, evaluating in the analysis a range of $K_{cb\ full}$ for $f_{c\ eff\text{-}full} = 0.8$ (0.7-1.1) based on tabulated literature values (Allen et al., 2005). The cross-validation algorithm was not considered to be necessary here due to the low variability of the two hydrological years of study (2015-2016 and 2016-2017).

3.3. Results and Discussion

3.3.1. Parametrization of the VI-ETo Model over the Dehesa Ecosystem and Open Grassland

The application of the *VI-ET*$_o$ model to the study site has combined measured and estimated soil and vegetation parameters. Regarding the soil, the observed physical properties and the computed vegetation root depth resulted in a total amount of water being available for evaporation in the root zone of 283 mm, a value similar to the 280 mm zone computed by Campos et al. (2013) for the same landscape. For the vegetation, the calibrated model parameters were K_{cb} for full cover vegetation, $K_{cb\ full}$, and the depletion fraction, *p*. As can be observed in Figure 3.2, the sensitivity of the model to the depletion

factor is very low in both the whole system and the open grassland components, providing very similar results in the range of 0.4-0.6. Allen et al. (1998) discussed the variability of the fraction *p* as a function of the evaporation power of the atmosphere and the soil type. However, a constant value of $p = 0.5$ is commonly used for a wide variety of crops, rather than a daily variation. Attending to the results (Figure 3.2), *p* was chosen to be equal to 0.5 here for the two situations studied. This value was higher than the 0.3 selected by Campos et al. (2013) in the same type of ecosystem. However, different soil or evaporative conditions could contribute to this difference, which as can be derived from Figure 3.2, has a limited impact on the final *ET* estimations.

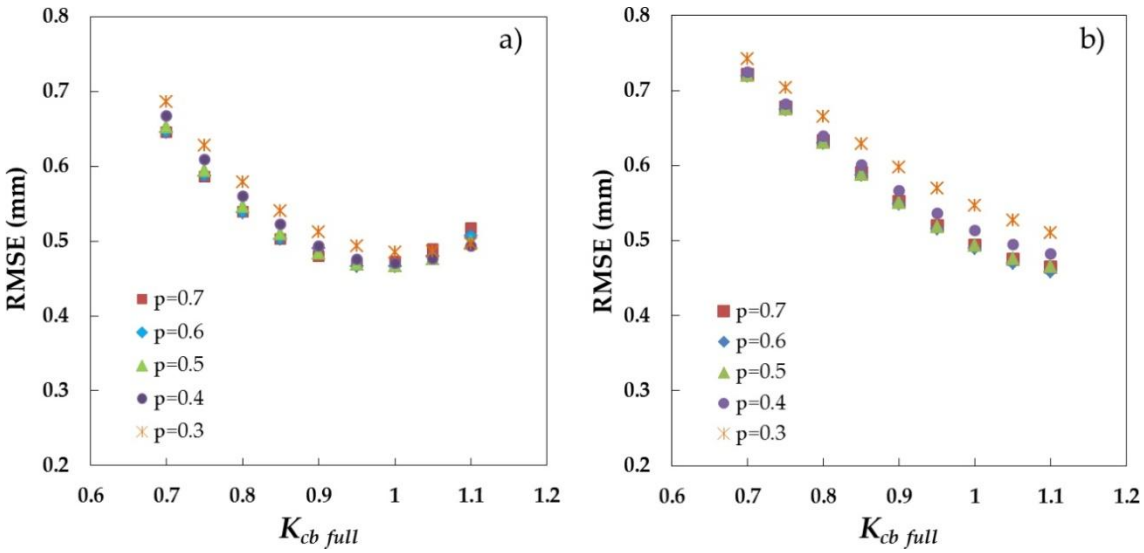

Figure 3.2. Performance (Root Mean Square Error, RMSE) of the soil water balance over the (**a**) *Dehesa* ecosystem and (**b**) grassland area, with a range of basal crop coefficients for full cover vegetation ($K_{cb\ full}$) (0.7-1.1) and depletion fractions (*p*) (0.3-0.7) parameters.

On the other hand, the selection of $K_{cb\ full} = 1$ for the whole system resulted in a reduction in RMSE of 0.2 mm when compared with the minimum value considered ($K_{cb\ full} = 0.7$). Therefore, the values of the parameters selected for the model application were $K_{cb\ full} = 1$ and $p = 0.5$ (with RMSE =0.47 mm day^{-1}). In open grassland modeling (Figure 3.2b), the simulation of increasing $K_{cb\ full}$ seemed to improve the final RMSE, until it reached a minimum of around $K_{cb\ full} = 1.1$, corresponding to the tabulated value of annual herbaceous crops used in previous works (Allen et al., 1998; González-Dugo et al., 2009; Padilla et al., 2011). These results are consistent with the results for the combined *dehesa* system and the tabulated values for other Mediterranean tree crops (e.g., olive trees) that have similarities with oak trees. The consideration of a $K_{cb\ full}$ value equal to 1 for the whole system and to 1.1 for grassland implies that $K_{cb\ full}$ for oak trees might be around 0.7, which is a reasonable value considering that it is similar to the values recommended by some authors for other Mediterranean tree species (Allen et al., 1998; Mateos et al., 2013). The selected values of

the parameters for model application over grassland, producing a RMSE = 0.47 mm day^{-1}, were $K_{cb\ full}$= 1.1 and p = 0.5.

3.3.2. Dead Grass Impact on ET Estimations during the Dry Season

Figure 3.3 presents the measured spectral signatures of green grass, senescent grass, and bare soil, with the red and near-infrared regions used to compute *NDVI* and *SAVI* highlighted in dark and light pink, respectively. One can observe the low separability of the bare soil and non-photosynthetic grass in the *VIS–NIR* region (Nagler et al., 2003), as well as the differences in the shortwave infrared region (2.0–2.2 μm), which can be useful for distinguishing both covers.

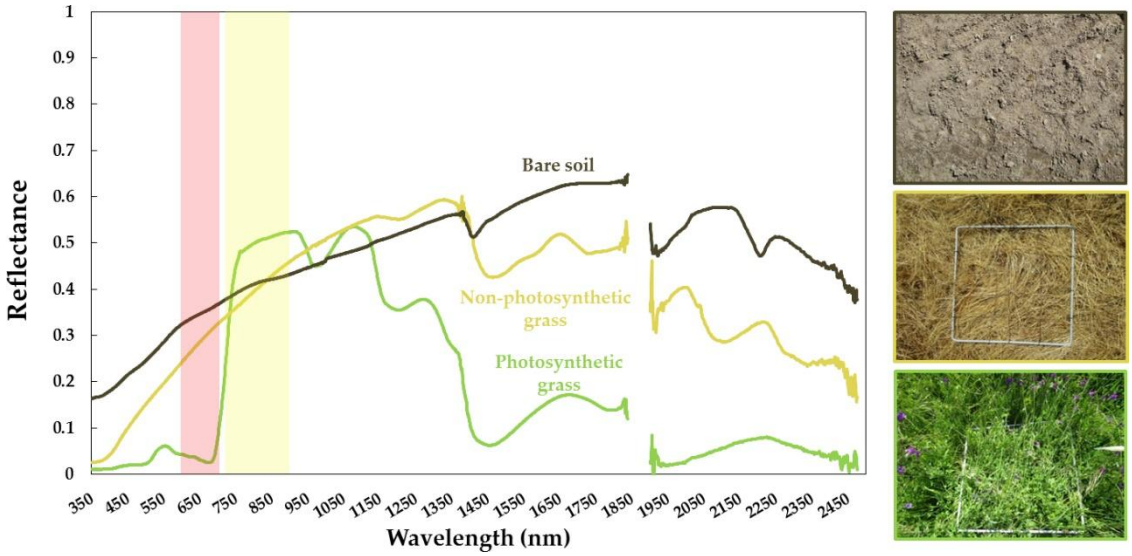

Figure 3.3. The spectral response measured with the spectroradiometer of bare soil, along with images of photosynthetic and non-photosynthetic grass under full vegetation conditions.

The field measurements resulted in *NDVI* and *SAVI* values of 0.24 and 0.19, respectively, for dead grass, which were significantly higher than values commonly used for soils, with *SAVI* in the range of 0.08-0.09 and NDVI of 0.1-0.14 (Pôças et al., 2020). Xu et al. (2014) obtained an *NDVI* of about 0.12 from a simulated relationship between the index and the dead cover, while the *NDVI* determined by Nagler et al. (2000) ranged between 0.25 and 0.3 for dry and wet forest litter, respectively, which was more similar to the values measured in this study. Summer *SAVI* values derived from the satellite data over the footprint of the open grassland tower when only dead grass is present are always higher than the selected value for soil, which is equal to 0.09, confirming the contribution of dead grass cover to the SAVI values used to estimate f_c.

In the final classification map of land cover on Santa Clotilde farm (Figure 3.4a), 96.6% of the validation points were classified correctly. The highest mismatches were

found in mixed tree and shadow pixels and pure shadows. The classification map obtained for the 1 × 1 km area surrounding the installation (Figure 3.4c) showed 75% background area (bare soil or non-photosynthetic grass, $f_{c\ grass+soil}$) and 25% tree fractional cover ($f_{c\ tree}$), similar to the fractional cover computed by Andreu et al. (2018). Considering only the tower footprint area used to compute the whole system *VIs*, $f_{c\ grass}$ was equal to 78.5% and $f_{c\ tree}$ equal to 21.5%. The tree fractional cover on the pasture lower tower footprint was confirmed to be equal to 0%, as originally designed.

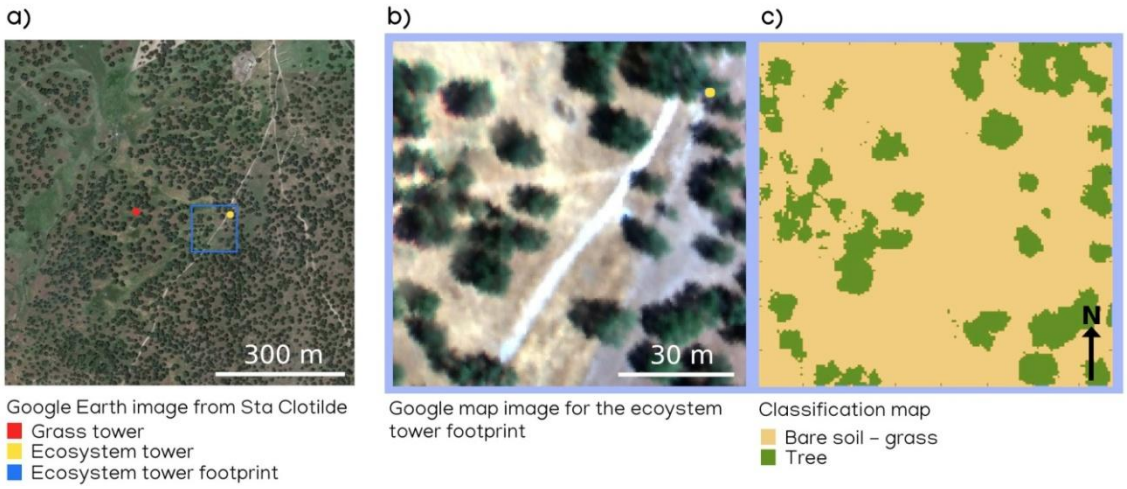

Figure 3.4. Classification map for the ecosystem eddy covariance tower.

The average estimation of the oak tree fractional cover of the ecosystem tower footprint area using satellite-derived *SAVI* values of the end of the summer (August) and all the years studied yielded a value of $f_{c\ tree}$ = 24%. The specific value corresponding to 28 August 2015 (when the reference flight was conducted) was equal to 23%. Both values are slightly higher than the 21.5% tree fractional cover computed with the reference classification method. Over the open grassland tower footprint, satellite-estimated summer $f_{c\ tree}$ was always >0%.

The difference of 1.5% in f_c suggests a certain influence of the dead grass on the satellite *VI*. However, its size does not seem large enough to justify the use of more precise spectral mixing models or higher complexity algorithms. The accuracy analysis presented in Section 3.3.3 was also used to support this decision.

3.3.3. Daily ET and Water Stress Monitoring over the Dehesa Ecosystem (Tree + Grass)

The modeled daily evapotranspiration is in reasonable agreement with the tower observations for the four hydrological years of the study (2013-2014 to 2016-2017; Figure 3.5), yielding an RMSE of 0.47 mm day^{-1} and a relatively low bias of -0.15 mm day^{-1}. This deviation is consistent with previous studies using the *VI-ET$_o$* FAO-56 dual crop coefficient

method in similar ecosystems (Campos et al., 2013; Andreu et al., 2019) for woody, sparse, semi-arid crops (Cammalleri et al., 2013; Consoli and Vanella, 2014; Campos et al., 2016) and for field crops (Padilla et al., 2011; González-Dugo et al., 2013; Mateos et al., 2013). Despite the low bias, a slight underestimation of the ET rates can be observed, with a greater impact on the highest *ET* rates (>4mm) in spring and a higher dispersion during this season. This underestimation might have an influence on the seasonal or annual computations of water consumption by the system. As an example, during the hydrological year 2016-2017, average weekly *ET* underestimation changed from 1.8 mm week^{-1} on average to values of around 5-7 mm week^{-1} for the springtime (between mid-May and mid-June 2017), decreasing again to 1.6 mm week^{-1} for the summer. The observed underestimation might be caused by a slight overestimation of some canopy parameters limiting the estimations ($SAVI_{max}$, $f_{c,full}$). The selection of representative values, accounting for the inter- and intra-annual variability and the behavior of the two vegetation layers, is a challenge, especially if ones wishes to avoid increasing the model's complexity, which could hinder the final operative applications. Adaptations to account for the major phenological periods were applied over savanna systems to estimate *ET* using a surface energy balance model (Burchad-Levine et al., 2020), which had a high sensitivity to f_c and to parameters related to the vegetation structure. Nevertheless, a daily error of 0.47 mm day^{-1}can be considered to be admissible to support management actions in the *dehesa*, with the precision reaching the accuracy requirements for agriculture and water management applications.

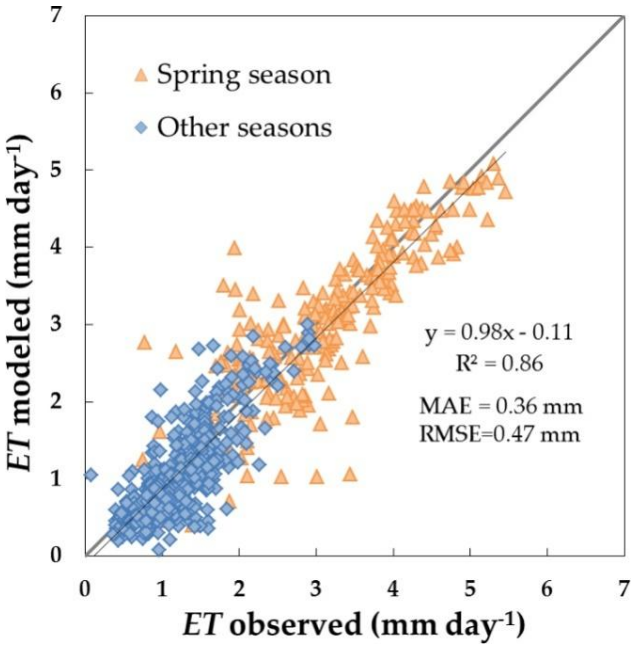

Figure 3.5. Comparison between observed and modeled daily evapotranspiration (*ET*) values (mm) for the *dehesa* system (tree + grass) for the four hydrological years analyzed (between 2013-2014 and 2016-2017). Root Mean Square Error (RMSE) and Mean Absolute Error (MAE) are presented in the figure.

Figure 3.6 shows a daily time step *ET* series generated for the four hydrological years analyzed (between 2013-2014 and 2016-2017) by the *VI-ET*$_o$ approach, together with *ET* measurements acquired by the *dehesa* ECT system and the rainfall data for the period. It can be seen that *ET* rates present an annual bimodal behavior, with two clear peaks of different sizes. The largest one occurs during the spring, reaching maximum values of around 4-4.5 mm day^{-1} in the first two years and higher ones of around 5 mm day^{-1} in the following years. A second smaller peak with maximum values of around 2 mm day^{-1} appears in the fall. This pattern is closely linked to the distribution of the annual rainfall and is also influenced by variables controlling the availability of energy for the evaporation. Although the average annual rainfall was similar in the first 3 years (653, 633, and 623 mm, respectively) with a wetter final year (731 mm), rainfall distribution is irregular throughout the seasons. The rainiest springs corresponded to the last 2 years (292 and 160 mm, respectively), which were followed by the *ET* rates, reaching their maxima during the spring of 2016 and the spring of 2017. During the long dry summers, the transpiration of the system was low (1.5 mm on average for the months of July and August) and minima of around 0.5-0.6 mm day^{-1} were measured at the end of the season (normally in early September before the first rainfall). *ET* rates during the summer, when the grass was dry and the oak trees transpired at a very low rate, showed the tolerance of this species to water stress. Oak tree roots explore extensive and deep volumes of soil, reaching the groundwater, in addition to forming both arbuscular and ectotrophic mycorrhizae accessing many different resources (Cubera and Moreno, 2007; Allen, 2015). The *ET* rates estimated here were lower but in the same range as values presented by David et al. (2007), who found that oak trees maintained transpiration rates of above 0.7 mm day^{-1} during the summer drought.

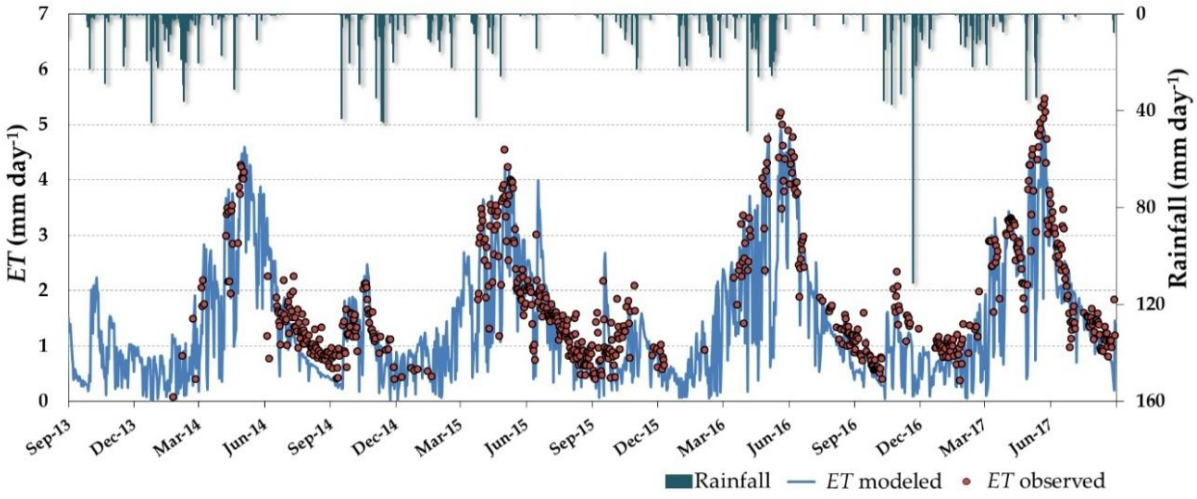

Figure 3.6. Daily evapotranspiration (*ET*) monitoring over the *dehesa* ecosystem, considering basal crop coefficients for full cover vegetation, $K_{cb\ full} = 1$, and the depletion fraction, p = 0.5. Dark green bars illustrate rainfall events.

Figure 3.6 shows that modeled *ET* accurately reproduced the temporal dynamics of the water consumed by the *dehesa* vegetation measured by the flux tower. Due to rainfall events (e.g., July 2015, October 2015, November 2016), isolated *ET* peaks measured by the ECT were reproduced precisely by the estimations. The temporal resolution of the satellite images was key to mimicking the fast *ET* pulses in those events and preventing a loss of information. Accounting for intense, short-term events is important for the total annual budgets and for understanding the system's functioning, and it highlights the value of high temporal resolution satellite data.

The ratio of *ET* to reference *ET* (ET/ET_o) at a daily time step for the period 2013-2017 is presented in Figure 3.7. This index ranges from ~1 when the actual *ET* covers the atmospheric evaporative demand to approximately 0 as the water deficit develops and the evaporation is close to zero. In this location, ET/ET_o abruptly decreased from the end of May or beginning of June, depending on the year, with a slope of ~−1.5% for all years. The ecosystem's "dry peak" (ET/ET_o = 0.11) is found at the end of the summer, after a long season without rain. With the first rainfall, this ratio increased until reaching the annual maxima in around May. The falls and winters were noisy and highly influenced by the rainfall, but ET/ET_o varied at values of around >0.6, which can be considered to be the threshold of vegetation water stress. At the end of 2015, there was a small valley in the ET/ET_o values, representing a short period when the vegetation suffered a mild water stress at an unusual time of year. The later recovery from that situation was slower, with growing but lower values than other years, even if ET/ET_o reached the same maximum values afterwards. The results suggest the potential capability of this index as a monitoring tool for assessing anomalous dry periods and events, which can be used to guide management actions leading to maintaining the ecosystem's stability, both environmentally and economically.

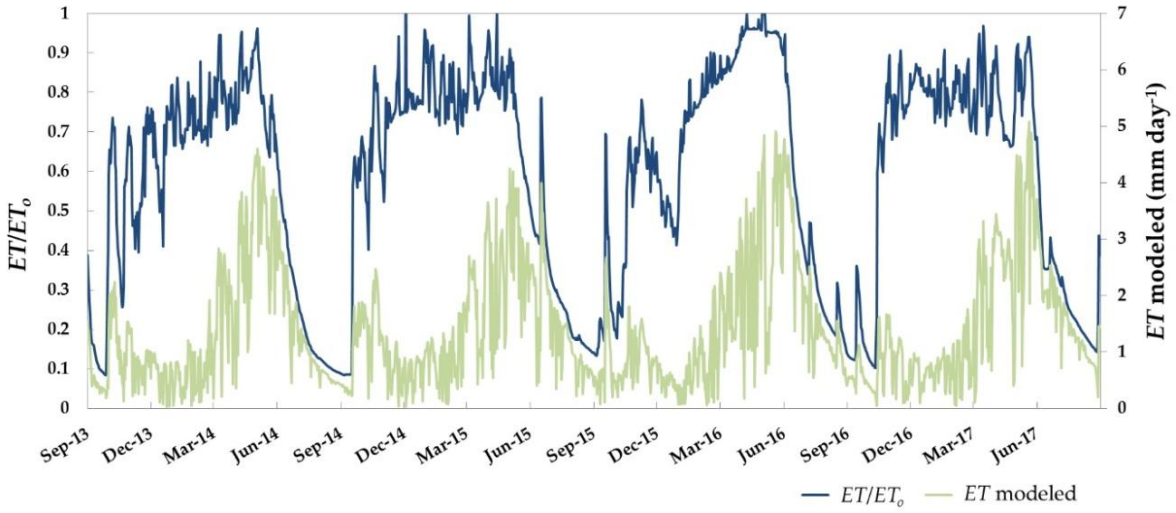

Figure 3.7. Daily evapotranspiration (*ET*) monitoring and water stress (ratio between evapotranspiration and reference evapotranspiration, ET/ET_o) over the *dehesa* ecosystem.

3.3.4. Estimation of Evapotranspiration of Grass in Open Areas

The RMSE of the estimation of the daily evapotranspiration of grass for the hydrological years 2015-2016 and 2016-2017 was equal to 0.47 mm day^{-1} when compared with tower measurements (Figure 3.8). This error is equal to the one obtained over the whole system and consistent with other studies using the *VI-ET$_o$* approach in field crops (González-Dugo et al., 2009; Padilla et al., 2011; Mateos et al., 2013). A bias of -0.03 mm day^{-1} was found, which was lower than that for the whole system and with a greater complexity. A clear deviation is found in a number of points, with *ET* modeled at around ~2 mm day^{-1} but measured at close to zero mm day^{-1}. These points corresponded to a period during the month of November 2016 (Figure 3.9), coinciding with some rainfall events. In this case, the modeled data seemed to be better aligned with the previous and following *ET* rates, and the effect of rainfall water on the instruments could have produced noisy measurements, which were difficult to correct with the automatic data processing.

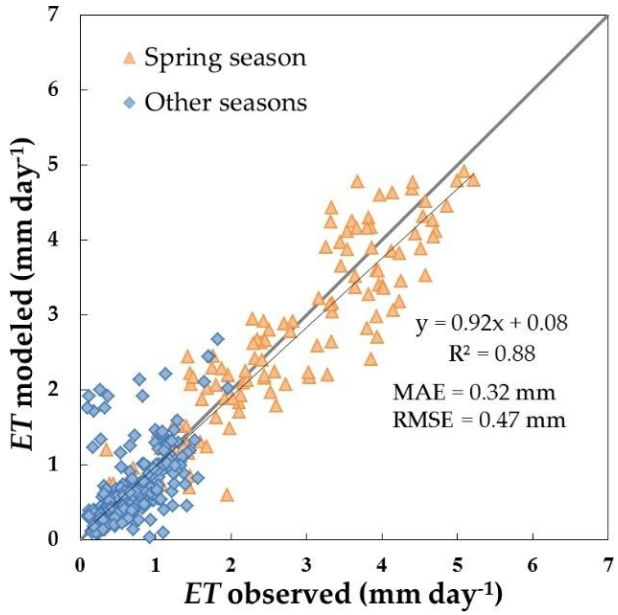

Figure 3.8. Comparison between observed and modeled daily evapotranspiration (*ET*) values over the grass area (mm) for the hydrological years 2015-2016 and 2016-2017. Root Mean Square Error (RMSE) and Mean Absolute Error (MAE) are presented in the figure.

Figure 3.9 shows the daily time step *ET* series for the open grassland estimated for the two hydrological years analyzed (2015-2016 to 2016-2017), together with *ET* measurements at the open grass tower and rainfall data. The different phenology of the grasses in comparison with the combined system can be observed in Figure 3.9, with lower rates shown for the dry season, when the grass is dry and the trees are still transpiring. As for the whole tree-grass system, a bimodal shape was also clear for 2015. However, the peak in the fall was not observed in 2016. *ET* rates reached the maximum values during

spring (~5 mm day^{-1}, similar to the maxima for the whole ecosystem), sharply decreasing with the drying of the grass, with both maximum values and the *ET* decreasing process being accurately reproduced by the model, especially in 2017, while in 2016 a slight underestimation can be observed.

Several short-time phenomena measured during this period were also accurately reproduced by the model. In this sense, it is worth mentioning a sharp reduction in the vegetation transpiration in May 2016 as a consequence of an unusually long rainfall event, which was well reproduced by the estimations. It is also possible to observe that the model captured the impact on *ET* of small isolated rain events, which increased the evaporation rates during the summer of 2016 when the grass fractional cover was close to zero. The identification of the starting dates of grass greening and drying, and the date when the grass layer reached *ET* maximum rates, which can be derived from the *ET* series, are key points for management purposes that may help to decide on the livestock grazing period in each field without compromising the conservation of the ecosystem. As mentioned for the system, the importance of the temporal resolution of the remote sensors in the monitoring of this vegetation layer is noted here, where the drying process usually occurs in a few days as a function of the fast depletion of soil water content and increasing evaporative demand. Information on the system's functioning could be lost with a lower frequency of available images, which at this time of the year can also be affected by cloudiness. The temporal resolution of Sentinel-2 was found to be well suited for this application.

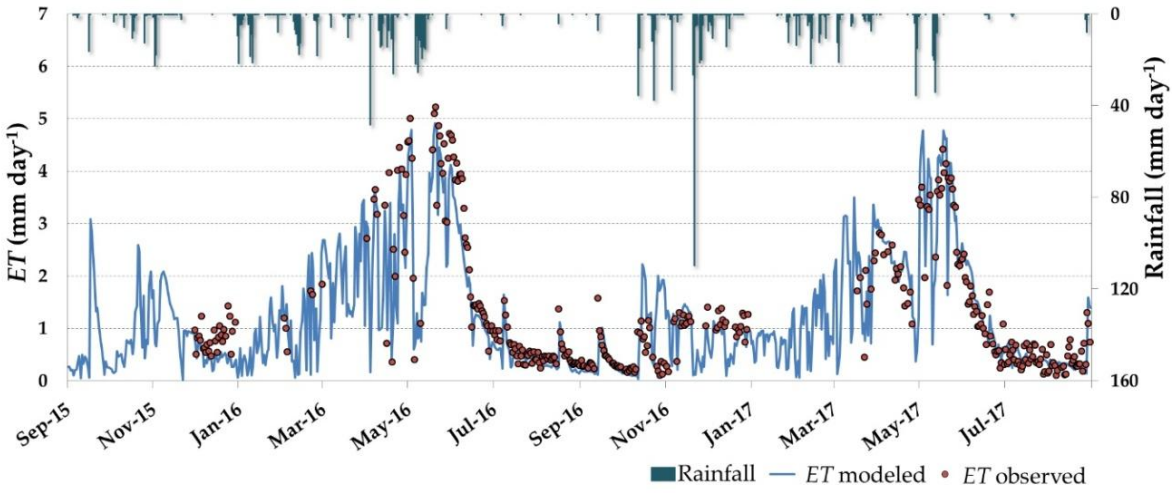

Figure 3.9. Daily evapotranspiration (*ET*) monitoring over grassland, considering the basal crop coefficient for full cover vegetation, $K_{cb\ full}$ =1.1, and the depletion fraction, p = 0.5. Dark green bars illustrate rainfall events.

ET basal rates (0.3-0.4) were maintained during the dry season, where no rainfall was observed and the grass was mostly dry. This could be explained by the presence of morning

dew and humidity condensing in the dry grass pockets and later evaporating, with a small percentage being due to the metabolism of heterotrophs and dead grass becoming converted into organic matter by microorganisms (Xu et al., 2004; Fischer and Blazka, 2015). In addition, a scattering of photosynthetically active plants were still found throughout the summer. Small *gramineae* individuals even survived in August, as they were protected by dry grass cover, but the most abundant species was *Senecio jacobaea* L., a tap-rooted *compositae* that explores deeper soil profiles.

The comparison of the estimated stress coefficient K_s and the soil water content is presented in Figure 3.10. It can be seen that the K_s curve is, in general, consistent with the evolution of the water content. When the soil moisture reached a threshold equal to field capacity, the K_s took and maintained the maximum value. Values of soil water content below 0.15 cm^3 cm^{-3}, in agreement with Gómez-Giráldez et al. (2020), generally marked the starting of K_s reduction.

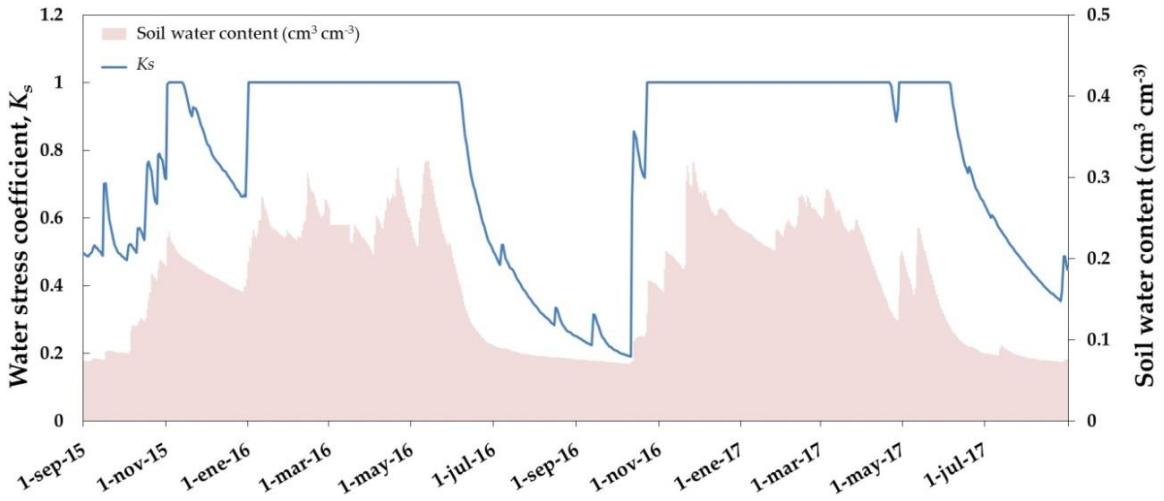

Figure 3.10. Daily evolution of water stress coefficient, K_s, computed by the *VI-ET*$_o$ method and soil water content over the open grassland.

3.4. Conclusions

The *VI-ET*$_o$ model accurately reproduced the temporal dynamics of daily water consumption of a *dehesa* ecosystem measured by an eddy covariance flux tower over four years. The results yielded an RMSE value of 0.47 mm day^{-1} and a low bias (-0.15 mm day^{-1}), similar to the errors presented in the literature for more homogeneous systems using similar approaches. Moreover, a separate application in an open grassland—the predominant component in the occupied area—produced similar results, with an RMSE of 0.47 mm day^{-1} and a bias of -0.03 mm day^{-1} for the two years analyzed. This work has provided effective parameters for applying a remote sensing-based water balance method over an oak-grass savanna, in addition to analyzing each of its components. Reasonable

parameters for one component of the system, the grass, were proposed and tested, while suggested values for the oak trees are yet to be validated. This proposal opens up new insights into the high diversity in water use of different grassland communities in the *dehesa*, the role of oak trees in the hydrology of the systems, and the potential impact of the possible reduction in water availability in the future.

The *ET* of the system presented an annual bimodal behavior, with two clear peaks of different sizes in spring (*ET* of 4.5-5 mm day^{-1}) and fall (*ET* around 2 mm day^{-1}). This pattern was repeated for all the years studied and could be closely linked to the distribution of the annual rainfall. The water stress of the whole system and the grassland was monitored using the ET/ET_o ratio. This index helped to identify periods of water stress, which were confirmed for the grassland by the soil water content measured.

The temporal resolution of the satellite images and the modeling scheme allowed the reproduction of fast and isolated *ET* pulses that are important for computing accurate annual budgets and for understanding the hydrologic behavior of the system. The identification of the starting dates of grass greening and drying, as well as the date when the grass reaches maximum *ET* rates, could be useful for management and conservation purposes, such as making decisions on the livestock grazing period in every field. Thus, the temporal resolution of Sentinel-2 was found to be well suited for the monitoring of these processes.

The effect of the non-photosynthetic grass layer on f_c estimation was evaluated using field measurements, airborne data, and satellite data. A slight deviation in tree f_c estimation (1.5 %) using summer satellite *VIs* was corroborated, although it was not considered large enough to justify the use of more precise spectral mixing models or higher complexity algorithms.

3.5. Acknowledgements

This research was funded by the SensDehesa project (PP.PEI.IDF201601.16), co-funded at 80% by the European Regional Development Fund (ERDF) as part of the Andalusian operational program 2014–2020. Elisabet Carpintero's work was developed under the "Formación de Profesorado Universitario" FPU subprogram (Ministerio de Educación, Cultura y Deporte - Gobierno de España), and Ana Andreu was funded by the European Union's Horizon2020 Research and Innovation program under the Marie Skłodowska-Curie grant agreement No703978. The authors would like to thank Hector Nieto and Pablo Zarco-Tejada for the use of the high-resolution image from 27 August 2015 over Santa Clotilde. We also would like to acknowledge Mario Ramos for his help with installation and maintenance of instruments. Finally, we thank the owner of Santa Clotilde farm for kindly letting us use his facilities.

3.6. References

Aase, J.K., Tanaka, D.L., 1991. Reflectances from Four Wheat Residue Cover Densities as Influenced by Three Soil Backgrounds. Agron. J. 83, 753–757. https://doi.org/10.2134/agronj1991.00021962008300040020x.

Allen, M.F., 2015. How Oaks Respond to Water Limitation, in: Standiford, Richard B.; Purcell, Kathryn L., tech. cords. Proceedings of the seventh California oak symposium: managing oak woodlands in a dynamic world. Gen. Tech. Rep. PSW-GTR-251, Berkeley, CA, pp-13–21.

Allen, R.G., Pereira, L.S., Raes, D., Smith, M., 1998. FAO Irrigation and Drainage Paper No. 56 -Crop Evapotranspiration, Rome, Italy.

Allen, R.G., Pereira, L.S., Smith, M., Raes, D., Wright, J.L., 2005. FAO-56 dual crop coefficient method for estimating evaporation from soil and application extensions. J. Irrig. Drain. Eng. 131, 2–13. https://doi.org/10.1061/(ASCE)0733-9437(2005)131:1(2).

Anderson, M.C., Zolin, C.A., Sentelhas, P.C., Hain, C.R., Semmens, K., Tugrul Yilmaz, M., Gao, F., Otkin, J.A., Tetrault, R., 2016. The Evaporative Stress Index as an indicator of agricultural drought in Brazil: An assessment based on crop yield impacts. Remote Sens. Environ. 174, 82–99. https://doi.org/10.1016/j.rse.2015.11.034.

Andreu, A., Dube, T., Nieto, H., Mudau, A.E., González-Dugo, M.P., Guzinski, R., Hülsmann, S., 2019. Remote sensing of water use and water stress in the African savanna ecosystem at local scale – Development and validation of a monitoring tool. Phys. Chem. Earth 112, 154–164. https://doi.org/10.1016/j.pce.2019.02.004.

Andreu, A., Kustas, W.P., Polo, M.J., Carrara, A., González-Dugo, M.P., 2018a. Modeling surface energy fluxes over a dehesa (oak savanna) ecosystem using a thermal based two-source energy balance model (TSEB) I. Remote Sens. 10, 1–27. https://doi.org/10.3390/rs10040567.

Arlot, S., Celisse, A., 2010. A survey of cross-validation procedures for model selection. Stat. Surv. 4, 40–79. https://doi.org/10.1214/09-SS054.

Baldocchi, D.D., Xu, L., 2007. What limits evaporation from Mediterranean oak woodlands - The supply of moisture in the soil, physiological control by plants or the demand by the atmosphere? Adv. Water Resour. 30, 2113–2122. https://doi.org/10.1016/j.advwatres.2006.06.013.

Bausch, W.C., 1995. Remote sensing of crop coefficients for improving the irrigation scheduling of corn. Agric. Water Manag. 27, 55–68. https://doi.org/10.1016/0378-3774(95)01125-3.

Birot, Y., Gracia, C., Palahí, M., 2011. Water for Forests and People in the Mediterranean: A Challenging Balance. What Science Can Tell Us; European Forest Institute, Helsinki, Finland.

Browne, M.W., 2000. Cross-Validation Methods. J. Math. Psychol. 44, 108–132. https://doi.org/10.1006/jmps.1999.1279.

Burchard-Levine, V., Nieto, H., Riaño, D., Migliavacca, M., El-Madany, T.S., Perez-Priego, O., Carrara, A., Martín, M.P., 2020. Seasonal adaptation of the thermal-based two-source energy balance model for estimating evapotranspiration in a semiarid tree-grass ecosystem. Remote Sens. 12. https://doi.org/10.3390/rs12060904.

Calera, A., Campos, I., Osann, A., D'Urso, G., Menenti, M., 2017. Remote sensing for crop water management: From ET modelling to services for the end users. Sensors (Switzerland) 17, 1–25. https://doi.org/10.3390/s17051104.

Cammalleri, C., Ciraolo, G., Minacapilli, M., Rallo, G., 2013. Evapotranspiration from an Olive Orchard using Remote Sensing-Based Dual Crop Coefficient Approach. Water Resour. Manag. 27, 4877–4895. https://doi.org/10.1007/s11269-013-0444-7.

Campos, I., Balbontín, C., González-Piqueras, J., González-Dugo, M.P., Neale, C.M.U., Calera, A., 2016. Combining a water balance model with evapotranspiration measurements to estimate total available soil water in irrigated and rainfed vineyards. Agric. Water Manag. 165. https://doi.org/10.1016/j.agwat.2015.11.018.

Campos, P., Huntsinger, L., Oviedo, J., Díaz, M., Starrs, P., Standiford, R., Montero, G., 2013. Mediterranean Oak Woodland Working Landscapes: Dehesas of Spain and Ranchlands of California, Springer: Dordrecht, The Netherlands.

Campos, I., Neale, C.M.U., Calera, A., Balbontín, C., González-Piqueras, J., 2010. Assessing satellite-based basal crop coefficients for irrigated grapes (Vitis vinifera L.). Agric. Water Manag. 98, 45–54. https://doi.org/10.1016/j.agwat.2010.07.011.

Campos, I., Villodre, J., Carrara, A., Calera, A., 2013. Remote sensing-based soil water balance to estimate Mediterranean holm oak savanna (dehesa) evapotranspiration under water stress conditions. J. Hydrol. 494, 1–9. https://doi.org/10.1016/j.jhydrol.2013.04.033.

Canadell, J., Jackson, R.B., Ehleringer, J.R., Mooney, H.A., Sala, O.E., Schulze, E.D., 1996. Maximum rooting depth of vegetation types at the global scale. Oecologia 108, 583–595. https://doi.org/10.1007/BF00329030.

Carpintero, E., Mateos, L., Andreu, A., González-Dugo, M.P., 2020. Effect of the differences in spectral response of Mediterranean tree canopies on the estimation of evapotranspiration using vegetation index-based crop coefficients. Agric. Water Manag. 238, 106201. https://doi.org/10.1016/j.agwat.2020.106201.

Coelho, C.; Ferreira, A.J.D., Laouina, A., Hamza, A., Chaker, M., Naafa, R., Regaya, K., Boulet, A. K., Keizer, J.J., Carvalho, T.M.M., 2004. Changes in Land Use and Land Management Practices Affecting Land Degradation within Forest and Grazing Ecosystems in the Western Mediterranean, in: Schnabel, S., Ferreira, A. (Eds.), Sustainability of Agrosylvopastoral Systems, Dehesas, Montados, Schweizerbart Science Publishers: Stuttgart, Germany, pp. 137–154.

Consoli, S., Vanella, D., 2014. Mapping crop evapotranspiration by integrating vegetation indices into a soil water balance model. Agric. Water Manag. 143, 71–81. https://doi.org/10.1016/j.agwat.2014.06.012.

Cubera, E., Moreno, G., 2007. Effect of single Quercus ilex trees upon spatial and seasonal changes in soil water content in dehesas of central western Spain. Ann. For. Sci. 64, 355–364. https://doi.org/10.1051/forest:2007012.

David, T.S., Henriques, M.O., Kurz-Besson, C., Nunes, J., Valente, F., Vaz, M., Pereira, J.S., Siegwolf, R., Chaves, M.M., Gazarini, L.C., David, J.S., 2007. Water-use strategies in two co-occurring Mediterranean evergreen oaks: Surviving the summer drought. Tree Physiol. 27, 793–803. https://doi.org/10.1093/treephys/27.6.793.

Er-Raki, S., Chehbouni, A., Guemouria, N., Duchemin, B., Ezzahar, J., Hadria, R., 2007. Combining FAO-56 model and ground-based remote sensing to estimate water consumptions of wheat crops in a semi-arid region. Agric. Water Manag. 87, 41–54. https://doi.org/10.1016/j.agwat.2006.02.004.

Fischer, Z., Blažka, P., 2015. Soil Respiration in Drying of an Organic Soil. Open J. Soil Sci. 05, 181–192. https://doi.org/10.4236/ojss.2015.59018.

Gao, F., Masek, J., Schwaller, M., Hall, F., 2006. On the blending of the landsat and MODIS surface reflectance: Predicting daily landsat surface reflectance. IEEE Trans. Geosci. Remote Sens. 44, 2207–2218. https://doi.org/10.1109/TGRS.2006.872081.

García-Ruiz, J.M., López-Moreno, I.I., Vicente-Serrano, S.M., Lasanta-Martínez, T., Beguería, S., 2011. Mediterranean water resources in a global change scenario. Earth-Science Rev. 105, 121–139. https://doi.org/10.1016/j.earscirev.2011.01.006.

Gauquelin, T., Michon, G., Joffre, R., Duponnois, R., Génin, D., Fady, B., Bou Dagher-Kharrat, M., Derridj, A., Slimani, S., Badri, W., Alifriqui, M., Auclair, L., Simenel, R., Aderghal, M., Baudoin, E., Galiana, A., Prin, Y., Sanguin, H., Fernandez, C., Baldy, V., 2016. Mediterranean forests, land use and climate change: a social-ecological perspective. Reg. Environ. Chang. 18, 623–636. https://doi.org/10.1007/s10113-016-0994-3.

Giorgi, F., Lionello, P., 2008. Climate change projections for the Mediterranean region. Glob. Planet. Change 63, 90–104. https://doi.org/10.1016/j.gloplacha.2007.09.005.

Glenn, E.P., Nagler, P.L., Huete, A.R., 2010. Vegetation Index Methods for Estimating Evapotranspiration by Remote Sensing. Surv. Geophys. 31, 531–555. https://doi.org/10.1007/s10712-010-9102-2.

Glenn, E.P., Neale, C.M.U., Hunsaker, D.J., Nagler, P.L., 2011. Vegetation index-based crop coefficients to estimate evapotranspiration by remote sensing in agricultural and natural ecosystems. Hydrol. Process. 25, 4050–4062. https://doi.org/10.1002/hyp.8392.

Gómez-Giráldez, P.J., Pérez-Palazón, M.J., Polo, M.J., González-Dugo, M.P., 2020. Monitoring grass phenology and hydrological dynamics of an oak-grass savanna ecosystem using sentinel-2 and terrestrial photography. Remote Sens. 12. https://doi.org/10.3390/rs12040600.

González-Dugo, M.P., Escuin, S., Cano, F., Cifuentes, V., Padilla, F.L.M., Tirado, J.L., Oyonarte, N., Fernández, P., Mateos, L., 2013. Monitoring evapotranspiration of irrigated crops using crop coefficients derived from time series of satellite images. II. Application on basin scale. Agric. Water Manag. 125, 92–104. https://doi.org/10.1016/j.agwat.2013.03.024.

González-Dugo, M.P., Mateos, L., 2008. Spectral vegetation indices for benchmarking water productivity of irrigated cotton and sugarbeet crops. Agric. Water Manag. 95, 48–58. https://doi.org/10.1016/j.agwat.2007.09.001.

Gonzalez-Dugo, M.P., Neale, C.M.U., Mateos, L., Kustas, W.P., Prueger, J.H., Anderson, M.C., Li, F., 2009. A comparison of operational remote sensing-based models for estimating crop evapotranspiration. Agric. For. Meteorol. 149, 1843–1853. https://doi.org/10.1016/j.agrformet.2009.06.012.

Gonzalez-Piqueras, J., Calera, A., Gilabert, M.A., Cuesta, A., De la Cruz Tercero, F., 2004. Estimation of crop coefficients by means of optimized vegetation indices for corn. Remote Sens. Agric. Ecosyst. Hydrol. V 5232, 110. https://doi.org/10.1117/12.511317.

Hsieh, C.I., Katul, G., Chi, T.W., 2000. An approximate analytical model for footprint estimation of scalar fluxes in thermally stratified atmospheric flows. Adv. Water Resour. 23, 765–772. https://doi.org/10.1016/S0309-1708(99)00042-1.

Huete, A. R., 1988. A soil-adjusted vegetation index (SAVI). Remote Sens. Environ. 25, 295-309.

Hunsaker, D.J., Pinter, P.J., Barnes, E.M., Kimball, B.A., 2003. Estimating cotton evapotranspiration crop coefficients with a multispectral vegetation index. Irrig. Sci. 22, 95–104. https://doi.org/10.1007/s00271-003-0074-6.

Hunsaker, D.J., Pinter, P.J., Kimball, B.A., 2005. Wheat basal crop coefficients determined by normalized difference vegetation index. Irrig. Sci. 24, 1–14. https://doi.org/10.1007/s00271-005-0001-0.

Jacob, D., Petersen, J., Eggert, B., Alias, A., Christensen, O.B., Bouwer, L.M., Braun, A., Colette, A., Déqué, M., Georgievski, G., Georgopoulou, E., Gobiet, A., Menut, L., Nikulin, G., Haensler, A., Hempelmann, N., Jones, C., Keuler, K., Kovats, S., Kröner, N., Kotlarski, S., Kriegsmann, A., Martin, E., van Meijgaard, E., Moseley, C., Pfeifer, S., Preuschmann, S., Radermacher, C., Radtke, K., Rechid, D., Rounsevell, M., Samuelsson, P., Somot, S., Soussana, J.F., Teichmann, C., Valentini, R., Vautard, R., Weber, B., Yiou, P., 2014. EURO-CORDEX: New high-resolution climate change projections for European impact research. Reg. Environ. Chang. 14, 563–578. https://doi.org/10.1007/s10113-013-0499-2.

Jayanthi, H., Neale, C.M.U., 2001. Seasonal evapotranspiration estimation using canopy reflectance: A case study involving pink beans. IAHS-AISH Publ. 2000, 302–305.

Jayanthi, H., Neale, C.M.U., Wright, J.L., 2007. Development and validation of canopy reflectance-based crop coefficient for potato. Agric. Water Manag. 88, 235–246. https://doi.org/10.1016/j.agwat.2006.10.020.

Joffre, R., Rambal, S., 1993. How tree cover influences the water balance of Mediterranean rangelands. Ecology 74, 570–582. https://doi.org/10.2307/1939317.

Lee, G., Kim, W., Oh, H., Youn, B.D., Kim, N.H., 2019. Review of statistical model calibration and validation—from the perspective of uncertainty structures. Struct. Multidiscip. Optim. 60, 1619–1644. https://doi.org/10.1007/s00158-019-02270-2

Mateos, L., González-Dugo, M.P., Testi, L., Villalobos, F.J., 2013. Monitoring evapotranspiration of irrigated crops using crop coefficients derived from time series of satellite images. I. Method validation. Agric. Water Manag. 125, 81-91. https://doi.org/10.1016/j.agwat.2012.11.005.

Mauder, M., Genzel, S., Fu, J., Kiese, R., Soltani, M., Steinbrecher, R., Zeeman, M., Banerjee, T., De Roo, F., Kunstmann, H., 2018. Evaluation of energy balance closure adjustment methods by independent evapotranspiration estimates from lysimeters and hydrological simulations. Hydrol. Process. 32, 39–50. https://doi.org/10.1002/hyp.11397.

Mbah, C.N., 2012. Determining the field capacity, wilting point and available water capacity of some Southeast Nigerian soils using soil saturation from capillary rise. Niger. J. Biotechnol. 24, 41–47.

Melendo, M., 1998. Cartografía y ordenación vegetal de Sierra Morena: Parque Natural de las sierras de Cardeña y Montoro, Universidad de Jaén, Jaén.

Milano, M., Ruelland, D., Fernandez, S., Dezetter, A., Ardoin-Bardin, S., Fabre, J., Thivet, G., Servat, E., 2011. Assessing the impacts of global changes on the water resources of the Mediterranean basin. IAHS-AISH Publ. 347, 165–172.

Milano, M., Ruelland, D., Fernandez, S., Dezetter, A., Fabre, J., Servat, E., Fritsch, J.M., Ardoin-Bardin, S., Thivet, G., 2013. Current state of Mediterranean water resources and future trends under climatic and anthropogenic changes. Hydrol. Sci. J. 58, 498–518. https://doi.org/10.1080/02626667.2013.774458.

Mishra, A.K., Singh, V.P., 2010. A review of drought concepts. J. Hydrol. 391, 202–216. https://doi.org/10.1016/j.jhydrol.2010.07.012.

Moreno, G., Cáceres, Y., 2016. System report: Iberian Dehesas, Spain. AGFORWARD. Agroforestry for Europe, Plasencia.

Moreno, G., Obrador, J.J., Cubera, E., Dupraz, C., 2005. Fine root distribution in Dehesas of Central-Western Spain. Plant Soil 277, 153–162. https://doi.org/10.1007/s11104-005-6805-0.

Moreno G., Pulido F.J., 2009. The Functioning, Management and Persistence of Dehesas, in: Rigueiro-Rodróguez A., McAdam J., Mosquera-Losada M.R. (Eds.), Agroforestry in Europe. Advances in Agroforestry, vol 6, Springer, Dordrecht.

Mueller-Wilm, U., Devignot, O., Pessiot, L., 2017. Sen2Core Configuration and User Manual. Ref. S2-PDGS-MPC-L2ASUM-V2.3 eesa Sentinel 2. Version: 1 November 2017. Available online: https://step.esa.int/thirdparties/sen2cor/2.4.0/Sen2Cor_240_Documenation_PDF/S2-PDGS-MPC-L2A-SUM-V2.4.0.pdf (accessed on 14 October 2019).

Nagler, P.L., Daughtry, C.S.T., Goward, S.N., 2000. Plant litter and soil reflectance. Remote Sens. Environ. 71, 207–215. https://doi.org/10.1016/S0034-4257(99)00082-6.

Nagler, P.L., Inoue, Y., Glenn, E.P., Russ, A.L., Daughtry, C.S.T., 2003. Cellulose absorption index (CAI) to quantify mixed soil-plant litter scenes. Remote Sens. Environ. 87, 310–325. https://doi.org/10.1016/j.rse.2003.06.001.

Odi-Lara, M., Campos, I., Neale, C.M.U., Ortega-Farías, S., Poblete-Echeverría, C., Balbontín, C., Calera, A., 2016. Estimating evapotranspiration of an apple orchard using a remote sensing-based soil water balance. Remote Sens. 8. https://doi.org/10.3390/rs8030253.

Padilla, F.L.M., González-Dugo, M.P., Gavilán, P., Domínguez, J., 2011. Integration of vegetation indices into a water balance model to estimate evapotranspiration of wheat and corn. Hydrol. Earth Syst. Sci. 15, 1213–1225. https://doi.org/10.5194/hess-15-1213-2011.

Pierret, A., Maeght, J.L., Clément, C., Montoroi, J.P., Hartmann, C., Gonkhamdee, S., 2016. Understanding deep roots and their functions in ecosystems: An advocacy for more unconventional research. Ann. Bot. 118, 621–635. https://doi.org/10.1093/aob/mcw130.

Plieninger, T., Rolo, V., Moreno, G., 2010. Large-scale patterns of Quercus ilex, Quercus suber, and Quercus pyrenaica regeneration in central-western Spain. Ecosystems 13, 644–660. https://doi.org/10.1007/s10021-010-9345-2.

Pôças, I., Calera, A., Campos, I., Cunha, M., 2020. Remote sensing for estimating and mapping single and basal crop coefficientes: A review on spectral vegetation indices approaches. Agric. Water Manag. 233, 106081. https://doi.org/10.1016/j.agwat.2020.106081.

Polade, S.D., Pierce, D.W., Cayan, D.R., Gershunov, A., Dettinger, M.D., 2014. The key role of dry days in changing regional climate and precipitation regimes. Sci. Rep. 4. https://doi.org/10.1038/srep04364.

Pulido-Fernández, M., Schnabel, S., Lavado-Contador, J.F., Miralles Mellado, I., Ortega Pérez, R., 2013. Soil organic matter of Iberian open woodland rangelands as influenced by vegetation cover and land management. Catena 109, 13–24. https://doi.org/10.1016/j.catena.2013.05.002.

Rivas Martínez, S., 1988. Bioclimatología, biogeografía y series de vegetación de Andalucía Occidental. Lagascalia 15, 91–120.

Roberts, D.A., Smith, M.O., Adams, J.B., 1993. Green vegetation, nonphotosynthetic vegetation, and soils in AVIRIS data. Remote Sens. Environ. 44, 255–269. https://doi.org/10.1016/0034-4257(93)90020-X.

Rodríguez, J., Sotelo, A., Monge, G., De la Rosa, D., 2008. Sistema de inferencia espacial de propiedades de los suelos de Andalucía, Consejería de Agricultura y Pesca, Sevilla.

Rolo, V., López-Díaz, M.L., Moreno, G., 2012. Shrubs affect soil nutrients availability with contrasting consequences for pasture understory and tree overstory production and nutrient status in Mediterranean grazed open woodlands. Nutr. Cycl. Agroecosystems 93, 89–102. https://doi.org/10.1007/s10705-012-9502-4.

Román-Sánchez, A., Vanwalleghem, T., Peña, A., Laguna, A., Giráldez, J. V., 2018. Controls on soil carbon

storage from topography and vegetation in a rocky, semi-arid landscapes. Geoderma 311, 159–166. https://doi.org/10.1016/j.geoderma.2016.10.013.

Schleussner, C.F., Lissner, T.K., Fischer, E.M., Wohland, J., Perrette, M., Golly, A., Rogelj, J., Childers, K., Schewe, J., Frieler, K., Mengel, M., Hare, W., Schaeffer, M., 2016. Differential climate impacts for policy-relevant limits to global warming: The case of 1.5 °c and 2 °c. Earth Syst. Dyn. 7, 327–351. https://doi.org/10.5194/esd-7-327-2016.

Schoups, G., Van De Giesen, N.C., Savenije, H.H.G., 2008. Model complexity control for hydrologic prediction. Water Resour. Res. 44, 1–14. https://doi.org/10.1029/2008WR006836.

Seneviratne, S.I., Wartenburger, R., Guillod, B.P., Hirsch, A.L., Vogel, M.M., Brovkin, V., Van Vuuren, D.P., Schaller, N., Boysen, L., Calvin, K. V., Doelman, J., Greve, P., Havlik, P., Humpenöder, F., Krisztin, T., Mitchell, D., Popp, A., Riahi, K., Rogelj, J., Schleussner, C.F., Sillmann, J., Stehfest, E., 2018. Climate extremes, land-climate feedbacks and land-use forcing at 1.5°C. Philos. Trans. R. Soc. A Math. Phys. Eng. Sci. 376. https://doi.org/10.1098/rsta.2016.0450.

Stegman, E.C., Musick, J.T., Stewart, J.I., 1980. Irrigation water management, in: Design and Operation of Farm Irrigation Systems. American Society of Agricultural Engineers., Michigan, pp. 763–768.

Tegegne, G., Park, D.K., Kim, Y.O., 2017. Comparison of hydrological models for the assessment of water resources in a data-scarce region, the Upper Blue Nile River Basin. J. Hydrol. Reg. Stud. 14, 49–66. https://doi.org/10.1016/j.ejrh.2017.10.002.

Webb, E.K., Pearman, G.I., Leuning, R., 1980. Correction of flux measurements for density effects due to heat and water vapour transfer. Q. J. R. Meteorol. Soc. 106, 85–100. https://doi.org/10.1002/qj.49710644707.

Wright, J.L., 1982. New Evapotranspiration Crop Coefficients. J. Irrig. Drain. Div. - ASCE 108, 57–74.

Xu, L., Baldocchi, D.D., Tang, J., 2004. How soil moisture, rain pulses, and growth alter the response of ecosystem respiration to temperature. Global Biogeochem. Cycles 18, n/a-n/a. https://doi.org/10.1029/2004GB002281

Xu, D., Guo, X., Li, Z., Yang, X., Yin, H., 2014. Measuring the dead component of mixed grassland with Landsat imagery. Remote Sens. Environ. 142, 33–43. https://doi.org/10.1016/j.rse.2013.11.017.

Chapter 4

Combination of lumped hydrological and remote-sensing models to evaluate water resources in a semi-arid high altitude ungauged watershed of Sierra Nevada (Southern Spain)

Jódar, J., **Carpintero, E.,** Martos-Rosillo, S., Ruiz-Constán, A., Marín-Lechado, C., Cabrera-Arrabal, J.A., Navarrete-Mazariegos, E., González-Ramón, A., Lambán, L.J., Herrera, C., González-Dugo, M.P., 2018. Combination of lumped hydrological and remote-sensing models to evaluate water resources in a semi-arid high altitude ungauged watershed of Sierra Nevada (Southern Spain). Sci. Total Environ. 625, 285–300. https://doi.org/10.1016/j.scitotenv.2017.12.300

Abstract

Assessing water resources in high mountain semi-arid zones is essential to be able to manage and plan the use of these resources downstream where they are used. However, it is not easy to manage an unknown resource, a situation that is common in the vast majority of high mountain hydrological basins. In the present work, the discharge flow in an ungauged basin is estimated using the hydrological parameters of an HBV (Hydrologiska Byråns Vattenbalansavdelning) model calibrated in a "neighboring gauged basin". The results of the hydrological simulation obtained in terms of average annual discharge are validated using the VI-ET_o model. This model relates a simple hydrological balance to the discharge of the basin with the evaporation of the vegetal cover of the soil, and this to the SAVI index, which is obtained remotely by means of satellite images. The results of the modeling for both basins underscore the role of the underground discharge in the total discharge of the hydrological system. This is the result of the deglaciation process suffered by the high mountain areas of the Mediterranean arc. This process increases the infiltration capacity of the terrain, the recharge and therefore the discharge of the aquifers that make up the glacial and periglacial sediments that remain exposed on the surface as witnesses of what was the last glaciation.

4.1. Introduction

In high-altitude hydrological systems located in semi-arid zones, practically all the necessary water resources available in the low zones are generated to satisfy the demand of both the biological activity of the associated ecosystems (Taylor et al., 2012) and of the users who depend on this resource (Vivirolí et al., 2007; García-Vera, 2013; López-Moreno et al., 2014). At the head of these basins, global warming is directly affecting the accumulation and melting of snow, modifying the response of these hydrological systems, at least in the discharge flows and their seasonality, causing the main peak of the hydrograph to be brought forward (Andermann et al., 2012; Hood and Hayashi, 2015; Cowie et al., 2017). In the Mediterranean region, in addition to the rise in temperature, the occurrence of prolonged dry periods and greater evaporation is also forecasted, which could increase the frequency and intensity of droughts in the areas of southern Europe (Mishra and Singh, 2010), where conditions of hydrological aridity already prevail (Wanders et al., 2010; Van Lanen et al., 2013).

In the Alpine basins of the Mediterranean arc, global change is producing a rapid retreat of the few remaining glaciers as a consequence of the 0 °C thermocline elevation (Nogués-Bravo et al., 2008; González Trueba et al., 2008; Grunewald and Scheithauer, 2010). This glacial retreat generates large permeability changes in the upper part of the basins by exposing high permeability glacial and periglacial materials that facilitate both, rainfall to infiltrate and groundwater to flow (Fedeli and Castillo, 1997; Millares et al.,

2009). Additionally, the thermocline elevation has generated a reduction in the permafrost affected area and changes in the basin land use and management (Benito et al., 2011; García-Ruiz et al., 2015). The global change is modifying the role played by the different processes that control the behavior of the hydrological systems located in high mountain zones. This has to be taken into account when establishing or even updating the conceptual model of such hydrological systems.

Despite their strategic importance, the Alpine basins of the Mediterranean arc are little studied (Bocchiola et al., 2010). Furthermore, characterizing behavior of such basins is not easy, given the difficulty of access, the adverse climatic conditions of great part of the year and the instrumentation necessary to characterize the operation of the system, especially in relation to groundwater (Langston et al., 2013; Molina et al., 2014; Hood and Hayashi, 2015). As a result, the majority of the high mountain hydrological basins are completely ungauged.

Making reliable Predictions in "Ungauged Basins" (PUB, Sivapalan, 2003) has long been recognized by hydrologic sciences (Sivapalan et al., 2003; Kundzewicz, 2007). A better understanding of the hydrological processes involved and the effect on them of the different landscapes and landcover changes (Pisano et al., 2017) are necessary to characterize the response of hydrological systems. These geographical features can be considered one of the most rapid drivers of global change (Slaymaker et al., 2009). Additionally, it is also necessary to obtain coherent and concurrent data at different spatio-temporal scales to correctly define the hydrological systems dynamics (Blöschl et al., 2007; Wagener et al., 2007; Hrachowitz et al., 2013). The problem may be even more complex if it is not clear how different hydrological processes (e.g. evapotranspiration, surface runoff generation, percolation and underground discharge) interact with each other to end up generating total discharge from the basin.

The use of hydrological models reduces the problem of PUB to the appropriate selection of the effective parameters corresponding to the "ungauged basin". Despite the hydrological aphorism that each basin is different ('uniqueness in place', Beven, 2000), the most common practice is to apply the concept of regionalization (Buytaert and Beven, 2009), through which the model parameters that have been calibrated in the gauged basin are migrated to the ungauged one. In the literature, there are several regionalization techniques whose functional complexity varies from the nearest neighbor (Merz and Blöschl, 2004) to the use of complex functional dependencies and statistical techniques (see Vandewiele and Elias, 1995; Sefton and Howarth, 1998; Wagener et al., 2004; Hundecha and Bárdossy, 2004; Wagener and Wheater, 2006; Skøien and Blöschl, 2006).

To facilitate the process of regionalization, several authors suggest the use of "parsimonious conceptual rainfall-run-off models" (see Seibert, 1999; Bergström et al., 2002; Merz and Blöschl, 2004; Parajka and Blöschl, 2008; Skaugen et al., 2015). These models express, through more or less simple functions, the different physical processes that

control the operation of the hydrological processes governing the functioning of the basin. From the perspective of parameterization, these models are the most efficient (parsimonious), and avoid the problems generated by the over parameterization of the model in the identification of parameters (Kirchner, 2006; McDonnell et al., 2007; Wagener et al., 2007).

Nowadays, due to the availability of new sensors on board the satellites it is possible to estimate the discharge of some rivers remotely (Smith et al., 1996; Bjerklie et al., 2003; Alsdorf et al., 2007; Temimi et al., 2007; Smith and Pavelsky, 2008; Neal et al., 2009; Birkinshaw et al., 2010; Tarpanelli et al., 2013a, 2013b; Tarpanelli et al., 2015), something that is fundamental to be able to validate the discharge flows calculated in the "ungauged basins". Although the different techniques for estimating the flow through the rivers have great potential, their application in "ungauged basins" is still limited, since the flow estimate finally depends on detail information of the basin that cannot be obtained completely remotely (e.g. flow rate through different river control sections, river bed depth, river rating curve, etc.). However, remote observation of hydrological variables, such as the extension of flood zones (Di Baldassarre et al., 2009; Domeneghetti et al., 2014), the soil uses and the associated evapotranspiration (Anderson et al., 2012), or even the depth of the water table (Urqueta et al., 2018) have recently been postulated as an additional source of information to help to establish the conceptual model of hydrological systems, and to improve the calibration of corresponding numerical models.

This work evaluates the discharge of the Mecina River basin, an ungauged basin located in a high mountain area in the SE Iberian Peninsula, from the response observed in the neighboring Bérchules River basin. From the perspective of the global change impact on the hydrological systems located in high mountain zones, both basins are examples of what could happen in other higher latitude basins. The Bérchules and Mecina basins are located in Sierra Nevada, a mountain area where the latest glaciers disappeared by the middle of the last century (Hughes and Woodward, 2009), almost the total permafrost has disappeared (Oliva and Gómez-Ortiz, 2012), glacial and periglacial quaternary sediments favor the infiltration capacity of practically all the precipitations, increasing the underground component (Jódar et al., 2017), and where the vegetation has adapted to arid conditions that bear no relation with the prevailing climate conditions in high mountain basins located at high latitudes in the Northern Hemisphere, which have been the object of a deeper research (Theurillat and Guisan, 2001; Kullman, 2002; Benito et al., 2011).

In this work, a lumped hydrological HBV model (Bergström, 1976, 1992, 1995) has been calibrated to simulate the observed response in the discharge flow of the Bérchules basin. This conceptual rainfall-runoff model has not only been thoroughlly used in hydrological characterization studies (Singh and Woolhiser, 2002; Bergström, 2006, Seibert and McDonnell, 2013 and references therein), but also in numerous regionalization studies (Seibert, 1999; Merz and Blöschl, 2004; Parajka et al., 2005; Götzinger and Bárdossy,

2007; Samuel et al., 2011); however, its implementation has been limited in high mountain basins with semi-arid conditions. With the parameters of the calibrated model of the Bérchules basin, the hydrological response is simulated in the ungauged basin of the Mecina River. These results are validated independently using a model (hereinafter called VI-ETo) that integrates the data from the Soil Adjusted Vegetation Index (Huete, 1988), obtained from the Landsat-8 satellite images (Roy et al., 2014). Besides the validation of the results, the combination of the HBV and VI-ET_o models allows improving the knowledge of the variability of the water resources in the basin, not only temporally but also spatially, given the aggregated and distributed nature of the HBV and VI-ET_o models, respectively. The applied methodology may be used in any ungauged basin, opening the possibility of remotely estimating the basin discharge flows by only using satellite images, which is essential for the management and planning of the available water resources in high mountains watersheds.

4.2. Study area

The study area is located at the southern slope of Sierra Nevada, a mountain range in southern Spain (Figure 4.1), one of the higher massifs in Europe. More than 30 peaks in the range overtake three thousand meters of altitude, one of them (Mulhacén, 3482 m a.s.l.) being the highest in the Iberian Peninsula. The recognized ecological value of the Sierra Nevada endemic ecosystems, together with its landscapes and cultural heritage, has favored its protection through different ecological figures, such as Biosphere Reserve (1986) and National Park (1999).

The regional structure of Sierra Nevada is an E-W antiform (90 km long and 40 km wide) that mainly deforms metamorphic rocks at its core. The hydrographic network is composed of numerous gullies, preferentially striking in the N-S direction. Gullies from the southern slope of the cordillera discharge water into the Mediterranean Sea, while those of the northern slope drain into the Guadalquivir River and, consequently, into the Atlantic Ocean. These water resources constitute the main water supply for agricultural and human consumption of the settlements located downstream.

The study zone is composed by the two adjacent watersheds of Bérchules and Mecina, located on the southern slopes of Sierra Nevada, the former to the west and the latter to the east, with the intervening NS water divide. The Bérchules basin discharges in the Guadalfeo River, whereas the Mecina basin tributes to the Adra River. Both watersheds present similar characteristics in size, shape, orientation, vegetation, soil and geological bedrock. The Bérchules basin covers an area of 68 km^2. Within about 17 km, altitude rises from 980 m a.s.l. at the outlet to about 2910 m at the highest point. Figure 4.2 shows a mean altitude for this basin close to 1950 m a.s.l., being the mean land surface slope of 11%. The main drainage network of the Bérchules basin is constituted by two rivers: (1) the

Bérchules River, which runs along the whole eastern side of the basin, and (2) the Chico River, which runs along 11 km through the western side of the basin up to lead into the Bérchules River. The Mecina basin is slightly smaller than the Bérchules one. The associated length and area are 15 km and 55 km^2, respectively. In the Mecina basin the elevation ranges between 1042 and 2618 m a.s.l., being 1710 m a.s.l the mean elevation and presenting a mean slope of 9%. In this basin the most important river is the Mecina River, which is 15 km long.

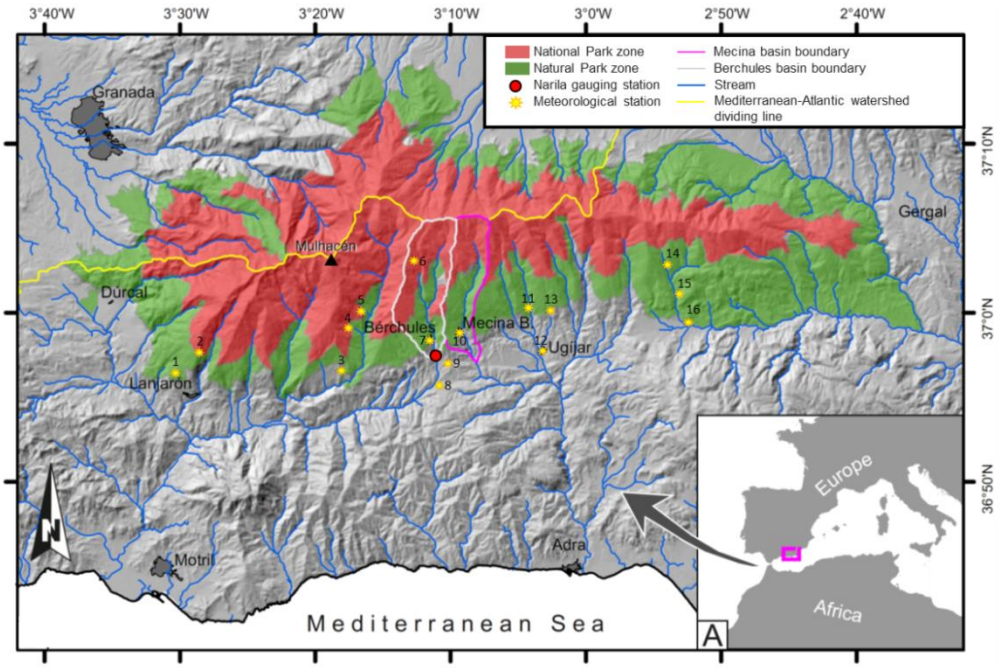

Figure 4.1. Location map of the study area. The red and green areas correspond to the National and Natural Park zones, respectively. The boundary of the Bérchules and the Mecina watersheds are indicated by the grey and the pink lines, respectively. The red point indicates the position of the Narila gauging station, at the outlet of the Bérchules basin. The meteorological stations are indicated with the yellow sun symbol. Numbers of the meteorological stations corresponded to those in Table 4.1. (For interpretation of the references to color in this figure legend, the reader is referred to the web version of this article).

The Bérchules and the Mecina watersheds are located over metamorphic rocks belonging to the Nevado Filábrade Complex (Egeler, 1964) that crop out in the core of the Sierra Nevada fold. The metamorphic materials are mainly constituted by mica-schists with alternating levels of quartzite with a total thickness greater than 1000 m. The schists show a penetrative foliation with a general dipping towards the N-NE that conditions the geometry of the slopes of both watersheds. The eastern slopes are gently, while the western ones are steeper. This fact highly conditions the irrigation network location and distribution (González-Ramón et al., 2015). Other factors that play an essential role in the hydrological and hydrogeological behavior of these watersheds are a well-developed alteration zone in

the upper part of the metamorphic rocks, the existence of periglacial sediments in areas located at elevations above 2000 m and the reduced slope of the upper parts of the hillsides.

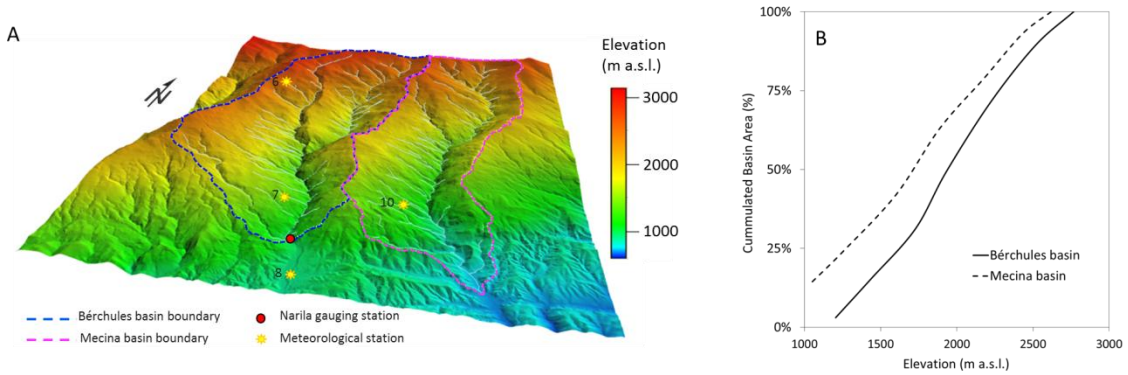

Figure 4.2. (A) Elevation map of the study area. The blue and pink dashed lines indicate the boundary of the Bérchules and the Mecina basins, respectively. The red point shows the position of the Narila gauging station. The yellow sun symbols indicate meteorological stations (numbers corresponding to those in Table 4.1). (B) Relationship between the cumulative basin area and elevation for the Bérchules and the Mecina basins. (For interpretation of the references to color in this figure legend, the reader is referred to the web version of this article).

The northern boundary of the study area is located along the main crest of Sierra Nevada, very close to the Mulhacén Peak (Figure 4.1). According to the Köppen–Geiger climate classification (Peel et al., 2007), it has a cold climate with a dry season, mild and cool summers, and significant altitudinal variations (AEMET/IM, 2011). Nevertheless, in the lower part of both watersheds, the climate is temperate Mediterranean. The presence and persistence of snow is restricted to elevations higher than 2400 m a.s.l. and to the months comprised between November and May. Precipitation is associated with wet winds coming from both, the Atlantic Ocean and the Mediterranean sea, in autumn, winter and, at a lower degree, during spring. At the Bérchules meteorological station (Table 4.1), located at 1319 m a.s.l., the mean annual temperature (T) is 13.3 °C, and the average precipitation (P) and potential evapotranspiration (PET) are 677 and 1012 mm/yr, respectively. In the case of the Mecina Bombarón meteorological station, with an elevation of 1200 m a.s.l., the mean annual T is 14.6 °C and the average P and PET are 593 and 1005 mm/yr, respectively. Figure 4.3 shows the monthly variation of P, T and PET for both meteorological stations.

The large variation in elevation between the highest and lowest parts of the study zone makes it necessary to account for vertical gradients of P and T. These gradients are obtained by analyzing the available precipitation and temperature time series coming from meteorological stations located at neighboring places, within the watershed (Table 4.1). The

vertical precipitation and temperature gradients are 20 mm/100 m and -0.56 °C/100 m, respectively.

Table 4.1. Meteorological stations used to complete the precipitation and temperature time series of the Bérchules and Mecina-Bombarón for the period 1970-2013, and also to estimate the vertical gradients of P and T for the study zone.

Code	Name	Latitude	Longitude	Elevation (m a.s.l.)	Precipitation (mm/yr)	Temperature (°C)
1	Posturas	36.94°	-3.50°	1050	493	14.2
2	Arquilla	36.95°	-3.48°	1652	570	11.6
3	Portugos	36.94°	-3.29°	1120	493	-
4	Busquistar-C. La Calahorra	36.99°	-3.28°	1400	660	-
5	Trévelez	37.00°	-3.27°	1476	694	-
6	Tajos de Breca	37.05°	-3.21°	2470	883	6
7	Bérchules	36.98°	-3.19°	1319	677	13.3
8	Cádiar	36.93°	-3.18°	950	587	-
9	Cadiar-C.P.G.	36.95°	-3.18°	940	557	15.3
10	MecinaBombarón	36.98°	-3.16°	1200	593	14.6
11	Velor-Nechite	37.00°	-3.07°	975	489	16.3
12	Ugíjar	36.97°	-3.05°	559	395	-
13	Mairena	37.00°	-3.05°	1080	391	16.2
14	Laujar-Cerecillo	37.05°	-2.91°	1800	661	10.6
15	Laujar-Monterrey	37.03°	-2.90°	1280	600	13.2
16	Laujar	37.00°	-2.89°	921	510	14.9

In the upper part of the Bérchules basin, the snow remains for almost half of the year. During the spring, water from the snow-melt flows through the Bérchules River, providing a resource for watering that the present dams partially divert into the existing network of irrigation channels. As a result, the river flowrate regime is slightly modified towards near-natural conditions (Stahl et al., 2010). The seasonal river hydrograph shows a pluvio-nival pattern, with maxima flow rates between January and May, and minima during August and September. Figure 4.3A shows the mean monthly basin discharge (green dashed line), along with the 20 and 80% percentiles (light green shadowed area) for the Bérchules basin obtained from the daily flowrates measured in the Narila gauging station.

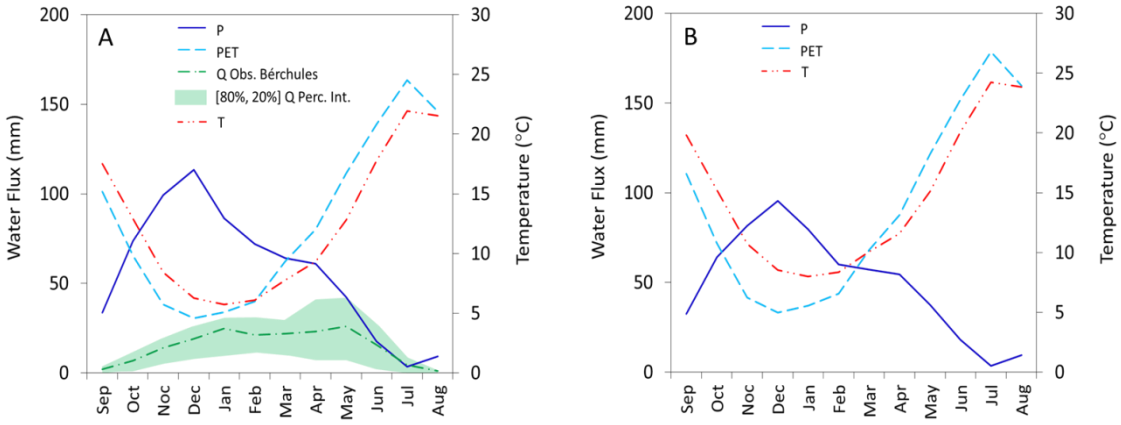

Figure 4.3. (A) Mean monthly precipitation, potential evapotranspiration, averaged runoff, 20 to 80% runoff percentile interval, and temperature for the Bérchules watershed. (B) Mean monthly precipitation, potential evapotranspiration and temperature for the Mecina watershed.

In relation to land cover uses, the study area is mainly characterized by natural vegetation of grassland, scrubs, conifers and oaks, followed by irrigated horticultural crops and rainfed fruit trees. Table 4.2 shows the spatial coverage corresponding to the main vegetation covers in both watersheds.

Table 4.2. Values of K_{cb}, and p used in this work for both deriving K_{cb} and computing the soil water balance.

Vegetation class	$K_{cb_{max}}$ [a] (-)	p [b] (-)
Grassland	0.70	0.60
Grassland with trees	0.70	0.60
Scrub	0.80	0.65
Scrub with trees	0.80	0.65
Conifers	0.95	0.70
Oaks	0.8	0.65
Conifers+oaks	0.80	0.70
Riparian vegetation	0.95	0.70
Permanent rainfed crops	0.65	0.60
Irrigated crops (tomato and bean)	1.12	0.42

[a] Maximum basal canopy coefficient.
[b] Depletion fraction.

4.3. Methods and materials

4.3.1. The HBV model

The HBV model (Bergström, 1976) is a conceptual rainfall-runoff model for catchment hydrology modeling. The basis of this model is the general water balance which is described as

$$P - E - Q = \frac{d}{dt}(SP + SM + UZ + LZ) \tag{4.1}$$

where P [LT^{-1}] is precipitation including rainfall and snowfall, E [LT^{-1}] is evapotranspiration, Q [LT^{-1}] is runoff, SP [L] is snowpack water equivalent volume storage, SM [L] is soil moisture storage, UZ [L] and LZ [L] are water storage in the upper and lower groundwater zone, respectively.

The HBV model provides daily basin discharge by subjecting daily precipitation to four subsequent conceptual modules: a snow routine, a soil moisture routine, a response routine, and a routing routine (Figure 4.4). Precipitation is simulated as rain or snow depending whether the temperature is above or below a threshold temperature. The snow accumulation and melting is computed according to a degree-day method by the snow routine. The combination of precipitation and meltwater is divided by the soil routine as soil infiltration recharge and added soil moisture as a potential function of the actual soil moisture (Seibert, 2005). This routine also calculates the actual evapotranspiration as a piecewise linear function of the actual soil moisture (Seibert, 2005). The response routine transforms excess water from the soil moisture routine to runoff. To this end, two stacked linear reservoirs are connected in series by a constant percolation rate (PERC). The upper reservoir generates surface and subsurface runoff (i.e. Q_0 and Q_1, respectively, in Figure 4.4), whereas the second reservoir plays the role of aquifer and generates groundwater runoff (i.e. Q_2 in Figure 4.4). The aquifer recharge (i.e. the water flux entering the lower reservoir) is therefore limited by the percolation rate between the upper and the lower reservoirs, and coincides with Q_2 in steady-state flow conditions. The HBV model sums the three runoff components (i.e. Q_0, Q_1 and Q_2) to generate the total basin runoff which is then transformed by the response routine to simulate the routing of the runoff to the catchment outlet. A complete description of the HBV model can be found in Bergström (1992, 1995) and Seibert (1999).

The HBV model provides an automatic calibration procedure that uses a genetic algorithm (Seibert, 2000) for mimicking the basin runoff evolution. The agreement between the observed (Q_{obs}) and simulated (Q_{sim}) catchment runoff is evaluated by the efficiency of the model R_{eff} [-] (Nash and Sutcliffe, 1970). To evaluate the uncertainty on the estimated parameters, we apply the same Monte-Carlo simulation process proposed by Jódar et al.

(2017), in which the model efficiency R_{eff} is optimized for a large number (50000) of HBV input parameter sets.

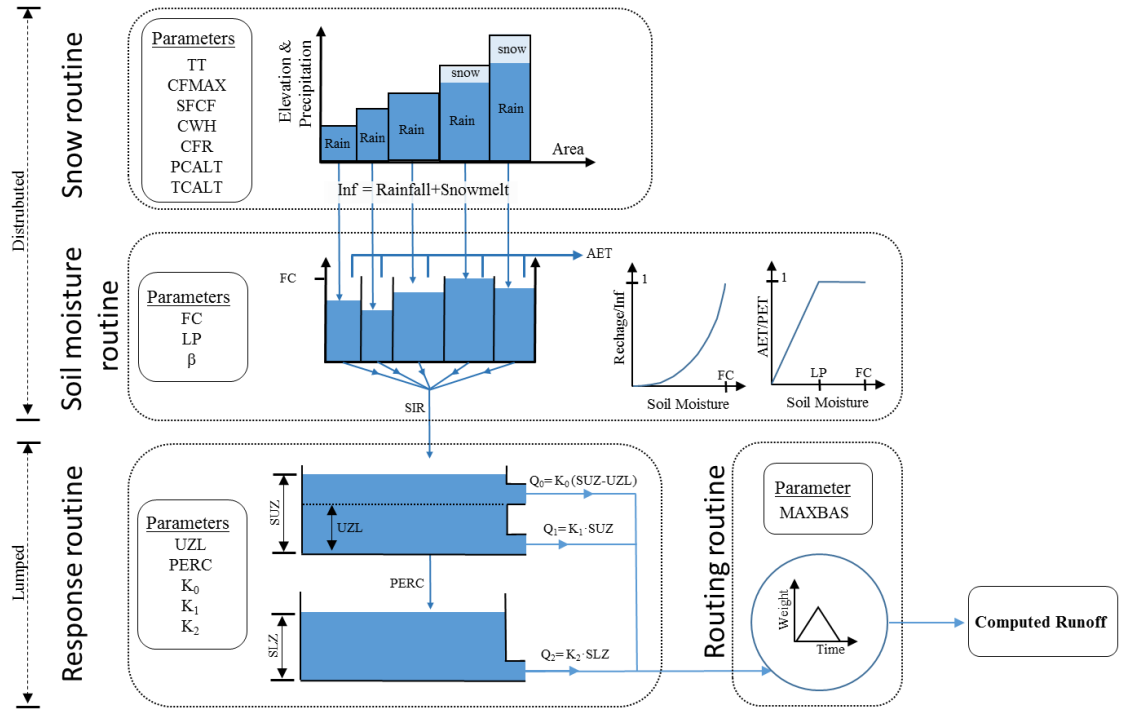

Figure 4.4. HBV model structure (modified from Seibert, 2000).

4.3.2. Remote sensing-based model to estimate evapotranspiration

Vegetation indices (VIs) obtained from satellite images are used in this work to estimate the water consumption of the different canopies in both watersheds for the hydrological years 2013/2014 and 2014/2015. An approach that integrates VIs in the method of FAO for computing crop water requirement (Allen et al., 1998) is applied here. This model has been tested and applied under a variety of conditions (González-Dugo and Mateos, 2008; González-Dugo et al., 2009, 2013; Mateos et al., 2013; Campos et al., 2013, 2016), and is based on the concepts of reference evapotranspiration ET_o [LT^{-1}] and the VI derived crop/canopy coefficient K_c [-]. The former takes into account the atmospheric demand, and it is calculated using the Hargreaves equation (Hargreaves et al., 1985). The latter accounts for the influence of the plant on the evapotranspiration, considering the effect of a specific canopy in relation to a given reference grass surface previously defined (Allen et al., 1998). For the estimation of the canopy coefficient, the dual method in the form popularized by the FAO manual (Allen et al., 1998) is used. The method separates canopy transpiration from soil surface evaporation and compute evapotranspiration following a daily scheme as (Allen et al., 1998; Wright, 1982):

$$ET = K_c ET_o \tag{4.2}$$

where ET [LT^{-1}] is evapotranspiration. The canopy coefficient K_c is obtained through the following equation:

$$K_c = K_{cb} K_s + K_e \tag{4.3}$$

where K_{cb} [-] is the basal canopy, K_s [-] is the water stress coefficient and K_e [-] is the soil evaporation coefficient.

The basal canopy coefficient K_{cb} determines the vegetation transpiration and depends on the vegetation class. It is derived from the spectral response of the canopy, which is provided by the satellite images. The relationship between K_{cb} and VI has been studied by different authors and there is not a complete agreement about its shape. Some authors consider it linear (Neale et al., 1989; Gonzalez-Piqueras et al., 2003), while others suggest non-linear approaches (Hunsaker et al., 2003, 2005). According to Choudhury et al. (1994), the linearity of these relationships depends on the canopy architecture and the definition of the VI applied. The equation proposed by González-Dugo et al. (2009) to compute the basal crop coefficient from the SAVI (Soil Adjusted Vegetation Index) index (Huete, 1988) is used here because it is a generalized equation for deriving K_{cb} from VI. It can be expressed as follows:

$$K_{cb} = \begin{cases} K_{cb_{max}} \left(\dfrac{f_c}{f_{c0}}\right) & ; \quad f_c < f_{c0} \\ K_{cb_{max}} & ; \quad f_c \geq f_{c0} \end{cases} \tag{4.4}$$

$$f_c = \left(\frac{SAVI - SAVI_{min}}{SAVI_{max} - SAVI_{min}}\right) \tag{4.5}$$

where $K_{cb_{max}}$ [-] is the maximum value of canopy coefficient (Table 4.2 shows the maximum value of canopy coefficient for the different vegetation classes existing in the watersheds), $SAVI_{max}$ [-] and $SAVI_{min}$ [-] are the corresponding values of the SAVI [-] index for very large ground coverage of the vegetation and bare soil, respectively, f_c [-] is the canopy ground-cover fraction, f_{c0} [-] is the canopy ground-cover fraction when $K_{cb} = K_{cb_{max}}$. The parameters f_{c0}, $SAVI_{max}$ and $SAVI_{min}$ have been assumed to be constant for all canopies, with values of 0.8, 0.75 and 0.09, respectively (González-Dugo et al., 2013), and the evolution of the spatial distribution of SAVI index is obtained from the Landsat-8 images, available every 16 days, when the satellite overpasses the study area. To obtain daily SAVI time series from two consecutive Landsat-8 images, a linear interpolation is applied between the two observed SAVI values.

The stress coefficient K_s quantifies the variation in transpiration due to the evolution of soil water deficit (Figure 4.5) in the root zone. The root zone depth is computed for each vegetation type as a function of K_{cb} values. K_s is calculated as:

$$K_s = \begin{cases} \dfrac{\sum - \Psi}{(1-p)\sum} & ; \Psi < \Psi_{Th} \\ 1 & ; \Psi \geq \Psi_{Th} \end{cases} \quad (4.6)$$

where Σ [L] is the root zone water holding capacity defined as the water length between the soil field capacity (maximum soil water content) and the wilting point (minimum soil water content), Ψ [L] is the root zone water deficit, Ψ_{Th} [L] is the root zone water deficit threshold value below which a shortage of water is found in the root zone, and p [-] is the fraction of Σ above Ψ_{Th} (Table 4.2). Ks is equal to 1 for non water stress conditions and smaller than 1 when a shortage of water is found in the root zone (Allen et al., 1998).

The daily evolution of the root zone water deficit can be estimated by solving the following soil water balance equation

$$\Psi_i = \Psi_{i-1} + \widehat{\hat{P}}_i - \widehat{ET}_{I-1} \quad (4.7)$$

where ET [LT^{-1}] is evapotranspiration and P [LT^{-1}] is the sum of rainfall and irrigation, R [LT^{-1}] is the water loss out of the soil zone by deep percolation, and RO [LT^{-1}] is runoff from the soil surface. The subscript i indicates the i^{th} day and the circumflex accent indicates that the corresponding flux variable has been temporally integrated on a daily basis.

Following heavy rain or irrigation, the soil water content in the root zone might exceed field capacity. In this situation, the surplus water is considered surface runoff.

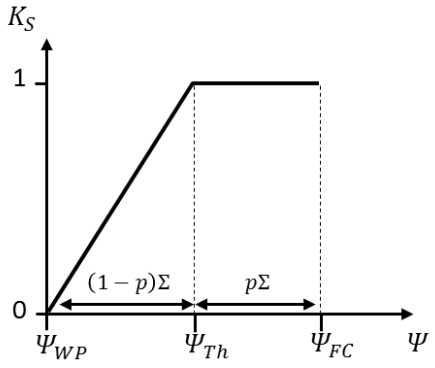

Figure 4.5. Relationship between the water stress coefficient K_s and the root zone water deficit Ψ, where Ψ_{WP}, Ψ_{FC} and Ψ_{Th} are the root zone water deficit corresponding to the wilting point, the field capacity, and the threshold value, respectively.

The balance equation described above is recursive, so for the first day it needs to know the initial value of the root zone water deficit (Ψ_0). As the soil water balance begins in August 2013 (in the middle of summer season for the study area), the value of Ψ_0 is assumed different for rainfed and irrigated canopies:

(1) Field capacity for irrigated horticultural crops (tomato and bean), so $\Psi_0 = 0$

(2) The root zone water holding capacity for the remaining vegetation types due to the long previous dry period, so $\Psi_0 = \Sigma$

The soil evaporation coefficient K_e [-] is obtained as:

$$K_e = \min\left[\left(f_{ew} \cdot K_{c_{max}}\right);\ K_r\left(K_{c_{max}} - K_{cb}\right)\right] \quad (4.8)$$

where $K_{c_{max}}$ [-] is the maximum value of K_c corresponding to the previous rainfall or irrigation event, f_{ew} [-] is the fraction of the soil surface that is both exposed (i.e. not covered by vegetation) and wetted, and K_r [-] is a dimensionless evaporation reduction coefficient that depends on topsoil water depletion (Allen et al., 1998). After a rain or irrigation episode, $K_r = 1$, but when the soil surface dries, the value of K_r linearly decreases along with the cumulative evaporation, becoming $K_r = 0$ when the soil is dry up and no water is left for evaporation.

4.3.3. Remotely sensed input data

A total of 26 cloud-free Landsat-8 images between August 2013 and October 2015 were selected (Table 4.3). The images were calibrated and atmospherically corrected to obtain surface reflectance values. The atmospheric correction of the optical bands was performed using the FLAASH (Fast Line-of-Sight Atmospheric Analysis of Spectral Hypercube) correction code (Adler-Golden et al., 1998) based on the radiative transfer model Modtran4 (Berk et al., 1989) and on monthly aerosol and atmospheric water vapour content data generated with the 6S model (Vermote et al., 1997).

Bad pixels and clouds have been masked out. During the winter, the low solar elevation caused that the steepest areas were not illuminated at sensor overpass time. These areas have been also masked out for the image processing and its subsequent use. Due to the lack of cloudy free Landsat-8 images between September and October 2015, the need to complete the satellite series for the year 2014/2015 led to the selection of lower spatial resolution images. Four MODIS images (product MOD09Q1, DOY 257, 265, 289 and 297) were selected, interpolated and added to the input data series.

Table 4.3. Acquisition dates of Landsat-8 satellite images (scene 200-34) for the hydrological years 2013/2014 and 2014/2015

Year 2013/2014	Year 2014/2015
11 August 2013	17 October 2014
12 September 2013	2 November 2014
15 November 2013	18 November 2014
19 February 2014	20 December 2014
23 March 2014	5 January 2015
8 April 2014	6 February 2015
24 April 2014	22 February 2015
26 May 2014	10 March 2015
27 June 2014	27 April 2015
13 July 2014	13 May 2015
29 July 2014	30 June 2015
15 September 2014	1 August 2015
17 October 2014	2 September 2015

4.3.4. Description of meteorological, runoff and soil-uses data

To simulate the hydrologic catchment behavior with the HBV model, it is necessary the availability of the meteorological data (i.e. P, T and PET) and of the runoff time series for the Bérchules and the Mecina watersheds. Cabrera and Martos-Rosillo (2014) analyzed the available meteorological data in the southern part of Sierra Nevada. As a result, complete time series of daily P and T were obtained, for the period 1970–2013, for the Bérchules and the Mecina meteorological stations. The corresponding PET time series were computed by applying the Hargreaves's method (Hargreaves and Samani, 1982).

To apply the VI-ET_o approach and estimate the water consumption of the different canopies, additional daily meteorological data were provided by automatic weather stations belonging to the following networks: Agroclimatic Information Network of Andalusia (RIA), Phytosanitary Alert and Information Network of Andalusia (RAIF) and the Spanish Meteorological Agency (AEMET). Variables including rainfall, solar radiation, air temperature and humidity, and wind speed were selected. The daily point data were spatially interpolated to obtain distributed information at the pixel resolution (30 × 30 m) of the Landsat-8 images. The hydrological model WiMMed (Herrero et al., 2011) was used to interpolate using the inverse distance IDW method, and taking into account the altitudinal

factor. For each cell, information from the seven nearest weather stations was employed for the interpolation.

In the case of runoff data, it was used a daily flow rate time series for the period 1970–2013 (Figure 4.6) measured at the Narila gauging station, which is located at the outlet of the Bérchules watershed (Figure 4.1).

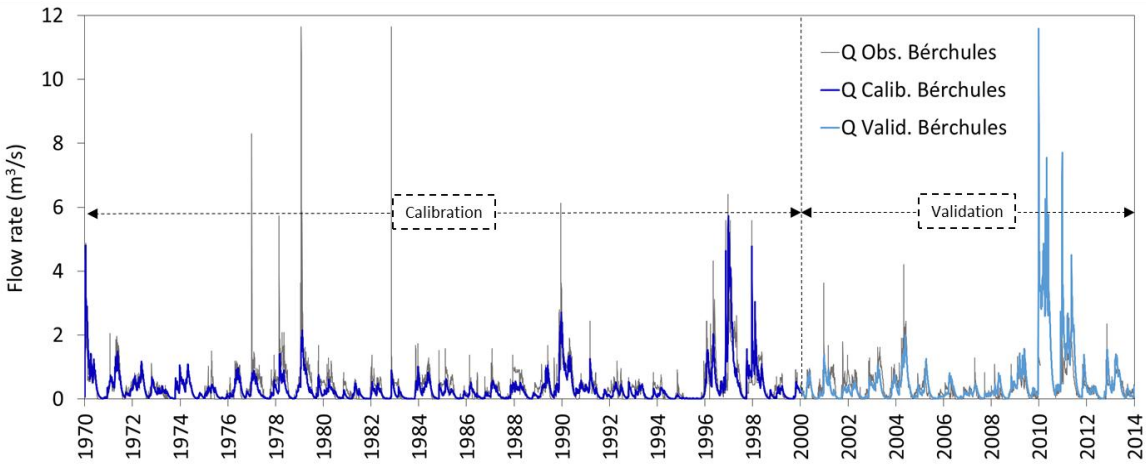

Figure 4.6. Time series of observed (grey line) and computed (blue and azure lines for the calibration and the validation periods, respectively) daily discharge flow rates obtained by the HBV model for the Bérchules watershed, in the Narila gauging station (located at the outlet of the Bérchules watershed). (For interpretation of the references to color in this figure legend, the reader is referred to the web version of this article.)

The vegetation types and their spatial distribution within the limits of both watersheds have been obtained from the Information and Soil Uses System of Spain (SIOSE) (http://www.siose.es/). A simplified land cover map (Figure 4.7) has been produced grouping vegetation species into different classes with similar structural and physiological characteristics and, therefore, similar spectral response. For refining the identification of irrigated horticultural crops areas, satellite images and data provided by the Environment and Water Agency of Andalusia have also been used. The information about irrigated areas was complemented with crop identification and radiometry measurements performed during a field campaign in the summer of 2014. Table 4.4 presents the soil use/land cover area for each basin.

In general terms, both watersheds present similar spatial distribution of vegetation types, with slight differences, such as a greater extension of conifers in Bérchules basin while Mecina has a greater cover of oak and permanent rainfed crops (Table 4.4). The irrigated horticultural crops are predominant in the south of Bérchules and more distributed between the southern and the central part in Mecina (Figure 4.7). In this work, a standard

irrigation schedule is assumed for the irrigated crops. It is based on a common practice in the area, which consists in watering to reach the soil field capacity every two days along the irrigation season, from mid-May to mid-October.

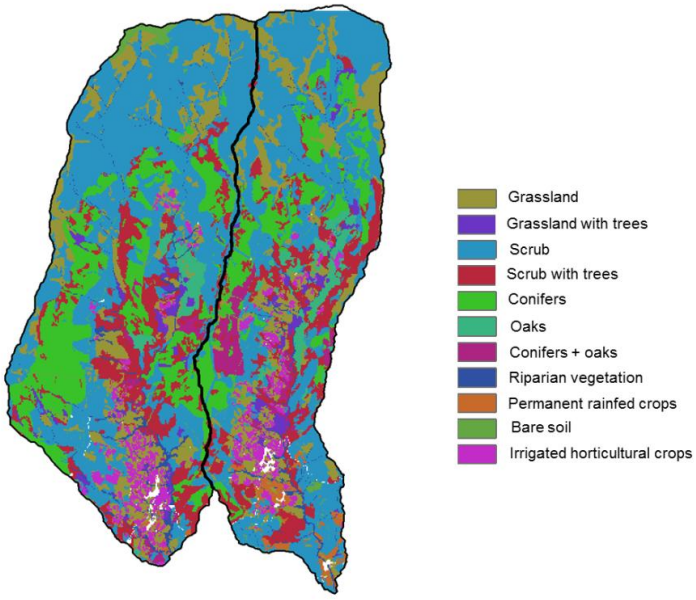

Figure 4.7. Land cover map of Bérchules and Mecina watersheds.

Table 4.4. Land cover area for Bérchules and Mecina watersheds, expressed in hectare and percentage of the total watershed area.

Land cover	Berchules ha (% watershed)	Mecina ha (% watershed)
Grassland	925.02 (13.73)	833.49 (15.21)
Grassland with trees	143.28 (2.13)	118.53 (2.16)
Scrub	2877.03 (42.71)	2202.30 (40.18)
Scrub with trees	841.05 (12.48)	729.18 (13.30)
Conifers	1179.99 (17.52)	671.04 (12.24)
Oaks	130.77 (1.94)	208.98 (3.81)
Conifers + Oaks	71.46 (1.06)	205.56 (3.75)
Riparian vegetation	160.38 (2.38)	97.92 (1.79)
Permanent rain-fed crops	20.07 (0.30)	117.45 (2.14)
Bare soil	141.30 (2.10)	79.11 (1.44)
Irrigated horticultural crops	245.61 (3.65)	217.44 (3.97)
Total	6735.96 (100)	5481.00 (100)

The vegetation ground cover fraction (f_c) is derived from the SAVI images taking advantage of the linear relationship existing between these two variables (Equation (4.5)). Figure 4.8 shows the monthly evolution of f_c for both watersheds (Bérchules and Mecina) along the hydrological year 2013-2014. Although the spatial distribution of f_c is heterogeneous, the lowest and the highest values can be found in the upper and the western-sunny hillside part of the basins, respectively. The lower f_c values correspond to high mountain grasslands and scrubs and show a seasonal variation, whereas the highest values correspond to conifers areas whose f_c values remain stable along the year. At the southern part of the basins where irrigated horticultural crops are predominant, fc is highly variable along the year, showing its maximum during the spring and summer seasons.

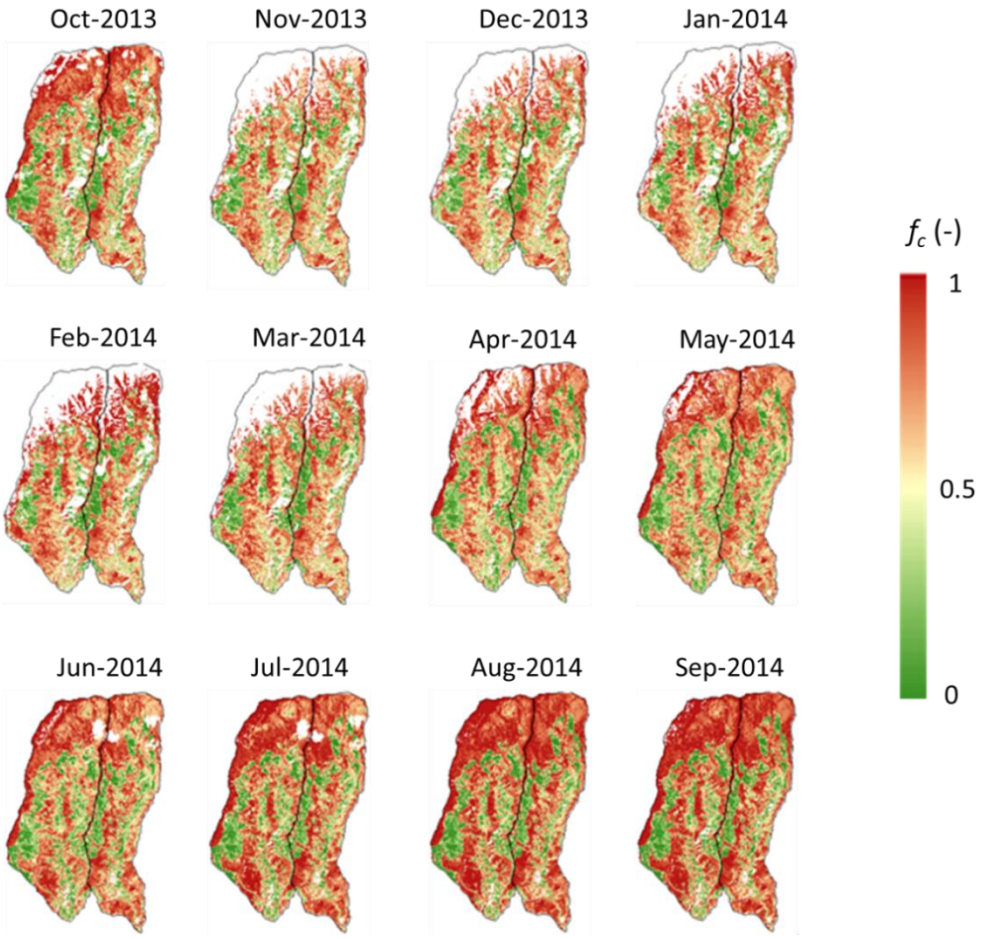

Figure 4.8. Monthly evolution of vegetation ground cover fraction f_c for the hydrological year 2013/14.

Soil parameters for the VI-ET_o approach are provided by regional soil maps produced by the Agricultural Department of Andalusia (CAPMA, 2008). These maps contain distributed information (with 250 m of spatial resolution) of different soil related properties, such as

texture (as % of sand, clay and silt), water content at field capacity and wilting point, and soil depth.

4.4. Results

4.4.1. The HBV model

The total time interval (i.e. 1970–2014) is divided into two parts of 2/3 and 1/3 of the total time length. The former (i.e. 1970–1999) is used for calibrating the HBV model parameters and the latter interval (2000–2014) is used for validating the previous calibration. The value of the calibrated HBV model parameters and their corresponding standard deviation obtained from the Monte-Carlo simulating process are presented in Table 4.5. The efficiency parameter R_{eff} obtained for the calibration and the validation period are 0.52 and 0.26, respectively. Figure 4.6 shows the performance of the model calibration in terms of the Bérchules basin runoff. There is a good agreement between Q_{obs} and Q_{sim}. Although the calibrated HBV model underestimates the measured flowrate peaks, the computed flow rates resemble the observed ones by following the observed temporal variation of the basin runoff. The calibrated HBV model reproduces the basin mean discharge at the outlet of the basin, which is critical from a perspective of water resources management. The calibrated mean annual basin discharge for the Bérchules basin is 12.61 hm^3/yr, and the corresponding standard deviation is 12.31 hm^3/yr. This high value underlines the high variability of the mean annual basin discharge.

The calibrated HBV parameter set obtained for the Bérchules watershed is used as input parameter set for simulating the hydrological response of the Mecina watershed. The simulated hydrologic response of the Mecina watershed resembles the simulated response of the Bérchules watershed but applying to the latter a dumpening factor (Figure 4.9). The simulated mean annual basin discharge and the associated standard deviation for the Mecina watershed are 6.32 hm^3/yr and 5.67 hm^3/yr respectively.

The monthly averaged values of the relevant mass balance flux terms are shown in Figure 4.10. In both basins, all the water flux terms show a seasonal pattern, in which precipitation, runoff (surface and subsurface) and groundwater discharge present the maximum and the minimum in December and July, respectively, and actual evapotranspiration follows the temporal dependence shown by the potential evapotranspiration (Figure 4.3) with the maximum and the minimum in July and December, respectively. Moreover, in both basins surface and subsurface runoff (i.e. Q_0 and Q_1, respectively) are almost negligible along the year. As a result, the monthly variation of the averaged basin runoff reflects the monthly variation of the averaged groundwater discharge (i.e. Q_2).

Table 4.5. Values of the calibrated HBV model parameters and their corresponding Monte-Carlo simulation initial and final interval values.

HBV Parameter	Calibrated value	Standard deviation (Monte-Carlo)
PERC (mm)	20.00	2.6
UZL (mm)	20.00	13.4
K_0 (día^{-1})	0.10	6.6E-02
K_1(día^{-1})	0.05	6.7E-03
K_2(día^{-1})	0.04	4.8E-03
MAXBAS (-)	7.00	2.3
TCALT (˚C/100m)	-0.56	[-,-]
CFMAX (mm/d/˚C)	3.00	1.5
SFCF (-)	1.80	1.0
CFR (-)	5.00	1.8
CWH (-)	6.00	1.7
TT (˚C)	5.00	1.5
FC (mm)	2000	555.8
LP (mm)	0.50	0.1

The simulated mean annual groundwater recharge for the Bérchules and the Mecina basins represents the 26% and 19% of the mean annual basin precipitation, respectively. The difference in the ratio between recharge and precipitation is coherent with the existing vertical precipitation gradient in the study zone and the different areal distribution with elevation of both basins (Figure 4.2B).

Groundwater discharge plays a major role in dynamics of both watersheds, representing the 95% and 98% of the total runoff for the Bérchules and the Mecina watersheds, respectively. These results are consistent with those obtained for the Bérchules watershed by Jódar et al. (2017), who using a coupled Témez-degree day (TDD) model estimated a groundwater contribution to total watershed discharge of 97%.

The basin runoff directly depends on soil infiltration recharge, which in turn depends on the sum of rainfall (RP) and snow-melt (SP) infiltration. In the case of the Bérchules watershed, RP and SP contribute 86% and 14% to the mean basin runoff, whereas in the case of the Mecina watershed these contributions are 97% and 3%, for RP and SP. The small SP value in the Mecina watershed shows that snowmelt plays a minor role and this

makes the basin runoff to follow the seasonal trend of RP, which has a maximum in January and monotonically decreases to reach the minimum in August.

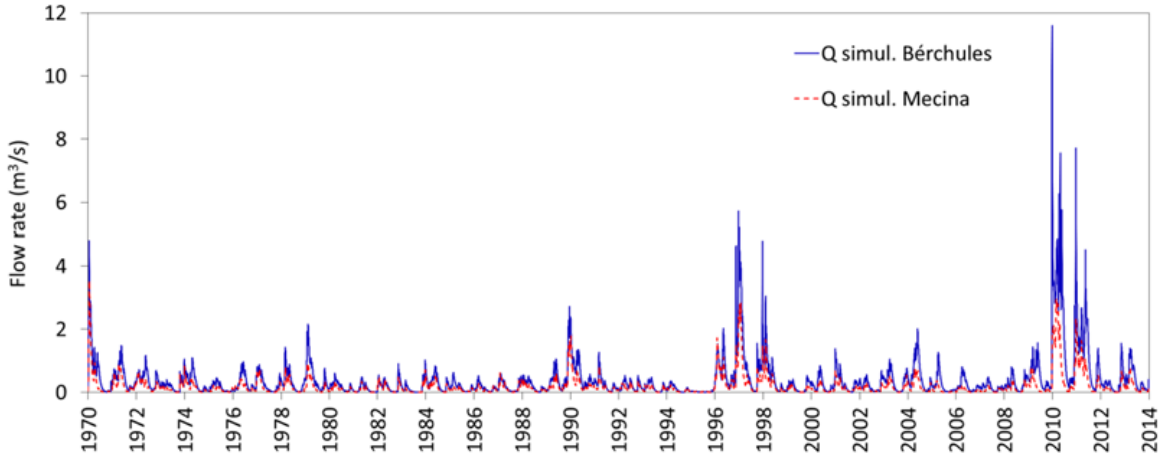

Figure 4. 9. Computed discharge flow rates for the Bérchules (blue dashed line) and the Mecina (red dashed line) basins. (For interpretation of the references to color in this figure legend, the reader is referred to the web version of this article).

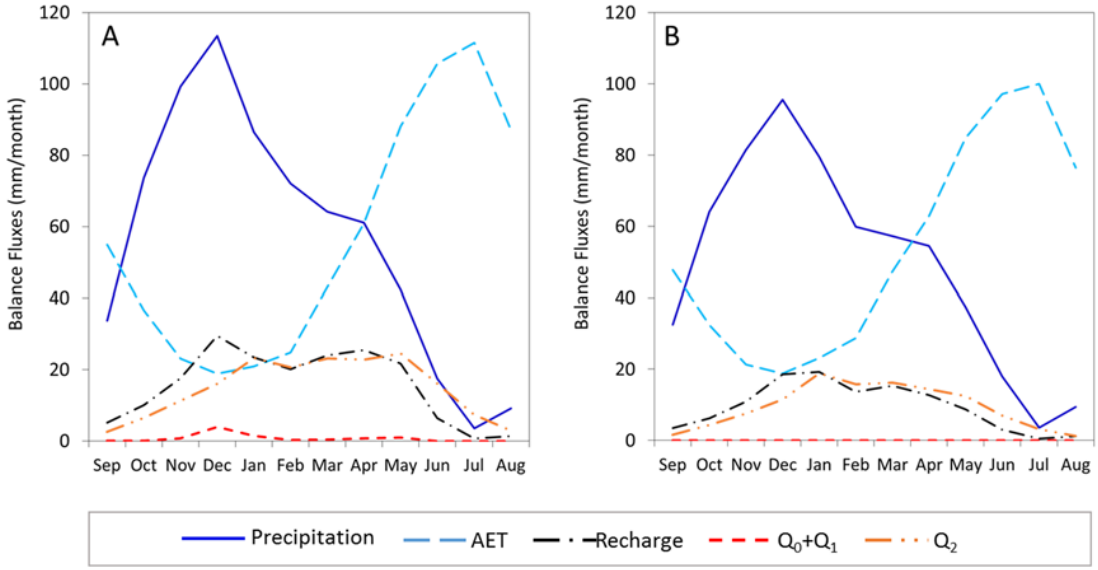

Figure 4.10. Monthly average of the different mass balance terms for (A) the Bérchules and (B) the Mecina basins obtained by simulating with the calibrated HBV parameters.

The discrepancy between the SP contribution to the total runoff for the Bérchules and the Mecina basins generates a differentiated hydrologic response in terms of the basin runoff seasonality. This discrepancy is due to the difference in the mean basin elevation of both watersheds (i.e. 1950 and 1710 m a.s.l. for the Bérchules and the Mecina watersheds, respectively). The 66% of the total area in the Mecina watershed has an elevation that falls

below the mean elevation of the Bérchules watershed (Figure 4.2B), whereas by definition the 50% of the total area in the Bérchules watershed falls below its mean basin elevation. The accumulation of precipitation as snowpack is more likely to occur in the Bérchules watershed than in the Mecina given (1) the larger area at higher elevations in the Bérchules watershed and (2) the existing temperature and precipitation vertical gradients in the study zone

4.4.2. The VI-ET_o approach

Daily spatially distributed ET values have been obtained at the pixel (30 × 30 m) scale for the hydrologic years 2013/2014 and 2014/2015. Figure 4.11 shows the accumulated monthly ET evolution for the former hydrologic year. In some cases, a masked out area can be observed in the highest part of both watersheds due to the snow cover that prevents the VI-ET_o model application, and therefore ET is not computed in these pixels. For analysis at the watershed scale, losses due to snow sublimation can produce a slight underestimation of total volumes.

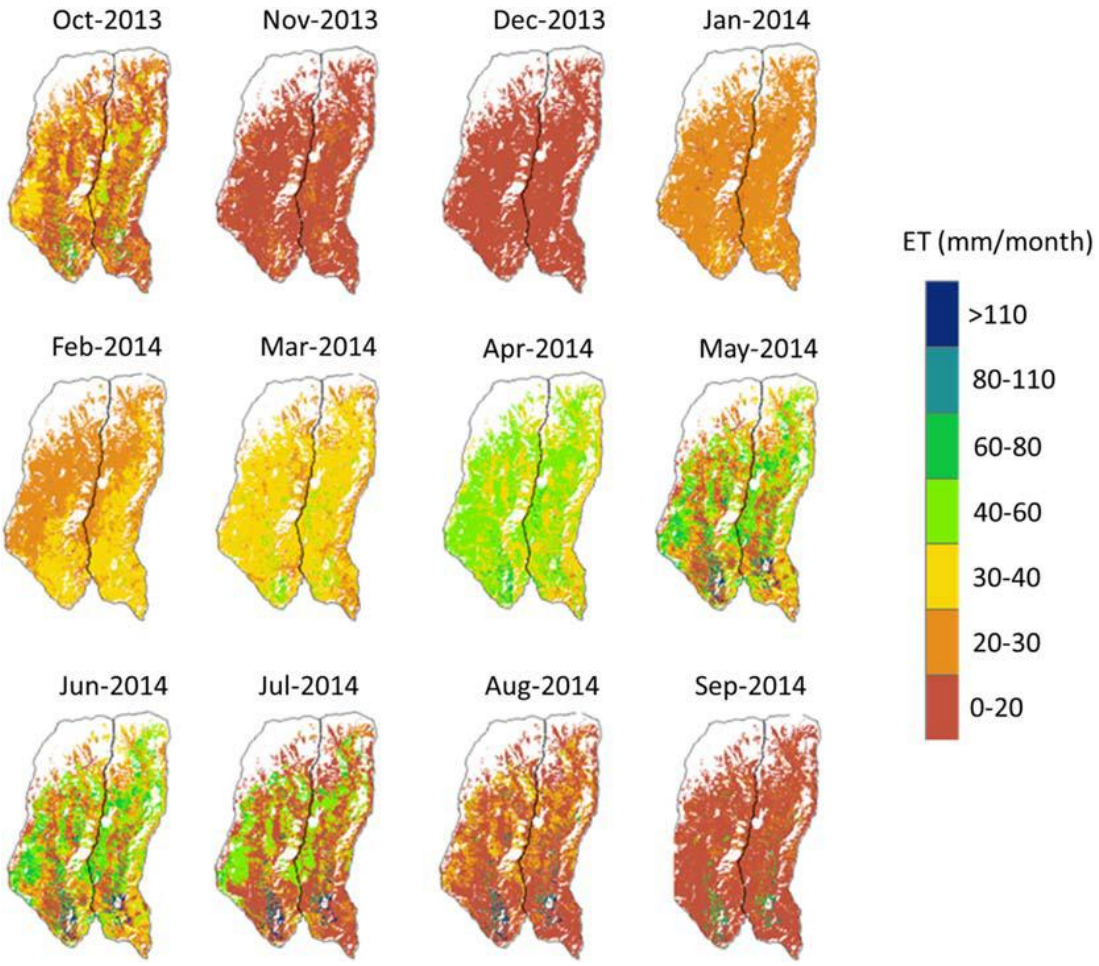

Figure 4.11. Monthly evolution of evapotranspiration values for the hydrological year 2013/14.

The monthly accumulation of the spatially integrated ET values corresponding to three representative vegetation types in the study zone (conifers, scrubs and irrigated horticultural crops) along the hydrological years 2013-2014 and 2014-2015 are shown in Figure 4.12. As can be shown, the monthly ET values are similar in both watersheds. This supports the hypothesis of assuming a similar hydrological behavior between both watersheds.

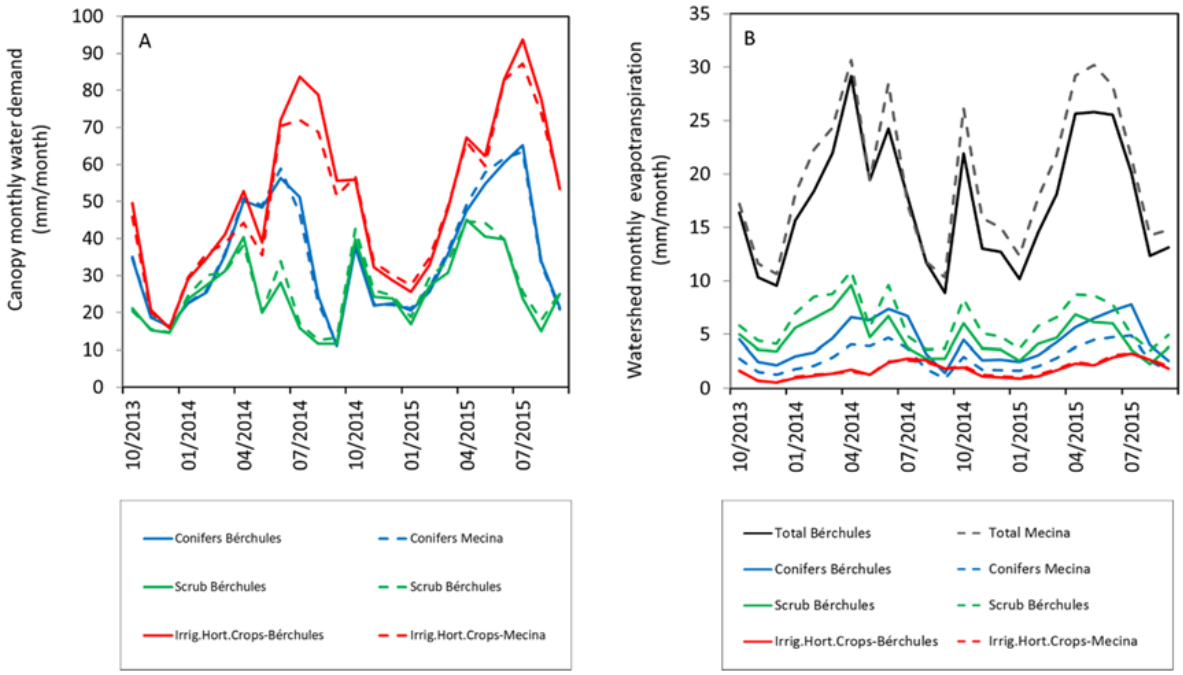

Figure 4.12. (A) Monthly unitary water demand for the different canopies (conifers in blue, scrubs in green and irrigated horticultural crops in red) existing in the Bérchules (line) and the Mecina (dashed line) watersheds. (B) Watershed monthly evapotranspiration obtained with the VI-ET_o approach along the hydrologic years 2013-2014 and 2014-2015 for the Béchules and the Mecina watersheds for the above canopies. The black line integrates ET corresponding to all the canopies considered in the model (Table 4.6). (For interpretation of the references to color in this figure legend, the reader is referred to the web version of this article.)

The evolution of monthly ET for the irrigated horticultural crops follows an annual pattern, with a similar trend in both years. It presents low values at the end of autumn and winter and increases gradually in spring, as a consequence of rain-fed pastures growing before the crop season in summer. A first peak of ET is observed until the soil is prepared for sowing. The crops start their cycle in May and the main annual peak in these areas is reached around the middle of the summer. The months of June, July and August accumulates the 37% of annual water consumption.

In the case of conifers, intra-annual changes are coupled with variations in the evaporative demand of the atmosphere, while maintaining quite regular vegetation coverage along the year. There were marked peaks in June 2014 and July 2015, coinciding

with high ET_o values for those months. The lowest values can be found at the end of the dry season, during the month of September, before the first rainfalls. Additionally, sparse scrubs presented low general values of ET, with minima of 3.2 and 2.8 mm/month in September 2014 and August 2015, respectively, and maxima of 10.2 and 7.8 mm/month in April 2014 and April 2015, respectively.

The annual accumulated ET values for the hydrological years 2013/14 and 2014/15 and every land cover of both watersheds are presented in Table 4.6. As can be shown, the contribution to the total ET of the irrigated horticultural crop represents, on average (i.e. for a given land cover averaging all the values of both watersheds), the 6.6% despite having the highest water demand per unit area (605 mm/yr on average). This low ET value is the result of the small percentage area (3.8% on average) associated to the irrigated horticultural crops in both watersheds (Table 4.4).

Table 4.6. Annual accumulated ET corresponding to the different land covers in the Bérchules and Mecina watersheds for the hydrologic years 2013/2014 and 2014/2015. For each watershed, ET values are provided in mm and percentage of the total basin ET for the corresponding hydrologic year.

Land cover	Annual evapotranspiration mm (% of the watershed annual ET)			
	2013/2014		2014/2015	
	Bérchules	Mecina	Bérchules	Mecina
Grassland	26.7 (9.0%)	29.2 (9.9%)	43.1 (11.3%)	49.3 (12.5%)
Grassland with trees	5.9 (2.0%)	7.3 (2.5%)	8.9 (2.3%)	9.1 (2.3%)
Scrub	111.3 (37.5%)	109.5 (37.3%)	149.9 (39.1%)	149.6 (38.0%)
Scrub with trees	37.1 (12.5%)	40.1 (13.6%)	47.5 (12.4%)	52.9 (13.4%)
Conifers	68.3 (23.0%)	47.4 (16.1%)	78.7 (20.5%)	54.7 (13.9%)
Oaks	7.4 (2.5%)	12.8 (4.4%)	7.4 (1.9%)	16.4 (4.2%)
Conifers + Oaks	4.5 (1.5%)	14.6 (5%)	4.5 (1.2%)	16.4 (4.2%)
Riparian vegetation	8.9 (3%)	5.5 (1.9%)	11.9 (3.1%)	7.3 (1.9%)
Permanent rain-fed crops	1.5 (0.5%)	5.5 (1.9%)	1.5 (0.4%)	9.1 (2.3%)
Bare soil	4.5 (1.5%)	1.8 (0.6%)	5.9 (1.5%)	3.6 (0.9%)
Irrigated horticultural crops	20.8 (7%)	20.1 (6.8%)	23.8 (6.2%)	25.5 (6.5%)
Total	306.9 (100%)	298.5 (100%)	400.1 (100%)	406.0 (100%)

On the contrary, scrubs (with and without trees) present relatively low water demands per unit area (329 mm/year on average) but cover more than 50% of the total area. They contribute up to 51% of total ET. The contribution of the conifer areas represent the 18.9% of total ET, while having a lower areal coverage (14.9% on average) but a higher annual water demand per unit area (422 mm/year on average) than scrubs.

It is possible to estimate the annual watershed runoff Q_{runoff} [LT^{-1}] considering the following surface water balance:

$$P\sim = ET\sim + I\sim + Q\sim_{runoff} \tag{4.9}$$

where I [LT^{-1}] is rainfall interception, which is assumed as 8% of rainfall according to Polo et al. (2013), who estimated I for different vegetation covers in Sierra Nevada Mountains. The tilde accent "~" indicates that the corresponding flux daily variable has been spatially integrated for the watershed and then temporal integrated on a yearly basis.

The annual runoff values measured at the Narila gausing station corresponding to the hydrologic years 2013/2014 and 2014/2015 are 87.3 and 78.8 mm, respectively (Table 4.7). The overall mean value for these two hydrologic years is 83.1 mm. These values are plotted against the corresponding annual runoff values obtained with the HBV model (Figure 4.13), where the correlation line is also included. As can be shown there is a good agreement between the annual runoff values obtained for the both models: The slope and the coefficient of determination of the correlation line ($Q\sim_{runoff\ VI-ETo}$ as dependent variable) are 1.08 and 0.96, respectively. $Q\sim_{runoff\ VI-ETo}$ is in average 5.3% smaller $Q\sim_{runoff\ HBV}$.

Table 4.7. Calculated annual runoff data for the Berchules and Mecina watersheds for the hydrological years 2013/14 and 2014/15.

Hydrologic Year	Annual runoff (mm)				
	Bérchules			Mecina	
	Observed[a]	VI-ET_o	HBV	VI-ET_o	HBV
2013/2014	87.3	81.9	80.1	45.9	51.9
2014/2015	78.8	83.2	89.1	58.1	63.0

[a] Observed in the gauging station of Narila, located at the outlet of the Bérchules watershed.

The annual runoff values obtained with the VI-ET_o approach corresponding to the hydrologic years 2013/2014 and 2014/2015 for the Bérchules and the Mecina watersheds are shown in Table 4.7, where the observed annual runoff values corresponding to the

Narila gauging station, which is located at the outlet of the Bérchules watershed, are also included for the same hydrologic years. As can be shown, the observed annual runoff values are similar to those obtained with HBV and VI-ET_o. In fact, their mean values for the whole period (2013-2015) are 83.1 mm, 82.6 mm and 84.6 mm, respectively.

The annual runoff values obtained with the VI-ET_o approach are plotted against the corresponding annual runoff values obtained with the HBV model (Figure 4.13), where the correlation line is also included. There is a good agreement between the annual runoff values obtained by both models in the watersheds: The slope and the coefficient of determination of the correlation line ($Q\sim_{runoff\ VI-ETo}$ as dependent variable) are 1.08 and 0.96, respectively. $Q\sim_{runoff\ VI-ETo}$ is, in average, 5.3% smaller than $Q\sim_{runoff\ HBV}$.

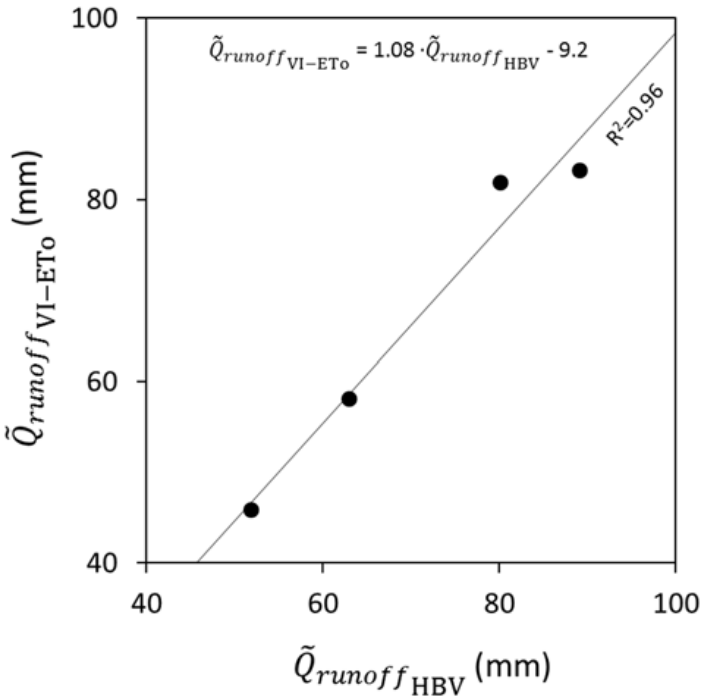

Figure 4.13. Annual runoff values obtained with the VI-ET_o approach and the HBV model and the corresponding regression line.

4.5. Discussion

The Bérchules and Mecina basins are located in the southern most high mountain area of the European continent. Because of its location, this area is more sensitive to the temperature increase generated by climate change than the high mountain basins located at greater latitude. This makes the study area an ideal laboratory to anticipate the impact of climate change on other high mountain basins of high latitudes, since its characteristics include:

- Strong vertical gradients of precipitation and temperature that are not yet so evident in high latitudes (Wanner et al., 2000; Oliva and Gómez-Ortiz, 2011).
- Strong rainfall seasonality, occurring the 80% of the annual precipitation between autumn and winter (October to April). During this period, precipitation occurs as snow 95% of the times above 2500 m a.s.l. (Gómez-Ortiz et al., 2015). In the spring the snow melt starts, a process that typically extends until the end of summer (September).
- Continuous intensification of aridity from the Middle Holocene (Oliva and Gómez-Ortiz, 2012). This has caused that the isotherm of 0 °C has been ascending in altitude, being now located around the 3300-3400 m a.s.l., very close to the maximum elevation of Sierra Nevada (3482 m a.s.l.). This has exposed the majority of the Quaternary glacial and periglacial formations that develop over the zone of alteration of the hard rocks that usually appear in the high mountain chains. The infiltration capacity of the glacial and periglacial materials is favored by the low slope and the high permeability of the quaternary materials. As a result of the continuous increase in temperature from the Middle Holocene, the infiltration capacity of the ground has increased even more due to the disappearance of the low permeability barrier that formed the permafrost, which deepened the materials of the zone of alteration. As a consequence of the increase in the soil infiltration capacity in these basins, its hydrological functioning regime has changed, increasing the underground component in the total discharge of the system, as it is observed in the Bérchules and Mecina basins, where the groundwater contribution to the total basin discharge is close to 95%.
- Continuing occupation and modification of the territory by the different civilizations (Romans, Visigoths, Muslim and Christian - Castillans) that have inhabited the middle mountain (Gómez-Ortiz et al., 2013). In this sense, in the southern margin of the Sierra Nevada, it is not difficult to find populations and fields of cultivation at heights above 1500 and 2200 m, respectively, which due to their activity have affected the base flows of the rivers, reducing the total river basin discharge, especially during the summer. In addition, reforestation during the second half of the 20th century over more than 25% of the mountain area, with dense masses of conifers where previously were scrubland (Jiménez-Olivenza et al., 2015), has influenced the operating regime of these rivers, with increased evapotranspiration (ET).
- The absence of a gauging station in most of its hydrological basins. The evaluation of these water resources is essential, both to manage the drinking water supply availability for the downstream depending population, and to know the base flow discharge of these watersheds, which is essential for the maintenance of the ecosystems.

Given the relevance of the increase in temperature in the modification of the hydrological response of the high mountain basins, it is necessary to take into account these changes in the planning of water resources under the scenario of climate change, especially in high mountain areas in semi-arid environments, since these generate practically the totality of the hydric resource available in those zones. When these discharge zones are located in karst areas then mountain discharge water is even more important given the typically paucity of water at the surface in these areas (LeGrand and Stringfield, 1973; White, 2002).

In this work, the parameters of the HBV model for the Bérchules basin have been calibrated. To this end, basin discharge data from an existing gauging station have been used. There is a good agreement between the observed and the computed basin runoffs. In terms of water budget, the obtained model results agree with those obtained by Jódar et al. (2017) for the same basin, but using a different hydrological model. Given the geomorphological similarities between the Bérchules and Mecina basins, the HBV parameters obtained for the Bérchules basin have been assumed to be valid for the Mecina basin.

Vegetation index field time series which are provided by satellite images have been used to obtain the evolution of the spatially distributed ET in both, the Bérchules and the Mecina basins. By using a simple surface water balance model the average annual discharge for both basins has been estimated. The obtained values are very similar to those calculated by the HBV model for the corresponding basins. This result validates (1) the use of the methodology presented to estimate the ET from the satellite images, and (2) the use of the HBV parameters obtained for the Bérchules basin to simulate the hydrological behavior of the Mecina basin.

The aggregate nature of the HBV model does not allow any spatial analysis of the mass balance terms considered in this model from its results. Moreover, this aggregate precipitation-contribution model does not allow us to know the impact that the spatial variation that certain hydrological variables have over time, such as changes in land use, in the basin response. Given the complementarity of the HBV and VI-ETo models for the Bérchules and Mecina basins, these issues can now be addressed, since the water balance in the soil used with VI-ET_o (Equation (4.8)) allows: (1) having a spatial distribution of the consumption of water by evaporation in both basins of the model, (2) determining the ET outputs associated to different vegetation cover, and (3) evaluating the impact of landcover changes on basin hydrology.

An example is the water demand of conifers (420 mm/year per square meter) which represents a total annual of 5 hm^3 for the study area, when considering a surface with this type of cover in both basins. This fact is of special interest, since the surface of conifers was practically null in the basin of the Bérchules River before 1956. In this sense, it must be indicated that the most significant land use changes occurred in Sierra Nevada in the last

50 years. Jiménez-Olivenza et al. (2015), after comparing the 1956 and 2011 digital orthophotographs of the Sierra Nevada, have shown that the area of wooded formations increased from 15% to 51.2%. In the case of conifers, repopulations carried out in the second half of the 20th century have made the area of Sierra Nevada range from 2.5 to 25%.

In the southern margin of Sierra Nevada, the main reforested zones correspond to spaces that were previously covered by scrubland and grasslands. Conifers have been used for reforestation and they have been planted following a pattern of coverage of maximum surface density. If the data resulting from this work are compared, reforestation implies an increase in the evaporation rate of 114 mm/year than if the reforested area would have been covered by the original thicket. Considering the 1180 ha of reforestation done in the Bérchules River basin, the ET increase in the basin is 1.35 hm^3/year, that is to say, these actions imply an increase in water consumption similar to that used for irrigation in the basin. If this increase in the evaporation rate (114 mm/year) is applied to the area repopulated (22.5%) in the Sierra Nevada area (171,985 ha) during the last 50 years, the ET increase reaches 44 hm^3/year, and it should not be forgotten that the flow associated with ET is subtracted directly from the total runoff of the hydrological system. The latter number shows that, when considering these types of actions, the variables to be analyzed, apart from the environmental benefits and the reduction of soil loss, should also include the assessment of the decrease of total runoff, especially in semi-arid areas where large mountains are the main source of supply of the population living in their environment and where aquatic ecosystems depend on very limited resources, and are therefore highly vulnerable to any change in the climatic conditions.

4.6. Conclusions

An HBV model for the Bérchules River basin has been calibrated using the flow data from the Narila gauging station, which is located at the mouth of the basin. The calibrated parameters of the HBV model have been used to simulate the hydrological response of the neighboring basin of the Mecina River, in which there is no gauging station. In both basins, the underground discharge component is higher than 95% of the total discharge of the basin, due to the outcropping of large areas of glacial and periglacial materials as a consequence of the deglaciation processes that occurred in Sierra Nevada. This fact demonstrates the importance of the effects of deglaciation on the hydrological functioning of the rivers of the low-latitude high mountains, by changing the infiltration capacity of the basin bedrock, as a consequence of the increase in temperature. This effect should be considered in simulations of future scenarios of the precipitation-contribution models in high mountain basins.

ET has been estimated in the hydrological basins of Bérchules and Mecina from the temporal variation of the vegetation index obtained by satellite images. A model of surface

water balance has been applied to estimate the annual flow of discharge of both basins, which are very similar to those obtained by the HBV model. This result validates the use of the parameters of the HBV model obtained for the basin in which the gauging station exists (Bérchules) in the non-instrumented basin (Mecina). This result also validates the VI-ET_o methodology for the estimation of ET in high mountain areas using satellite images.

The use of HBV and VI-ET_o models in high mountain hydrological basins allows the association of a spatial dependence to some of the variables of the hydrological model, such as ET infiltration and recharge that can give additional information of the operation of the system that would be hard to get other way.

The joint use of the HBV and VI-ET_o models opens the door to the validation of hydrological modeling results in ungauged basins mainly using remote information along with some amount of "ground truth", which is directly obtained from easy to obtain field measurements.

Future decisions about land-use changes, sanctioned by the river basin authorities, should take into account water consumptions, especially in the difficult conditions faced by this region in all global change predictions.

4.7. Acknowledgements

This research was undertaken as part of two projects funded by the Geological Survey of Spain (IGME), with reference numbers CANOA- 73.3.00.47.00 and 73.3.00.44.00, respectively; the Anillo Project, with reference number ACT-1203 funded by the CONICYT of Chile, and the Research Group RNM-126 which is funded by the Andalusian Government. The meteorological data have been provided by both, the Spanish State Meteorological Agency (AEMET) and the Environment and Water Agency of Andalusia (AMAYA).

We would also like to thank the editor D. Barceló and the anonymous reviewers for their constructive comments and suggestions which led to a substantial improvement of the paper.

4.8. References

Adler-Golden, S.M., Berk, A., Bernstein, L.S., Richtsmeier, S., 1998. FLAASH, a MODTRAN 4 atmospheric correction package for hyperspectral data retrievals and simulations. Proc. Sumaries 7th JPL Airborne Earth Sci. Workshop, pp. 1–9. AEMET/IM, 2011. Atlas Climático Ibérico–Iberian Climate Atlas. Madrid AEMET & IM (80 pp.).

Allen, R.G., Pereira, L.S., Raes, D., Smith, M., 1998. Crop Evapotranspiration: Guidelines for Computing Crop Requirements. Irrigation and Drainage Paper No. 56FAO, Roma, Italia.

Alsdorf, D.E., Rodriguez, E., Lettenmaier, D.P., 2007. Measuring surface water from space. Rev. Geophys. 45, RG2002. https://doi.org/10.1029/2006RG000197.

Andermann, C., Longuevergne, L., Bonnet, S., Crave, A., Davy, P., Gloaguen, R., 2012. Impact of transient groundwater storage on the discharge of Himalayan rivers. Nat. Geosci. 5: 127–132. https://doi.org/10.1038/NGEO1356.

Anderson, M.C., Allen, R.G., Morse, A., Kustas,W.P., 2012. Use of Landsat thermal imagery in monitoring evapotranspiration and managing water resources. Remote Sens. Environ. 122:50–65. https://doi.org/10.1016/j.rse.2011.08.025.

Benito, B., Lorite, J., Peñas, J., 2011. Simulating potencial effects of climatic warming on altitudinal patterns of key species in Mediterranean alpine ecosystem. Clim. Chang. 108 (3):471–483. https://doi.org/10.1007/s10584-010-0015-3.

Bergström, S., 1976. Development and Application of a Conceptual Runoff Model For Scandinavian Catchments, SMHI, Report No. RHO 7, Norrköping (134 pp.).

Bergström, S., 1992. The HBVModel – Its Structure and Applications, SMHI Hydrology, RH No. 4, Norrköping (35 pp.).

Bergström, S., 1995. The HBV model. In: Singh, V.P. (Ed.), Computer Models of Watershed Hydrology, Ch. 13, pp. 443±476. Water Resources Publications, Highlands Ranch, Colorado, USA (1130 pp.).

Bergström, S., 2006. Applications of the HBV hydrological model in prediction in ungauged basins. Large Sample Basin Experiments for Hydrological Model Parameterization: Results of the Model Parameter Experiment MOPEX. 307. IAHS Publ., pp. 97–107.

Bergström, S., Lindström, G., Petterson, A., 2002. Multi-variable parameter estimation to increase confidence in hydrological modeling. Hydrol. Process. 16:413–421. https:// doi.org/10.1002/hyp.332.

Berk, A., Bernstein, L.S., Robertson, D.C., 1989. MODTRAN: A Moderate Resolution Model for LOWTRAN7, GL-TR -89-0122. Air Force Geophys. Lab., Hanscom AFB,MA (38 pp.).

Beven, K.J., 2000. Uniqeness of place and process representations in hydrological modeling. Hydrol. Earth Syst. Sci. 4:203–213. https://doi.org/10.5194/hess-4-203-2000.

Birkinshaw, S.J., O'Donnell, G.M., Moore, P., Kilsby, C.G., Fowler, H.J., Berry, P.A.M., 2010. Using satellite altimetry data to augment flow estimation techniques on the Mekong River. Hydrol. Process. 24:3811–3825. https://doi.org/10.1002/hyp.7811.

Bjerklie, D.M., Dingman, S.L., Vorosmarty, C.J., Bolster, C.H., Congalton, R.G., 2003. Evaluating the potential for measuring river discharge from space. J. Hydrol. 278:17–38. https://doi.org/10.1016/S0022-1694(03)00129-X.

Blöschl, G., Ardoin-Bardin, S., Bonell, M., Dorninger, M., Goodrich, D., Gutknecht, D., Matamoros, D., Merz, B., Shand, P., Szolgay, J., 2007. At what scales do climate variability and land cover change impact on flooding and low flows? Hydrol. Process. 21 (9):1241–1247. https://doi.org/10.1002/hyp.6669.

Bocchiola, D., Mihalcea, C., Diolaiuti, G., Mosconi, B., Smiraglia, C., Rosso, R., 2010. Flow prediction in high altitude ungauged catchments: a case study in the Italian Alps (Pantano Basin, Adamello Group). Adv. Water Resour. 33 (10):1224–1234. https:// doi.org/10.1016/j.advwatres.2010.06.009.

Buytaert,W., Beven, K., 2009. Regionalization as a learning process. Water Resour. Res. 45, W11419. https://doi.org/10.1029/2008WR007359.

Cabrera, J.A., Martos-Rosillo, S., 2014. Evaluación de los recursos hídricos de las cabeceras de los ríos Bérchules yMecina (Sierra Nevada, Granada)mediante la aplicación de los modelos HBV y Témez-Grado–Día. IGME-AMAYA (141 pp.).

Campos, I., Villondre, J., Carrara, A., Calera, A., 2013. Remote sensing-based soil water balance to estimate Mediterranean holm oak savanna (dehesa) evapotranspiration under water stress conditions. J. Hydrol. 494:1–9. https://doi.org/10.1016/j.jhydrol.2013.04.033.

Campos, I., Gonzalez-Piqueras, J., Carrara, A., Villodre, J., Calera, A., 2016. Estimation of total available water in the soil layer by integrating actual evapotranspiration data in a remote sensing-driven soil water balance. J. Hydrol. 534:427–439. https://doi.org/10.1016/j.jhydrol.2016.01.023.

Choudhury, B.J., Ahmed, N.U., Idso, S.B., Reginato, R.J., Daughtry, C.S.T., 1994. Relations between evaporation coefficients and vegetation indices studied by model simulations. Remote Sens. Environ. 50:1–17. https://doi.org/10.1016/0034-4257(94)90090-6.

Consejería de Agricultura y Pesca, Junta de Andalucía (CAPMA), 2008. Sistema de Inferencia Espacial de Propiedades Físico-Químicas e Hidráulicas de los Suelos de Andalucía (Informe Final).

Cowie, R.M., Knowles, J.F., Dailey, K.R., Williams, M.W., Mills, T.J., Molotch, N.P., 2017. Sources of streamflow along a headwater catchment elevational gradient. J. Hydrol. 549:163–178. https://doi.org/10.1016/j.jhydrol.2017.03.044.

Di Baldassarre, G., Schumann, G., Bates, P.D., 2009. A technique for the calibration of hydraulic models using uncertain satellite observations of flood extent. J. Hydrol. 367: 276–282. https://doi.org/10.1016/j.jhydrol.2009.01.020.

Domeneghetti, A., Tarpanelli, A., Brocca, L., Barbetta, S., Moramarco, T., Castellarin, A., Brath, A., 2014. The use of remote sensing-derived water surface data for hydraulic model calibration. Remote Sens. Environ. 149:130–141. https://doi.org/10.1016/j.rse.2014.04.007.

Egeler, C.G., 1964. On the tectonics of the eastern Betic Cordilleras (SE Spain). International Journal of Earth Sciences, (Geologische Rundschau) 53 (1):260–269. https://doi.org/10.1007/BF02040750.

Fedeli, B., Castillo, A., 1997. Different kinds of morphogenetic springs in the upper Dilar valley (Sierra Nevada, Granada; Spain). In: IAH (Ed.), Hydrogeology of Hard Rocks, pp. 159–167.

García-Ruiz, J.M., López-Moreno, J.I., Lasanta, T., Vicente-Serrano, S.M., González-Sampériz, P., Valero-Garcés, B.L., Sanjuán, Y., Beguería, S., Nadal-Romero, E., Lana-Renault, N., Gómez-Villar, A., 2015. Los efectos geoecológicos del cambio global en el Pirineo Central español: una revisión a distintas escalas espaciales y temporales. Pirineos. 170:p. 012. https://doi.org/10.3989/Pirineos.2015.170005.

García-Vera, M.A., 2013. The application of hydrological planning as a climate change adaptation tool in the Ebro basin. International Journal of Water Resources Development 29 (2):219–236. https://doi.org/10.1080/07900627.2012.747128.

Gómez-Ortiz, A., Oliva, M., Salvà-Catarineu, M., Salvador-Franch, F., 2013. The environmental protection of landscapes in the high semiarid Mediterranean mountain of Sierra Nevada National Park (Spain): historical evolution and future perspectives. Appl. Geogr. 42:227–239. https://doi.org/10.1016/j.apgeog.2013.02.006.

Gómez-Ortiz, A., Oliva, M., Palacios, D., Salvador-Franch, F., Vázquez-Selem, L., Salvà-Catarineu, M., de Andrés, N., 2015. The deglaciation of Sierra Nevada (Spain), synthesis of the knowledge and new contributions. Cuadernos de Investigación Geográfica 41 (2). https://doi.org/10.18172/cig.2722.

González Trueba, J.J., Moreno, R.M., Martínez de Pisón, E., Serrano, E., 2008. Little Ice Age' glaciation and current glaciers in the Iberian Peninsula. The Holocene 18 (4): 551–568. https://doi.org/10.1177/0959683608089209.

González-Dugo, M.P., Mateos, L., 2008. Spectral vegetation indices for benchmarking water productivity of irrigated cotton and sugar beet crops. Agric. Water Manag. 95:48–58. https://doi.org/10.1016/j.agwat.2007.09.001.

González-Dugo, M.P., Neale, C.M.U., Mateos, L., Kustas,W.P., Prueger, J.H., Anderson, M.C., Li, F., 2009. A comparison of operational remote sensing-based models for estimating crop evapotranspiration. Agric. For. Meteorol. 149:1843–1853. https://doi.org/10.1016/j.agrformet.2009.06.012.

González-Dugo, M.P., Escuin, S., Mateos, L., Cano, F., Cifuentes, V., Padilla, F.L.M., Tirado, J.L., Oyonarte, N., Fernández, P., 2013. Monitoring evapotranspiration of irrigated crops using crop coefficients derived from time series of satellite images. II. Application on basin scale. Agric. Water Manag. 125:92–104. https://doi.org/10.1016/j.agwat.2013.03.024.

Gonzalez-Piqueras, J., Calera Belmonte, A., Gilabert, M.A., Cuesta García, A., De la Cruz Tercero, F., 2003. Estimation of crop coefficient by means of optimized vegetation indices for corn. Proc. SPIE 5232, 110–118.

González-Ramón, A., Martos, F.M., Marín, C., 2015. Factores geomorfológicos condicionantes de la hidrogeología de la cuenca alta del río Bérchules (Sierra Nevada, Granada). Málaga, 4(6). Proceedings of SIAGA 2015, pp. 283–294 Tomo 1.

Götzinger, J., Bárdossy, A., 2007. Comparison of four regionalisation methods for a distributed hydrological model. J. Hydrol. 333 (2):374–384. https://doi.org/10.1016/j.jhydrol.2006.09.008.

Grunewald, K., Scheithauer, J., 2010. Europe's southernmost glaciers: response and adaptation to climate change. J. Glaciol. 56, 129–142.

Hargreaves, G.H., Samani, Z.A., 1982. Estimation of potential evapotranspiration. Journal of Irrigation and Drainage Division. Proceedings of the American Society of Civil Engineers 108, 223–230.

Hargreaves, G.L., Hargreaves, G.H., Riley, J.P., 1985. Irrigation water requirements for Senegal river basin. Journal of Irrigation and Drainage Engineering, ASCE 111 (3): 265–275. https://doi.org/10.1061/(ASCE)0733-9437(1985)111:3(265).

Herrero, J., Millares, A., Aguilar, C., Díaz, A., Polo, M.J., Losada, M.A., 2011. WiMMed. Base Teórica. Grupo de Dinámica fluvial e Hidrología de la Universidad de Córdoba y Grupo de Dinámica de Flujos Ambientales de la Universidad de Granada, Spain.

Hood, J.L., Hayashi, M., 2015. Characterization of snowmelt flux and groundwater storage in an alpine headwater basin. J. Hydrol. 521:482–497. https://doi.org/10.1016/ j.jhydrol.2014.12.041.

Hrachowitz, M., Savenije, H.H.G., Blöschl, G., McDonnell, J.J., Sivapalan, M., Pomeroy, J.W., Arheimer, B., Blume, T., Clark, M.P., Ehret, U., Fenicia, F., Freer, J.E., Gelfan, A., Gupta, H.V., Hughes, D.A., Hut, R.W., Montanari, A., Pande, S., Tetzlaff, D., Troch, P.A., Uhlenbrook, S., Wagener, T., Winsemius, H.C., Woods, R.A., Zehe, E., Cudennec, C., 2013. A decade of Predictions in Ungauged Basins (PUB)—a review. Hydrol. Sci. J. 58 (6):1198–1255. https://doi.org/10.1080/02626667.2013.803183.

Huete, A.R., 1988. A soil-adjusted vegetation index (SAVI). Remote Sens. Environ. 25: 295–309. https://doi.org/10.1016/0034-4257(88)90106-X.

Hughes, P.D., Woodward, J.C., 2009. Chapter 12: glacial and periglacial environments. In: Woodward, J.C. (Ed.), The Physical Geography of the Mediterranean Basin. Oxford University Press, Oxford, pp. 353–383.

Hundecha, Y., Bárdossy, A., 2004. Modeling of the effect of land use changes on the runogeneration of a river basin through parameter regionalization of a watershed model. J. Hydrol. 292:281–295. https://doi.org/10.1016/j.jhydrol.2004.01.002.

Hunsaker, D.J., Pinter Jr., P.J., Barnes, E.M., Kimball, B.A., 2003. Estimating cotton evapotranspiration crop coefficient with a multispectral vegetation index. Irrig. Sci. 22: 95–104. https://doi.org/10.1007/s00271-003-0074-6.

Hunsaker, D.J., Pinter, P.R., Kimball, B.A., 2005. Wheat basal crop coefficients determined by normalized difference vegetation index. Irrig. Sci. 24, 1–14.

Jiménez-Olivenza, Y., Porcel-Rodríguez, L., Caballero-Calvo, A., Bonet, F.J., 2015. Evolución de los usos del suelo en Sierra Nevada en los últimos 50 años y cambios del paisaje. 54-56. 2015. In: Zamora, R., Pérez-Luque, A.J., Bonet, F.J., Barea, Azcón J.M., Aspizua, R. (Eds.), La huella del Cambio Global en Sierra Nevada: Retos para la conservación. Consejería de Medio Ambiente y Ordenación del Territorio. Junta de Andalucía.

Jódar, J., Cabrera, J.A., Martos-Rosillo, S., Ruiz-Constan, A., González-Ramón, A., Lambán, L.J., Herrera, C., Custodio, E., 2017. Groundwater discharge in high-mountain watersheds: a valuable resource for downstream semi-arid zones. The case of the Bérchules River in Sierra Nevada (Southern Spain). Sci. Total Environ. https://doi.org/10.1016/j.scitotenv.2017.03.190.

Kirchner, J.W., 2006. Getting the right answer for the right reasons: linking measurements, analysis, and models to advance the science of hydrology. Water Resour. Res. 42, W03S04. https://doi.org/10.1029/2005WR004362.

Kullman, L., 2002. Rapid recent range-margin rise of tree and shurb species in the Swedish Scandes. J. Ecol. 90 (1):68–77. https://doi.org/10.1046/j.0022-0477.2001.00630.x.

Kundzewicz, Z.W., 2007. Prediction in ungauged basins—a systemic perspective. Predictions in ungauged basins: PUB Kick-off. IAHS Publ. 309.

Langston, G., Hayashi, M., Roy, J.W., 2013. Quantifying groundwater–surface water interactions in a proglacial moraine using heat and solute tracers. Water Resour. Res. 49: 5411–5426. https://doi.org/10.1002/wrcr.20372.

LeGrand, H.E., Stringfield, V.T., 1973. Karst hydrology—a review. J. Hydrol. 20 (1973): 97–120. https://doi.org/10.1016/0022-1694(73)90034-6.

López-Moreno, J.I., Zabalza, J., Vicente-Serrano, S.M., Revuelto, J., Gilaberte, M., Azorin-Molina, C., Morán-Tejeda, E., García-Ruiz, J.M., Tague, C., 2014. Impact of climate and land use change on water availability and reservoir management: scenarios in the Upper Aragón River, Spanish Pyrenees. Sci. Total Environ. 493:1222–1231. https://doi.org/10.1016/j.scitotenv.2013.09.031.

Mateos, L., González-Dugo, M.P., Testi, L., Villalobos, F.J., 2013.Monitoring evapotranspiration of irrigated crops using crop coefficients derived from time series of satellite images. I. Method validation. Agric. Water Manag. 125:81–91. https://doi.org/10.1016/j.agwat.2012.11.005.

McDonnell, J.J., Sivapalan, M., Vaché, K., Dunn, S., Grant, G., Haggerty, R., Hinz, C., Hooper, R., Kirchner, J., Roderick, M.L., Selker, J.,Weiler, M., 2007. Moving beyond heterogeneity and process complexity: a new vision for watershed hydrology. Water Resour. Res. 43, W07301. https://doi.org/10.1029/2006WR005467.

Merz, R., Blöschl, G., 2004. Regionalisation of catchment model parameters. J. Hydrol. 287 (1):95–123. https://doi.org/10.1016/j.jhydrol.2003.09.028.

Millares, A., Polo, M.J., Losada, M.A., 2009. The hydrological response of base flow in fractured mountain areas. Hydrol. Earth Syst. Sci. 13:1261–1271. https://doi.org/10.5194/hess-13-1261-2009.

Mishra, A.K., Singh, V.P., 2010. A review of drought concepts. J. Hydrol. 391 (1):202–216. https://doi.org/10.1016/j.jhydrol.2010.07.012.

Molina, A.J., Latron, J., Rubio, C.M., Gallart, F., Llorens, P., 2014. Spatio-temporal variability of soil water content on the local scale in a Mediterranean mountain area (Vallcebre, North Eastern Spain). How different spatio-temporal scales reflect mean soil water content. J. Hydrol. 516:182–192. https://doi.org/10.1016/j.jhydrol.2014.01.040.

Nash, J., Sutcliffe, J.V., 1970. River flow forecasting through conceptual models part I—a discussion of principles. J. Hydrol. 10 (3):282–290. https://doi.org/10.1016/0022-1694(70)90255-6.

Neal, J., Schumann, G., Bates, P., Buytaert, W., Pappenberger, F., 2009. A data assimilation approach to discharge estimation from space. Hydrol. Process. 23:3641–3649. https://doi.org/10.1002/hyp.7518.

Neale, C.M.U., Bausch, W.C., Heerman, D.F., 1989. Development of reflectance-based crop coefficients for corn. Trans. ASAE 32 (4):1891–1899. https://doi.org/10.13031/2013.31240.

Nogués-Bravo, D., Araújo, M.B., Lasanta, T., López-Moreno, J.I., 2008. Climate change in Mediterranean mountains during the 21st century. AMBIO: A Journal of the Human Environment 37 (4):280–285. https://doi.org/10.1579/0044-7447(2008)37[280:CCIMMD]2.0.CO;2.

Oliva,M., Gómez-Ortiz, A., 2011. Holocene slope dynamics in Sierra Nevada (south Spain). Sedimentological analysis of solifluction landforms and lake deposits. Geological Society, London, Special Publications 2011 354:227–239. https://doi.org/10.1144/SP354.15.

Oliva, M., Gómez-Ortiz, A., 2012. Late Holocene environmental dynamics and climate variability in a Mediterranean high mountain environment (Sierra Nevada, Spain) inferred from lake sediments and historical sources. The Holocene 22 (8):915–927. https://doi.org/10.1177/0959683611434235.

Parajka, J., Blöschl, G., 2008. The value of MODIS snow cover data in validating and calibrating conceptual hydrological models. J. Hydrol. 358:240–258. https://doi.org/10.1016/j.jhydrol.2008.06.006.

Parajka, J., Merz, R., Blöschl, G., 2005. A comparison of regionalisation methods for catchment model parameters. Hydrol. Earth Syst. Sci. 9:157–171. https://doi.org/10.5194/hess-9-157-2005.

Peel, M.C., Finlayson, B.L., McMahon, T.A., 2007. Updated world map of the Köppen–Geiger climate classification. Hydrol. Earth Syst. Sci. 11:1633–1644. https://doi.org/10.5194/hess-11-1633-2007.

Pisano, L., Zumpano, V.,Malek, Ž.,Micu,M., Rosskopf, C.M., Parise,M., 2017.Multi-temporal landslide susceptibility maps and future scenarios for expected land cover changes (Southern Apennines, Italy) open image in new window. In:Mikoš,M., Vilímek, V., Yin, Y., Sassa, K. (Eds.), Advancing Culture of Living With Landslides. WLF 2017. Springer, Cham. https://doi.org/10.1007/978-3-319-53483-1_45.

Polo, M.J., Aguilar, C., Díaz-Gutiérrez, A., González-Dugo, M.P., 2013. Cuantificando la interceptación en cuencas heterogéneas: la cuenca del río Guadalfeo (Granada). Interceptación de la lluvia por la vegetación en España. 297–317. Instituto Euromediterráneo del agua.

Roy, D.P.,Wulder,M.A., Loveland, T.R.,Woodcock, C.E., Allen, R.G., Anderson, M.C., Helder, D., Irons, J.R., Johnson, D.M., Kennedy, R., Scambos, T.A., Schaaf, C.B., Schott, J.R., Sheng, Y., Vermote, E.F., Belward, A.S., Bindschadler, R., Cohen, W.B., Gao, F., Hipple, J.D., Hostert, P., Huntington, J., Justice, C.O., Kilic, A., Kovalskyy, V., Lee, Z.P., Lymburner, L., Masek, J.G., McCorkel, J., Shuai, Y., Trezza,

R., Vogelmann, J., Wynne, R.H., Zhu, Z., 2014. Landsat-8: science and product vision for terrestrial global change research. Remote Sens. Environ. 145:154–172. https://doi.org/10.1016/j.rse.2014.02.001.

Samuel, J., Coulibaly, P., Metcalfe, R.A., 2011. Estimation of continuous streamflow in Ontario ungauged basins: comparison of regionalization methods. J. Hydrol. Eng. 16 (5): 447–459. https://doi.org/10.1061/(ASCE)HE.1943-5584.0000338.

Sefton, C.E.M., Howarth, S.M., 1998. Relationships between dynamic response characteristics and physical descriptors of catchments in England and Wales. J. Hydrol. 211: 1–16. https://doi.org/10.1016/S0022-1694(98)00163-2.

Seibert, J., 1999. Regionalisation of parameters for a conceptual rainfall-runoff model. Agric. For. Meteorol. 98:279–293. https://doi.org/10.1016/S0168-1923(99)00105-7.

Seibert, J., 2000. Multi-criteria calibration of a conceptual runoffmodel using a genetic algorithm. Hydrol. Earth Syst. Sci. 4 (2):215–224. https://doi.org/10.5194/hess-4-215-2000.

Seibert, J., 2005. HBV Light Version 2. User's Manual. Uppsala University, Dept. of Earth Science, Hydrology, Uppsala, Sweden.

Seibert, J., McDonnell, J.J., 2013. Gauging the ungauged basin: relative value of soft and hard data. J. Hydrol. Eng. 20 (1), A4014004. https://doi.org/10.1061/(ASCE)HE.1943-5584.0000861.

Singh, V.P., Woolhiser, D.A., 2002. Mathematical modeling of watershed hydrology. J. Hydrol. Eng. 7 (4):270–292. https://doi.org/10.1061/~ASCE!1084-0699~2002!7:4~270!.

Sivapalan, M., 2003. Prediction in ungauged basins: a grand challenge for theoretical hydrology. Hydrol. Process. 17:3163–3170. https://doi.org/10.1002/hyp.5155.

Sivapalan, M., Takeuchi, K., Franks, S.W., Gupta, V.K., Karambiri, H., Lakshmi, V., Liang, X., Mcdonnell, J.J., Mendiondo, E.M., O'Connell, P.E., Oki, T., Pomeroy, J.W., Schertzer, D., Uhlenbrook, S., Zehe, E., 2003. IAHS Decade on Predictions in Ungauged Basins (PUB), 2003–2012: shaping an exciting future for the hydrological sciences. Hydrol. Sci. J. 48 (6):857–880. https://doi.org/10.1623/hysj.48.6.857.51421.

Skaugen, T., Peerebom, I.O., Nilsson, A., 2015. Use of a parsimonious rainfall-runoff model for predicting hydrological response in ungauged basins. Hydrol. Process. 29:1999–2013. https://doi.org/10.1002/hyp.10315.

Skøien, J.O., Blöschl, G., 2006. Catchments as space-time filters—a joint spatio-temporal geostatistical analysis of runoff and precipitation. Hydrol. Earth Syst. Sci. 10:645–662. https://doi.org/10.5194/hess-10-645-2006.

Slaymaker, O., Spencer, T., Embleton-Hamann, C., 2009. Geomorphology and Global Environmental Change. Cambridge University Press, Cambridge, p. 528.

Smith, L.C., Pavelsky, T.M., 2008. Estimation of river discharge, propagation speed, and hydraulic geometry from space: Lena River, Siberia. Water Resour. Res. 44, W03427. https://doi.org/10.1029/2007WR006133.

Smith, L.C., Isacks, B.L., Bloom, A.L., Murray, A.B., 1996. Estimation of discharge from three braided rivers using synthetic aperture radar satellite imagery. Water Resour. Res. 32 (7):2021–2034. https://doi.org/10.1029/96WR00752.

Stahl, K., Hisdal, H., Hannaford, J., Tallaksen, L., Van Lanen, H., Sauquet, E., Demuth, S., Fendekova, M., Jódar, J., 2010. Streamflow trends in Europe: evidence from a dataset of near-natural catchments. Hydrol. Earth Syst. Sci. 14, p-2367. https://doi.org/10.5194/hess-14-2367-2010.

Tarpanelli, A., Barbetta, S., Brocca, L., Moramarco, T., 2013a. River discharge estimation by using altimetry data and simplified flood routing modeling. Remote Sens. 5 (9): 4145–4162. https://doi.org/10.3390/rs5094145.

Tarpanelli, A., Brocca, L., Lacava, T., Melone, F., Moramarco, T., Faruolo, M., Pergola, N., Tramutoli, V., 2013b. Toward the estimation of river discharge variations using MODIS data in ungauged basins. Remote Sens. Environ. 136:47–55. https://doi.org/10.1016/j.rse.2013.04.010.

Tarpanelli, A., Brocca, L., Barbetta, S., Faruolo,M., Lacava, T.,Moramarco, T., 2015. Coupling MODIS and radar altimetry data for discharge estimation in poorly gauged river basins. IEEE Journal of Selected Topics in Applied Earth Observations and Remote Sensing 8 (1):141–148. https://doi.org/10.1109/JSTARS.2014.2320582.

Taylor, R.G., Scanlon, B., Doll, P., Rodell, M., Van Beek, R., Wada, Y., Longuevergne, L., Leblanc, M., Famiglietti, J.S., Edmunds, M., Konikow, L., Green, T.R., Chen, J., Taniguchi, M., Bierkens, M.F.P., MacDonald, A., Fan, Y., Maxwell, R.M., Yechieli, Y., Gurdak, J.J., Allen, D.M., Shamsudduha, M., Hiscock, K., Yeh, Pat J.-F., Holman, I., Treidel, H., 2012. Ground water and climate change. Nat. Clim. Chang. 3 (4): 322–329. https://doi.org/10.1038/nclimate1744.

Temimi,M., Leconte, R., Brissette, F., Chaouch, N., 2007. Flood and soil wetness monitoring over the Mackenzie River Basin using AMSR-E 37 GHz brightness temperature. J. Hydrol. 333:317–328. https://doi.org/10.1016/j.jhydrol.2006.09.002.

Theurillat, J.P., Guisan, A., 2001. Potential impact of climate change on vegetation in the European Alps: a review. Clim. Chang. 50:77–109. https://doi.org/10.1023/A:1010632015572.

Urqueta, H., Jódar, J., Herrera, C.,Wilke, H.G.,Medina, A., Urrutia, J., Custodio, E., Rodríguez, J., 2018. Land surface temperature as an indicator of the unsaturated zone thickness: a remote sensing approach in the Atacama Desert. Sci. Total Environ. 612:1234–1248.https://doi.org/10.1016/j.scitotenv.2017.08.305.

Van Lanen, H.A.J.,Wanders, N., Tallaksen, L.M., Van Loon, A.F., 2013. Hydrological drought across the world: impact of climate and physical catchment structure. Hydrol. Earth Syst. Sci. 17 (5):1715–1732. https://doi.org/10.5194/hess-17-1715-2013.

Vandewiele, G.L., Elias, A., 1995.Monthlywater balance of ungauged catchments obtained by geographical regionalization. J. Hydrol. 170:277–291. https://doi.org/10.1016/0022-1694(95)02681-E.

Vermote, E.F., Tamre, D., Deuze, J.L., Herman, M., Morcrette, J.J., 1997. Second Simulation of the Satellite Signal in the Solar Spectrum, 6s: An Overview. IEEE Trans. Geosci. Remote Sens. 35 (3):675–686. https://doi.org/10.1109/36.581987.

Vivirolí, D., Dür, H.H., Messerli, B., Meybeck, M., Weingartner, R., 2007. Mountains of the world, water towers for humanity: topology, mapping and global significance. Water Resour. Res. 43. https://doi.org/10.1029/2006WR005653.

Wagener, T., Wheater, H.S., 2006. Parameter estimation and regionalization for continuous rainfall-runoff models including uncertainty. J. Hydrol. 320:132–154. https://doi.org/10.1016/j.jhydrol.2005.07.015.

Wagener, T., Wheater, H.S., Gupta, H.V., 2004. Rainfall-runoff Modelling in Gauged and Ungauged Catchments. Imp. Coll. Press, London.

Wagener, T., Sivapalan,M., Troch, P.,Woods, R., 2007. Catchment classification and hydrologic similarity. Geography Compass 1 (4):901–931. https://doi.org/10.1111/j.1749-8198.2007.00039.x.

Wanders, N., Van Lanen, H.A.J., Van Loon, A.F., 2010. Indicators for drought characterization on a global scale. WATCH Technical Report No. 24 available at:. www.euwatch.org/publications/technical-reports, Accessed date: 9 January 2017.

Wanner, H., Holzhauser, H., Pfister, C., Zumbühl, H., 2000. Interannual to Century Scale Climate Variability in the European Alps (Die Klimavariabilität Im Europäischen Alpenraum Auf Der Zeitskala Von Jahren Bis Jahrhunderten). Erdkunde 54 (1):62–69 JSTOR. www.jstor.org/stable/25647250.

White,W.B., 2002. Karst hydrology: recent developments and open questions. Eng. Geol. 65 (2002):85–105. https://doi.org/10.1016/S0013-7952(01)00116-8.

Wright, J.L., 1982. New evapotranspiration crop coefficients. J. Irrig. Drain. Div. 108, 57–74.

Chapter 5

Estimating Evapotranspiration of Mediterranean Oak Savanna at Multiple Temporal and Spatial Resolutions. Implications for Water Resources Management

Carpintero, E., Anderson, M.C., Andreu, A., Hain, C., Gao, F., Kustas, W.P., González-Dugo, M.P., 2021. Estimating Evapotranspiration of Mediterranean Oak Savanna at Multiple Temporal and Spatial Resolutions. Implications for Water Resources Management. Remote Sens. 13 (18) 3701. https://doi.org/10.3390/rs13183701

Abstract

Mediterranean oak savanna is composed of a mixture of scattered oak trees, crops, pasture, and shrubs. It is the most widespread agroforestry landscape in Europe, and its conservation faces multiple threats including water scarcity, which has been exacerbated by global warming and greater climate variability. Evapotranspiration (ET) can be used as a proxy of the vegetation water status and response to water shortage conditions, providing relevant information about the ecosystem stability and its hydrological dynamics. This study evaluates a framework to estimate ET at multiple spatial and temporal scales and applies it to the monitoring of the oak savanna vegetation water consumption for the years 2013-2015. We used a remote sensing-based energy balance model (ALEXI/DisALEXI approach), and the STARFM data fusion technique to provide daily ET estimates at 30 m resolution. The results showed that modeled energy balance components compared well to ground measurements collected by an eddy covariance system, with root mean square error (RMSE) values ranging between 0.60 and 2.18 MJ m^{-2} d^{-1}, depending on the sensor dataset (MODIS or Landsat) and the flux. The daily 30 m ET series generated by STARFM presented an RMSE value of 0.67 mm d^{-1}, which yielded a slight improvement compared to using MODIS resolution or more simple interpolation approaches with Landsat. However, the major advantage of the high spatio-temporal resolution was found in the analysis of ET dynamics over different vegetation patches that shape the landscape structure and create different microclimates. Fine-scale ET maps (30 m, daily) provide key information difficult to detect at a coarser spatial resolution over heterogeneous landscapes and may assist management decisions at the field and farm scale.

5.1. Introduction

In water-controlled ecosystems with limited water resources, soil moisture dynamics play a central role in the existence and spatial distribution of the different vegetation functional types (Rodriguez-Iturbe et al., 2001; Rundel et al., 2016). The discontinuities in the functioning of these ecosystems are related to an alternation in the dry and wet periods (Gauquelin et al., 2016). A feedback relationship is observed in these environments, where the vegetation water consumption strongly conditions the hydrological balance of the system, while plants are impacted by water stress situations.

Higher variability in climate patterns coupled with an increase in water demand due to anthropogenic factors is expected to cause a considerable reduction in the quality and quantity of freshwater resources in the Mediterranean basin, intensifying recurrent water scarcity problems (Milano et al., 2013; Cramer et al., 2020). Climate forecasting models suggest that these regions will be subject to hotter and drier summers, with a higher occurrence of heatwaves and an increase in the frequency and severity of droughts (Thiébault et al., 2016; Lionello and Scarascia, 2018). Aridity and desertification processes

may lead to the abandonment of farmland and grazing areas and therefore, to land-use changes (García-Ruíz et al., 2011; Turco et al., 2014; Cramer et al., 2018). In this scenario of increased variability, accurate modeling of hydrological processes and their effects on the vegetation could assist decision-making when implementing government policies at different levels (local, regional, national, etc.), in order to mitigate global warming impact and reduce ecosystems' vulnerability.

Evapotranspiration (ET), or the water consumed by the canopy and evaporated from the soil, is a key process in semi-arid landscapes. ET functions as a proxy that reveals the vegetation water status, responding to situations of water scarcity. Moreover, regular monitoring of water consumption provides information about the system's stability and its hydrological dynamics. The use of thermal infrared (TIR) observations from satellite sensors in surface energy balance models to derive ET—as latent heat flux, the available energy for the ET process—has been widely validated over homogeneous crops and sparse vegetation covers (Diak and Whipple, 1995; Bastiaanssen et al., 1998; Timmermans et al., 2007; González-Dugo et al., 2009; Cammalleri et al., 2010), and more heterogeneous landscapes (Anderson et al., 2018; Knipper et al., 2019).

Some energy balance-based modeling approaches, such as the TSEB (Two Source Energy Balance) (Kustas and Norman, 1999) and SEBS (Surface Energy Balance System) (Su, 2002) models, have been applied with good results over savanna-type landscapes, at different spatial and time scales, with monitoring purposes (Andreu et al., 2018a, 2018b; Burchard-Levine et al., 2020; González-Dugo et al. 2021). The TSEB model proposes a separate estimation of the surface energy fluxes over the soil and the vegetation, based on the disaggregation of the radiometric surface temperature measured by the thermal sensors between these surface components. For large-area modeling, there are approaches for implementing the TSEB that have the advantage of not requiring any local observations as input, including the ALEXI model (Atmosphere-Land Exchange Inverse) (Anderson et al., 1997; 2007) and the associated flux disaggregation scheme named DisALEXI (Norman et al., 2003).

The European oak savanna landscape (known as *dehesa* in Spain and *montado* in Portugal) is the most widespread agroforestry system in the continent, occupying more than three million hectares (Moreno and Pulido, 2009) in the Iberian Peninsula. It has a canopy structure composed of a mosaic of scattered oak trees (mostly *Quercus Ilex* L. and *Quercus Suber* L.), crops, pasture, and shrubs. *Dehesas* provide multiple socio-economic uses (livestock, agriculture, hunting, etc.) with an essential role in the economy of rural areas (Moreno and Cáceres, 2016). They also are biodiversity reservoirs, listed in the EU directive as a habitat with community-wide interest (Díaz et al., 2013). Despite its importance, in recent decades numerous threats are endangering the *dehesa* conservation, such as the lack of natural regeneration of tree species (Plieninger et al., 2010), profitability problems, or soil degradation mainly caused by the intensification of agricultural and

livestock activities (Coelho et al., 2004; Moreno and Pulido, 2009). Climate change is worsening this fragile environment.

The multiple vegetation layers that compose this typical Mediterranean ecosystem vary in phenology, physiology, and function, each one contributing in a different way to the turbulent exchanges and the radiative transfer budget (Baldocchi et al., 2004), with impact on the local microclimate and hydrology. For instance, most tree species are evergreen and tolerate high irradiance while limiting carbon assimilation either by stomatal closure or a decrease of photosynthetic capacity, which are adaptation mechanisms to cope with the water scarcity conditions (Baldocchi and Xu, 2007; Joffre et al., 2008). Meanwhile, the underlayer of annual species emerges after the first rainfalls in autumn and dries up during the summer.

Although the *dehesa* can be considered a homogeneous system on a regional scale, differences in tree/grass/crops/scrub and bare soil cover fractions can be observed at finer scales. The combined differential functioning and characteristics of the different patches of vegetation affect the biogeochemical flux dynamics, resulting in a high spatial and temporal variability and creating distinct intra-ecosystem microclimates (Chen et al., 1999; Johnston et al., 2021). This structure plays an important role in *dehesas*' resilience, making the system an efficient convector of sensible heat and keeping the canopy surface temperature within the survival range (Baldocchi et al., 2004).

Within this context, the monitoring of ET with high resolution in both time and space can help to assess landscape structure and to perform a disaggregated evaluation of areas mostly covered by grasslands, and areas with higher tree or bush coverage. The analysis of the spatial and temporal variations in the hydrological conditions controlling the production of pastures and acorns, the two primary sources of livestock feed in the *dehesa*, can provide information critical for adjusting management practices at the farm scale, with an important impact on the ecosystem conservation and profitability.

Space agencies and companies are making major efforts to distribute high-resolution products, but the current satellite programs present limitations in offering thermal information with high spatial and temporal resolution (e.g., 30 m/daily) simultaneously. An additional problem is the presence of clouds that often result in longer periods without useful images. Multi-scale remotely sensed data fusion techniques are a viable alternative to improve the spatio-temporal resolution of ET estimates derived from thermal-based modeling. The Spatial and Temporal Adaptive Reflectance Fusion Model, STARFM, was developed by Gao et al. (2006) to initially integrate surface reflectance data from multiple sensors (Zhu et al., 2010; Walker et al., 2012), but more recently it has been applied to fuse ET retrievals with satisfactory results in homogeneous agricultural and forested/mosaic areas (Cammalleri et al., 2013, 2014; Semmens et al., 2016; Yang et al., 2017; Anderson et al., 2018; Knipper et al., 2019). These studies demonstrated that data fusion modeling

improved the accuracy in the estimation of the water consumed by the vegetation, identifying small areas with deficits or excessive irrigation.

This research monitors the vegetation water use in the oak-grass savanna landscape of a small Mediterranean watershed of Southern Spain at different spatial and temporal scales. The specific objectives of the study were:

i) To evaluate the utility of a surface energy balance model (ALEXI/DisALEXI) and the STARFM data fusion technique, using multiple remote sensing platforms (Landsat 7/8 and MODIS), to estimate high-resolution ET in time and space over the complex canopy structure of Mediterranean oak savannas.

ii) To analyze the opportunities offered by this high-resolution product to provide information that is useful to improve the water and vegetation management of this agroforestry system at a field scale. To do that, we evaluated the water use patterns of the herbaceous stratum and other small heterogeneous vegetation patches typical of the *dehesa* (e.g., scrubs, humid areas, creek shore), which shape the landscape structure and reflect the existence of different micro-ecosystems and climates. Finally, the cumulative monthly ET generated by the different approaches with different spatial resolutions (1 km and 30 m) was quantified over the same vegetation patches.

5.2. Materials and Methods

5.2.1. Description of the Study Area and Experimental Site

The study was conducted over the *Martin Gonzalo* watershed (48.4 km^2), part of the larger Guadalquivir River basin located in Southern Spain (Figure 5.1a,c). The elevation range varies from 760 m in the north to 280 m at the outlet of the watershed, where there is a dam. The continental Mediterranean climate of this area is highly seasonal, with moderately cold winters alternating with hot and long dry summers. The rainfall presents intra- and inter-year variability, with an annual average of 895 mm (from 1990 to 2015) concentrated during spring and fall.

The landscape is mainly occupied by homogeneous *dehesa*, along with some conifer forests and olive groves. *Dehesa* is a Mediterranean oak savanna, whose canopy structure is composed of sparse clumped trees and a grassland or crops understory. In this ecosystem, extensive livestock production fed with acorns and grass is the main economic activity, but they also provide other uses, such as cork, cereal production, hunting, mushroom harvesting, and beekeeping. They offer as well multiple environmental services, such as biodiversity hotspots, water provisioning, CO_2 fixation and high diversity of habitats (Campos et al., 2013; Moreno and Cáceres, 2016).

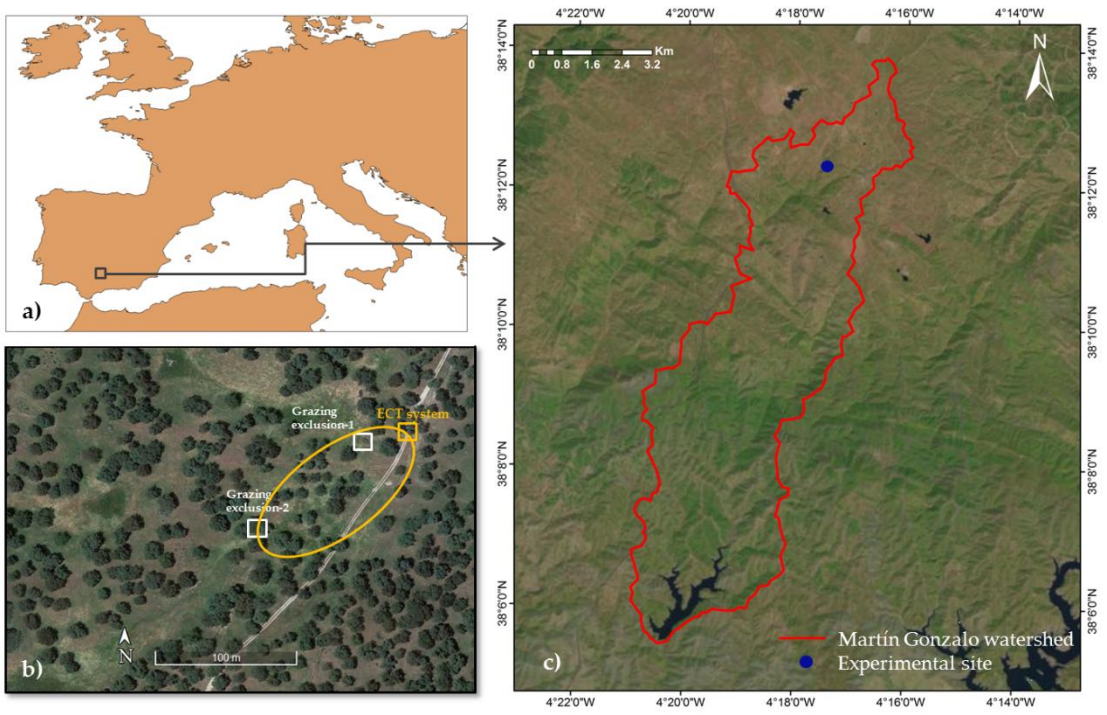

Figure 5.1. (a) and (c) Location of the study area and experimental site; (b) Aerial photograph of validation site showing the distribution of the three fields discussed in the text. ECT: eddy covariance tower. The orange ellipse represents the predominant fetch of the ECT.

Ground validation measurements were taken at an experimental site (*Santa Clotilde*, 38° 12′ N, 4° 17′ W, 736 m a.s.l, Figure 5.1c), located in a *dehesa* farm within the studied watershed. The setup included an eddy covariance tower (ECT) over the combined tree + grassland system and two grazing exclusion enclosures (over open grassland and under an oak tree respectively) to take into account the heterogeneity of the area (Figure 5.1b). All energy balance components: the turbulent fluxes of sensible heat (H) and latent heat (LE), net radiation (Rn) and the heat flux transport across the surface soil (G), were measured continuously.

The ECT system was installed on a tower at 18 m above ground level in April 2012, registering the ecosystem response as a whole (Figure 5.2a). The system included a 3D sonic anemometer (model CSAT3, Campbell Scientific Inc. Mention of trade names or commercial products in this publication is solely for the purpose of providing specific information and does not imply recommendation or endorsement by the U.S. Department of Agriculture) that measures horizontal and vertical fluctuations of temperature and wind speed, and a hygrometer (model KH20, Campbell Scientific Inc.) to estimate water vapor fluctuations, the latter being replaced in 2015 by an open Path CO_2/H_2O Gas Analyzer LICOR-7500, taking simultaneous measurements of carbon dioxide and water vapor in turbulent air structures (Figure 5.2b). These eddy covariance measurements were recorded

with a frequency of 10 Hz and corrected for density effects due to heat and water vapor transfer (Webb et al., 1980).

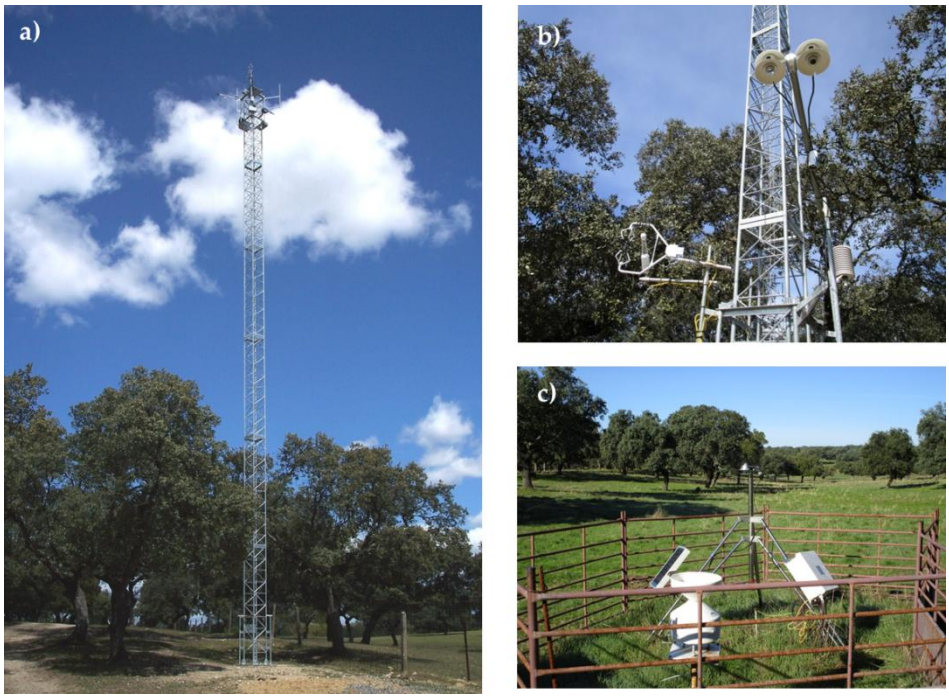

Figure 5.2. (a) Eddy covariance tower (ECT) over the combined tree + grassland system; (b) equipment installed on the tower; (c) Grazing exclusion enclosure over open grassland.

A relative humidity and air temperature probe (model HMP155, Vaisala) and a net radiometer (model NR-Lite, Kipp&Zonen, Delft, Netherlands) to obtain the net radiation were also installed at the tower. In 2015, the net radiometer was replaced by a four-component-net-radiation sensor (model NR01, Hukseflux Thermal Sensors, Delft, Netherlands) (Figure 5.2b). More information on the experimental site and the equipment can be found in Andreu et al. (2018a) and Carpintero et al. (2020).

The quality of the energy balance fluxes measured with the ECT was tested by Andreu et al. (2018a) for the 2012 summer season, resulting in an average closure balance ($Rn - G = LE + H$) of 86% of available energy. For the period 2014–2015, the closure balance was 91%. For the comparison with modeled LE, the latent heat fluxes obtained by forcing the closure of the energy balance with the residual method was preferred to direct LE measurement. This method assumes that the sensible heat, H, is correctly measured and LE is obtained by solving the surface energy balance equation. Daytime-integrated energy fluxes were calculated by averaging half-hourly values focusing on daytime fluxes and not considering overnight fluxes.

5.2.2. Modelling Framework

Figure 5.3 shows the flowchart of the modeling framework applied for the period 2013–2015. The process starts with a global ET product (5 km, daily) developed using the ALEXI model based on MODIS day-night temperature differences (Hain and Anderson, 2017). In the second step, the ALEXI ET fluxes are disaggregated to higher resolutions over the study area, using the flux disaggregation scheme DisALEXI applied to both MODIS (1 km, daily) and Landsat 7/8 (60-100 m, 16 days) images. Finally, both types of ET maps, the infrequent Landsat at 30 m resolution and the daily images at MODIS-scale generated by DisALEXI, are combined using the data fusion technique STARFM to provide ET estimates with both fine spatial (30 m) and temporal (daily) resolution.

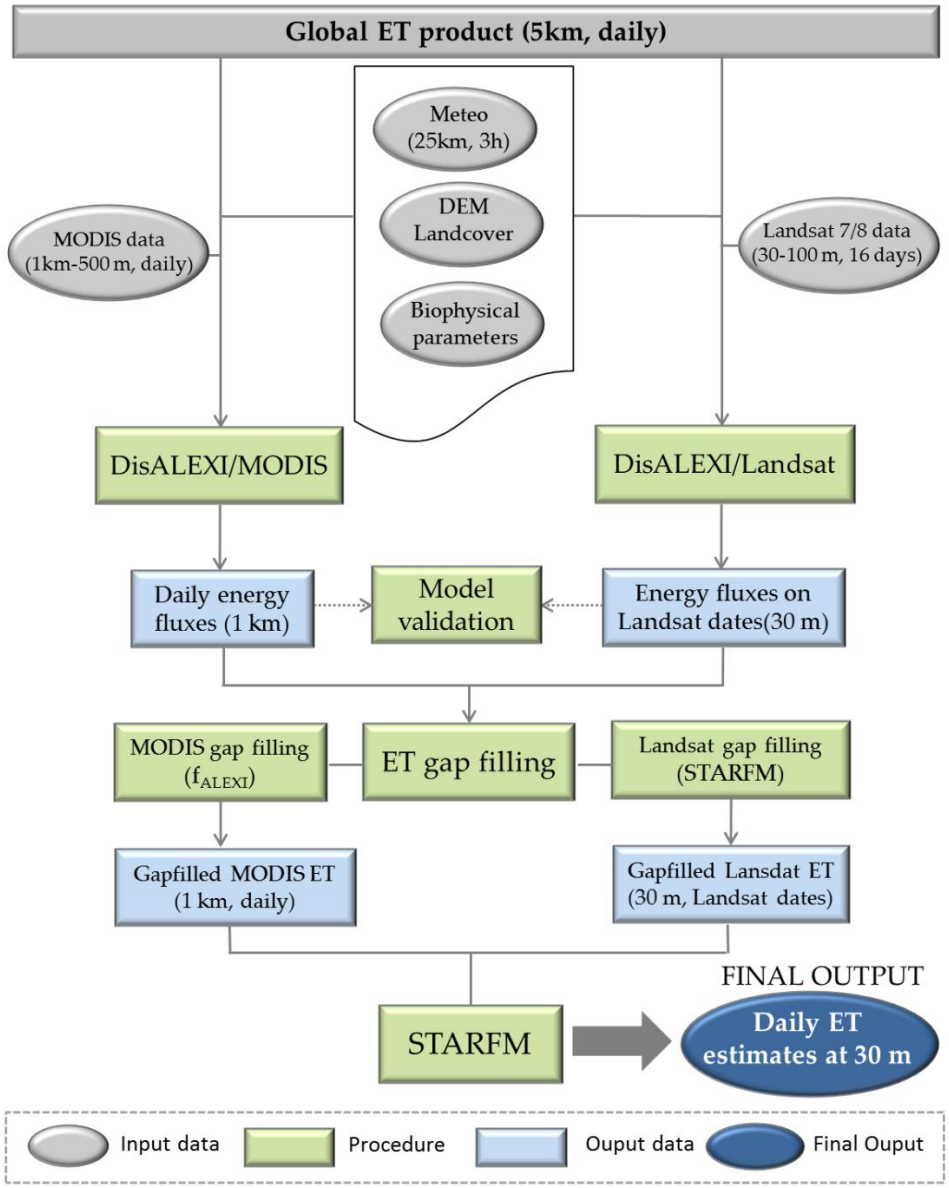

Figure 5.3. Flowchart of modeling framework applied to generate high resolution ET estimations.

5.2.2.1. ALEXI/DisALEXI Model

The Atmosphere-Land Exchange Inverse (ALEXI) model (Anderson et al., 1997, 2007) and the associated flux disaggregation technique (DisALEXI) (Norman et al., 2003) are based on the Two Source Energy Balance (TSEB) model.

The TSEB model partitions the surface blackbody radiance into the soil/substrate (T_S) and vegetated canopy (T_C) blackbody temperatures, being weighted by the cover fraction of each component at the sensor view angle, $f(\varphi)$, and resulting in:

$$T_{RAD}(\varphi) \approx (f(\varphi)T_c^4 + [1 - f(\varphi)]T_s^4)^{\frac{1}{4}} \quad (5.1)$$

The surface energy balance is solved for the whole soil-canopy-atmosphere system, and for each individual component, with Equations 5.2-5.3:

$$Rn_s = H_s + LE_s + G \quad (5.2)$$

$$Rn_c = H_c + LE_c \quad (5.3)$$

where the subscripts "*s*" and "*c*" represent fluxes from the soil and canopy, respectively. Norman et al. (1995) present a description of the original model, and further improvements can be found in Kustas and Norman (1999).

The ALEXI model was designed to reduce the use of ancillary meteorological data while maintaining a physically realistic representation of land-atmosphere exchange over a wide range of vegetation coverages. ALEXI implements the TSEB in a time-differential mode, applying this scheme two times during the morning, using surface radiometric temperature data generally provided by geostationary satellites. In this mode, the sensibility of the model to absolute temperature biases is reduced (Anderson et al., 2007). In ALEXI, TSEB is coupled with an atmospheric boundary layer model to internally simulate the effect of land-atmosphere feedback on the near-surface air temperature (Anderson et al., 2012). One limitation of this procedure is the dependence on geostationary datasets, with different calibrations and temporal extensions. For this reason, in this research, a global ET product developed using the non-geostationary MODIS sensor day-night temperature differences has been used. As a result, ALEXI generates surface energy fluxes at the continental scale, but at the coarse spatial resolution, of several km.

The DisALEXI scheme runs the TSEB using higher resolution thermal data from polar-orbiting satellites, such as MODIS or Landsat, for mapping finer spatial resolution fluxes. It iteratively adjusts the air temperature boundary conditions such that the disaggregated daily ET flux field reaggregates up to the coarse-resolution ALEXI regional baseline. This spatial disaggregation technique facilitates consistent flux evaluations at local to continental scales (Anderson et al., 2012). This ALEXI/DisALEXI framework has

been widely evaluated across the United States and Europe (Anderson et al., 2004, 2010, 2012).

5.2.2.2. Remote Sensing Data Fusion Method

The STARFM model (Gao et al., 2006) is a remotely sensed data fusion algorithm that allows an improvement of the temporal representation of ET variations between clear Landsat dates. It was originally designed to blend surface reflectance data, but the fusion of ET maps has been successfully conducted over a number of land covers by Cammalleri et al. (2013, 2014) over rain-fed and irrigated agricultural areas in the Midwestern United States and over irrigated crops in Texas, by Semmens et al. (2016) and Knipper et al. (2019) over California vineyards, by Anderson et al. (2018) over the California Delta and by Yang et al. (2017, 2021) over forested landscapes. It combines information at a high-temporal frequency from MODIS and high-spatial-resolution from Landsat. STARFM compares one or two Landsat/MODIS image pairs acquired on the same day to predict maps at Landsat spatial scale on other MODIS dates.

Following the weighting function (Equation 5.4), STARFM model predicts ET for the central pixel of a selected moving window at generic date (t_0):

$$L\left(x_{w/2}, y_{w/2}, t_0\right) = \sum_{i=1}^{w} \sum_{j=1}^{w} \sum_{k=1}^{n} W_{ijk}\left[M(x_i, y_j, t_0) + L(x_i, y_j, t_k) - M(x_i, y_j, t_k)\right] \quad (5.4)$$

where w is the searching window size; ($x_{w/2}$, $y_{w/2}$) is the central pixel of this moving window; n is the number of Landsat and MODIS pairs used (in this case only one pair) and W is the weighting factor. The weighting function (W) integrates the spatial differences between the Landsat (L) and MODIS (M) images on the acquisition date t_k and also the temporal differences between MODIS images from observed and predicted dates, t_k and t_0 respectively. The prediction for the central pixel only uses spectrally (or ET) similar pixels within the searching window. Further details about the STARFM model are provided by Gao et al. (2006).

5.2.2.3. ET Data Gap Filling

Prior to the fusion algorithm, MODIS and Landsat ET maps produced by DisALEXI were preprocessed to fill the gaps created by clouds or instrument issues (e.g., the failure of scan-line corrector in Landsat-7 ETM+). The gaps in MODIS images were filled to obtain a full daily coverage at 1 km resolution. To accomplish this, the ratio between MODIS and ALEXI ET was computed on MODIS days (f_{ALEXI} = ET MODIS/ET ALEXI), then smoothed and filled using the Savitsky–Golay method described by Sun et al. (2017). The

smoothed and filled f_{ALEXI} time series maps were then multiplied by daily ALEXI ET to obtain daily MODIS ET (Figure 5.3). The technique used to ensure optimal spatial coverage in Landsat maps employing the STARFM model was described by Yang et al. (2017) (Figure 5.3). It combines the gapped ET image with a prediction from STARFM on the target date using a nearby MODIS-Landsat date pair.

5.2.2.4. Simple ET Interpolation Methods

In parallel to the application of the STARFM framework to obtain a daily 30 m ET series, daily ET values obtained with a simpler data interpolation method were also generated for comparison purposes. It used the potential ET and MODIS ET as scaling fluxes. The objective was to evaluate the advantages of using the STARFM technique with respect to these simpler and less demanding methods. In this interpolation approach, the ratio between the Landsat ET and a daily scaling flux (potential and MODIS ET) was computed on clear dates. These ratios (FPET = Landsat ET/Potential ET and FMOD = Landsat ET/MODIS ET) were then linearly interpolated in time and fused in the daily ET estimation.

5.2.3. Model Input Datasets

5.2.3.1. Landsat Data

This work employed a set of 82 Pre-collection and Collection 1 scenes (path 200/row 33) from the Landsat 7 and 8 satellites, acquired from January 2013 to December 2015. Scenes with high cloud coverage were excluded. The Landsat surface reflectance climate data record (SR CDR) (http://espa.cr.usgs.gov/, accessed on 2 September 2017) (distributed atmospherically corrected) was used to compute the leaf area index (LAI) and albedo parameters. A simple approach proposed by Liang et al. (2000) was applied to calculate albedo at a 30 m resolution using six surface reflectance bands. To estimate LAI at 30 m on Landsat overpass dates, the regression tree approach developed by Gao et al. (2012a) was used, which was trained with samples from the MODIS LAI products and Landsat reflectance. This method has been successfully applied to annual and woody crops (Gao et al., 2012a; Semmens et al., 2016). Landsat thermal band data were corrected for atmospheric and surface emissivity effects using the atmospheric radiative transfer model MODTRAN (Berk et al., 1987), and subsequently sharpened to the shortwave bands' spatial resolution (30 m) using the Data Mining Sharpener (DMS) method (Gao et al., 2012b).

5.2.3.2. MODIS Data

MODIS images from Collection 5 (at 1 km spatial resolution) and Collection 6 (500 m) with variable temporal resolution were also used as inputs in the DisALEXI application, including data of land surface temperature (LST; MOD11_L2), geolocation (MOD03), and LAI (MCD15A3). The radiometric temperature with a daily frequency was derived from the 5-min swath LST product, MOD11_L2. The 4-day LAI product, integrated into the TIMESAT algorithm (Jönson et al., 2004), allowed for creating a smoothed and filled daily LAI time series.

As with other DisALEXI application inputs, the global albedo product from Boston University (ftp://rsftp.eeos.umb.edu/data02/Gapfilled/, accessed on 20 September 2017), in addition to the yearly and global MODIS product of land cover (MCD12Q1, 500 m) were included. The albedo data is a global gap-filled snow-free albedo product, which is temporally smoothed and composed over a global grid.

5.2.3.3. Meteorological Input Data and Vegetation Properties

The energy balance-based modeling framework requires several regional meteorological datasets: a series of surface atmospheric pressure, wind speed at 30 m, and air temperature and specific humidity at 2 m. These were provided every 3 h at a 25 km spatial resolution by the Climate Forecast System Reanalysis (CFSR) (Saha et al., 2010). Hourly insolation data at a spatial resolution of 25 km were also obtained from the CFSR. As part of the regional information, a global digital elevation model at a 30 m resolution from ASTER (a product of METI and NASA) and the Andalusian land cover map 2010 were also employed.

A set of biophysical parameters associated with the vegetation in Mediterranean savanna ecosystems were used. The vegetation ground cover fraction, clumping factor and canopy height were calculated following Andreu et al. (2018a).

5.2.3.4. Input Data Filtering

In order to isolate errors caused by poor input data quality, the insolation and LST data were filtered for fluxes comparison using ground information. It is known that the quality of insolation data is the primary driver of the total energy available for the ET process (Anderson et al., 2018), and TSEB is mostly driven by thermal information. Both variables were compared with the data measured at the experimental site, showing a mean relative error (mean absolute error/observed mean value; RE) of 9.4% in insolation and 14.5% in surface temperature. The days in which the RE value was higher than 25% in insolation data or higher than 50% in surface temperature were eliminated from the flux comparison analysis. Remotely sensed LST was compared with the half-hourly infrared temperature

value corresponding to the time of the satellite overpass. In this case, given the variations between both values and the mismatch representativeness (IR thermometer is mostly measuring canopy—Figure 5.2b), the threshold considered for filtering the data is less restrictive than for radiation.

5.2.4. Global Remotely Sensed ET Product

The 8-day total ET provided by a product at a 500 m pixel resolution (MOD16A2, Collection 6) was used for comparison purposes. This data collection uses Mu et al.'s (2011) improved algorithm. It is based on the logic of the Penman-Monteith equation which includes inputs of daily meteorological reanalysis data along with MODIS data, such as albedo, LAI, fraction of photosynthetically active radiation (FPAR) and land cover.

5.3. Results

5.3.1. Evaluation of Surface Energy Fluxes at the Flux Tower Site

The frequency distribution of the wind direction at the ECT for 2015 showed the southwest as the predominant fetch. A *footprint* analysis was performed by estimating the contribution areas to daily fluxes for 132 days of 2015 as described by Hsieh et al. (2000). An extensive description of the methodology can be found in Kustas et al. (2015). Over the period analyzed, it is observed that 78% of the system ECT fluxes were collected from an area within 130 m upwind (Figure 5.1b), with the maximum contribution to the measured energy fluxes at approximately 33 m upwind. According to these results, average values of a 3 × 3 grid cell (with 30x30 m size-cell and located to the southwest of the ECT) of the modeled fluxes were evaluated.

The relationship between the daily energy fluxes (daytime integrated fluxes) observed at the ECT and modeled by the DisALEXI application is plotted in Figure 5.4, using MODIS (Figure 5.4a) and Landsat images (Figure 5.4b). The comparison was made on days in which both in-situ measurements and input information for the model were available, with a larger set of usable field data corresponding to 2014 and 2015. In addition, 22 days were filtered from the comparison with DisALEXI/MODIS and 5 days for DisALEXI/Landsat, due to the lack of input data quality (for further information about the input data filtering, see Section 5.2.3.4). A total of 313 days were used in the comparison for MODIS data and 44 images for Landsat. In all three years, there was a general shortage of clear images and/or field measurements during the last part of the winter and early spring. This is the rainy season for this region and the absence of available data hindered incorporating enough observations representative of this period in the statistical analysis. Statistical metrics, such as mean absolute error (MAE), root mean square error (RMSE),

mean bias error (MBE) and coefficient of determination (R^2) are presented for all the daily energy fluxes generated by DisALEXI application for the period 2013-2015 (Table 5.1).

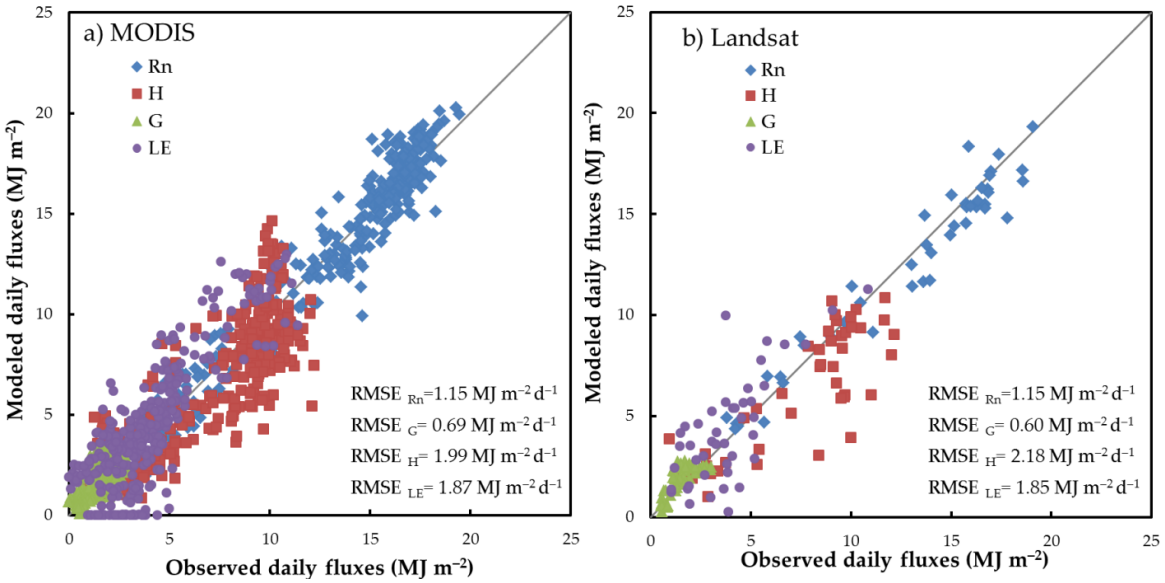

Figure 5.4. Comparison between observed and modeled daytime integrated energy fluxes obtained from DisALEXI procedure using (**a**) MODIS and (**b**) Landsat images for the years 2013–2015.

Table 5.1. Statistical metrics of daily energy fluxes generated by DisALEXI application with MODIS and Landsat images for 2013-2015.

	Flux	$\bar{O}$ (MJ m^{-2} d^{-1})	MAE (MJ m^{-2} d^{-1})	RMSE (MJ m^{-2} d^{-1})	MBE (MJ m^{-2} d^{-1})	R^2
MODIS	Rn	12.93	0.91	1.15	0.11	0.95
	G	1.59	0.56	0.69	0.35	0.52
	H	7.34	1.64	1.99	−0.60	0.69
	LE	4.01	1.54	1.87	0.37	0.69
Landsat	Rn	12.90	0.91	1.15	−0.33	0.94
	G	1.52	0.46	0.60	0.32	0.60
	H	7.52	1.56	2.18	−1.16	0.68
	LE	3.86	1.46	1.85	0.50	0.56

$\bar{O}$ = mean observed flux; MAE = mean absolute error; RMSE = root mean square error; MBE = mean bias error; R^2 = coefficient of determination.

Modeled Rn generally agreed with in-situ measurements (RMSE value of 1.15 MJ m^{-2} d^{-1} and R^2 = 0.94–0.95). Rn behavior was different depending on the satellite sensor, slightly overestimated with MODIS data and underestimated when using Landsat images. Insolation (solar incoming radiation) inputs for both applications were the same, but with different albedo and fractional cover values to derive the energy available for the photosynthesis process. The soil heat flux estimations presented a good agreement (RMSE of 0.69 for MODIS and 0.60 MJ m^{-2} d^{-1} for Landsat), worthy of mention in this ecosystem with bare soil patches and high temperatures, where G can use up to 20% of the available energy.

RMSE and MAE errors observed with Landsat images were equal or slightly lower than those generated with MODIS for Rn, G and LE, possibly due to the better footprint representation of the higher resolution input data. The RMSE value for H was equal to 1.99 MJ m^{-2} d^{-1} when using MODIS data, and 2.18 MJ m^{-2} d^{-1} with Landsat. A general underestimation of the H flux can be observed in Figure 5.4, corroborated by the negative MBE values obtained with both sensors. Modeled LE fluxes had RMSE values of 1.87 MJ m^{-2} d^{-1} with MODIS, and 1.85 MJ m^{-2} d^{-1} with Landsat (in mass flux units, 0.76 mm d^{-1}), with an overestimation of the modeled fluxes (MBE of 0.37 and 0.50 MJ m^{-2} d^{-1} or 0.15 and 0.20 mm d^{-1}, respectively), except for low LE values. On the other hand, the values of the coefficient of determination were in the range 0.56-0.69 using Landsat and MODIS for both convective fluxes (H and LE).

5.3.2. Analysis of ET Time Series from DisALEXI and STARFM

Figure 5.5 depicts the ET time series generated by DisALEXI (MODIS—1 km and Landsat—30 m) and STARFM approaches for the years 2013–2015, along with the closure-corrected ET measurements acquired by the *dehesa* ECT system and the rainfall observations. It can be observed in Figure 5.5 that in this ecosystem (with ~25% fraction tree cover) the annual ET curve is bimodal, with two distinct peaks of different sizes. The largest peak occurs during the spring, reaching maximum values of around 4–5 mm d^{-1}. A second and smaller peak appears in autumn, with maximum values of around 2–2.5 mm d^{-1} in 2013–2014 and 1.5 mm d^{-1} in 2015. This pattern is closely linked to the distribution of the annual rainfall throughout the year, defining the general pattern of soil water availability, and the vegetation growth dynamics, as well as by the energy available for evaporation.

The modeled ET reasonably reproduced the temporal dynamics of consumptive water use observed by the flux tower instruments. In general terms, the maximum peaks reached in the spring seasons, as well as the gradual decrease of ET during the end of the spring and summer seasons (periods with higher data available) were accurately reproduced by the STARFM and DisALEXI approaches (Figure 5.5).

The annual ET modeled by STARFM was equal to 600 mm in the hydrological year 2013/2014 (1 October to 30 September), and 578 mm in the year 2014/2015, with rainfall values of 704 mm and 511 mm for each hydrological year, respectively. These results reflect the evolving vegetation water needs and how the ecosystem adapts to differing water availability conditions, with 193 mm less rainfall during the second year. It also highlights the major role that ET plays in the water balance of the system.

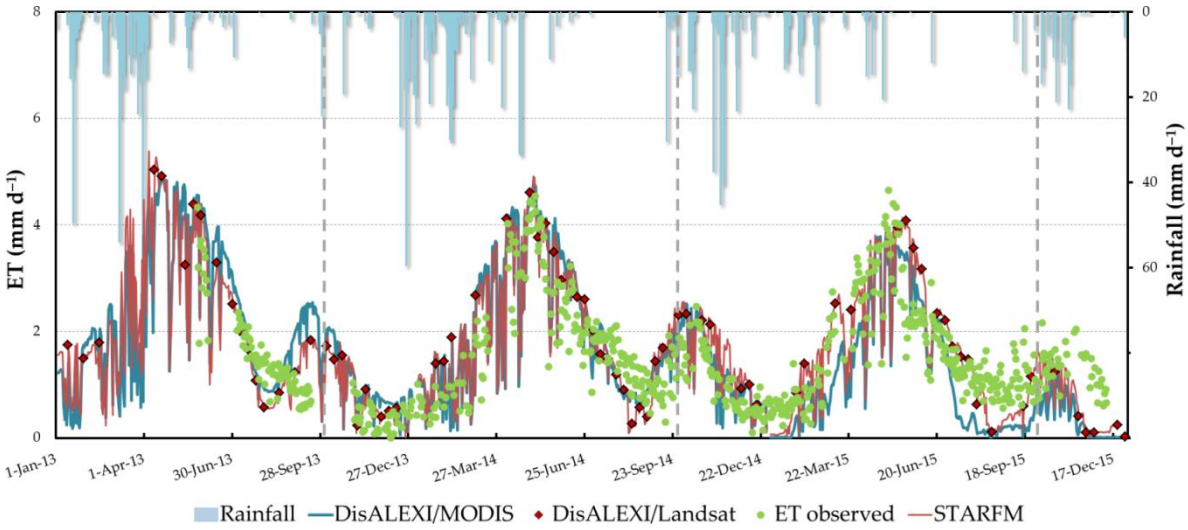

Figure 5.5. *ET* time series over the *dehesa* ecosystem from DisALEXI/MODIS, DisALEXI/Landsat, STARFM approach and observed data with closure correction for 2013, 2014 and 2015. Blue bars illustrate rainfall events and gray vertical lines indicate the starting of a hydrological year.

Looking at the details of seasonal water use more closely, we see that the water consumption in the spring of 2015 was similar to that of 2014, as well as the vegetation growth (NDVI values were similar for both years), even though the rainfall was considerably lower (spring rainfall of 120 mm in 2014 and 71 mm in 2015). In this case, the vegetation water consumption in the spring-2015 may have been tapping soil water storage from an unusually high rainfall in the previous autumn (311 mm in autumn—2014 compared to 103 mm of autumn—2013), pointing out the importance of the antecedent soil moisture conditions and the recharge of the subsurface layers.

During the summers, observed ET fell to low values (around 1.1 and 1.4 mm d^{-1} on average for the months of July and August), with minima around 0.7 mm d^{-1} at the end of the dry season (in early September before the first rainfalls). In addition to this summer-time soil-moisture limited minimum, a similar shut-down of the vegetation was observed

during the winter (average ET around 0.7 in January and February), due to the lack of insolation.

Despite the generally good fit of ET estimations with ECT observations during the study period, some seasonal mismatches between modeled and observed fluxes can be identified. For example, modeled ET increased at the end of the summer in 2013 (on September 3) after a light rainfall event (<2 mm), while ET observations continued to decrease. While the second peak in the observed flux series is missing due to a gap in the field data from September 28, it appears that the rise in ET outlined by Landsat and STARFM preceded the observed rise following rainfall on September 27 (36 mm event). At the end of the dry season of 2014, similar behavior was observed with a gradual increase of modeled estimates starting on September 1, although it was not until September 17 when a significant rainfall event happened (approx. 46 mm). During the wet season in mid-May of 2015, the model showed a lagged response to a drydown that caused the vegetation to dry quickly. This may be related to smoothing/gap-filling in the baseline ALEXI time series, which can tend to smooth out abrupt changes in fPET.

A comparative analysis between the different daily ET series and the observed measurements at the ECT is shown in Table 5.2 including the quantitative performance of the following daily ET retrievals: (a) from DisALEXI 1 km gap-filled MODIS, (b) STARFM from Landsat-MODIS, and (c) from a simple Landsat-only interpolation technique (using the potential ET as a daily scaling input, through the ratio FPET). The analysis was carried out for a period of 584 days. Results obtained with the Landsat interpolated ET series using MODIS as a daily scaling input (not shown) are similar to those obtained using FPET.

Table 5.2. Comparison of different daily ET retrievals modeled for the period 2013-2015.

	MODIS	**MODIS-Landsat (STARFM)**	**Interpolated Landsat (Using FPET)**
MAE (mm d^{-1})	0.589	0.539	0.596
RMSE (mm d^{-1})	0.737	0.673	0.749
MBE (mm d^{-1})	0.005	0.103	0.158

The data fusion algorithm for estimating daily 30 m ET outperformed the simpler interpolation technique based on FPET and using MODIS 1-km ET, yielding an RMSE value of 0.67 mm d^{-1}.

5.3.3. Evaluation of the MOD16A2 Global ET Product

Figure 5.6 shows data of the 8-day total ET layer provided by the global product MOD16A2 (500 m spatial resolution) at the tower pixel, together with the data observed at the ECT and the water consumption modeled by the STARFM approach. The MODIS ET product agreed poorly with the ECT observations (MAE = 0.79 mm d^{-1} and RMSE= 1.02 mm d^{-1}), with a significant underestimation (MBE = −0.56 mm d^{-1}). The error was unevenly distributed throughout the year, being more pronounced in the spring and summer seasons, and lessened in autumn and winter. This trend is observed in the three years and it highlights that the use of this product will underestimate ET rates over this semiarid ecosystem.

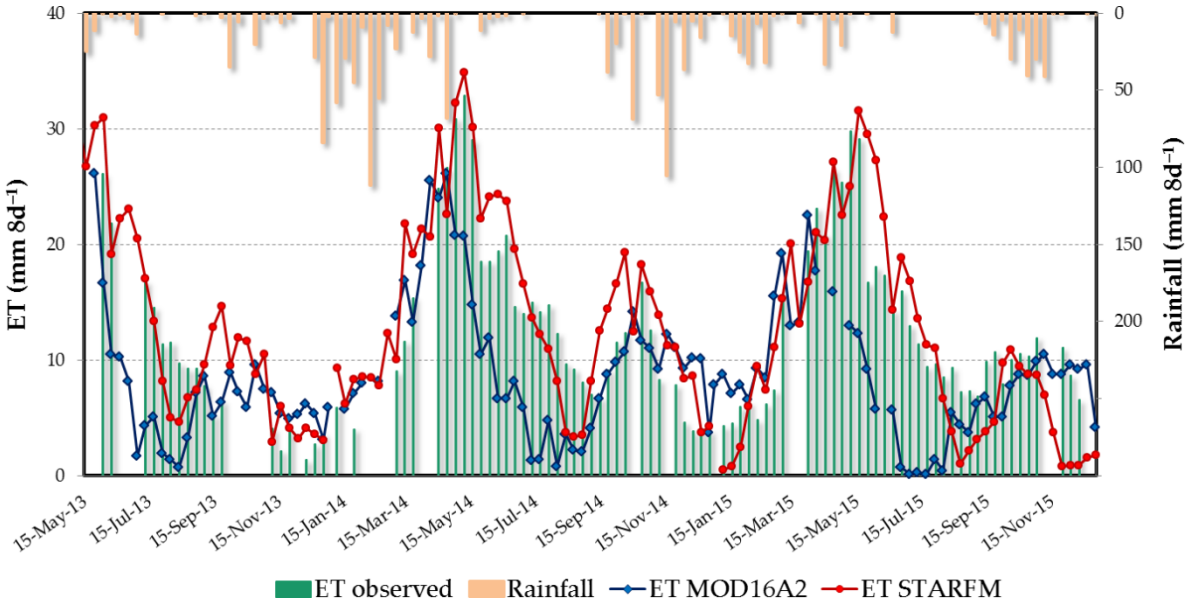

Figure 5.6. Comparison between observed, modeled by STARFM and MOD16A2 product ET for 2013-2015. Burnt orange bars illustrate rainfall events.

5.3.4. Water Resources Management at Field Scale Using High-Resolution ET Maps

At the field scale, the *dehesa* ecosystem presents variations in the distribution of vegetation strata (oak trees, grassland, crops, or scrubs) that affect the provisioning of ecosystem services and must be considered in the management of the livestock. Within this context, the evolution of daily ET at four characteristic micro-ecosystems/patches of the *dehesa* within the study area (Figure 5.1c), with different vegetation canopy structures and livestock feed production strategies has been analyzed at two spatial resolutions (30 m and 1 km) to evaluate the potential of Landsat-scale ET retrievals (Figure 5.7).

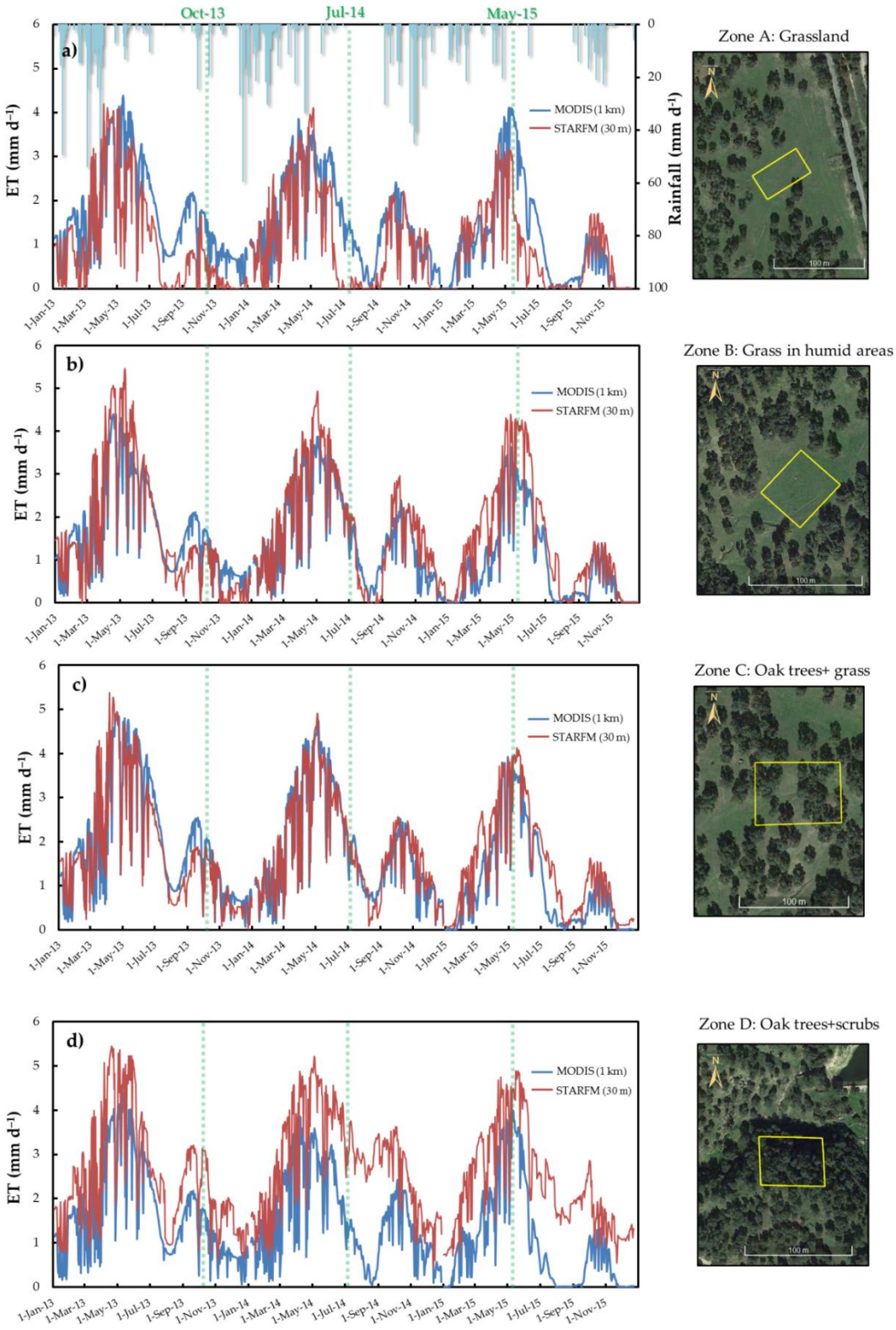

Figure 5.7. Evolution of daily ET generated by DisALEXI/MODIS (1 km) and STARFM (30 m) over an area (denoted by the yellow polygons) of grassland (a), of grass in humid areas (b), of combined oak tree and grassland (c) and of oak trees and scrub (d). The green vertical dashed lines correspond to dates that are analyzed in Section 5.3.4.

Zone A (1700 m^2) is an open grassland without trees. It is a grazing area, which exhibits high temporal and spatial variability in vegetation growth. Zone B (2400 m^2) is a pasture area where there is a land depression accumulating water through most of the year and maintaining high humidity conditions. Zone C (4300 m^2) is a mixture of tree/grass, with an average tree fractional cover of around ~25%, common in *dehesa* production systems and similar to the ECT surrounding area. Acorn production to feed Iberian pigs is usually the main economic use of these landscapes. The final area, zone D (3300 m^2), is located near a stream with a high ground fraction covered by trees and an evergreen underlayer of scrubs.

Significant differences were observed between the daily ET provided by DisALEXI/MODIS at a 1 km resolution and modeled ET with STARFM approach at a 30 m resolution, especially pronounced over zones A and D (Figure 5.7). Despite the relatively small area of these sites, the 30 m spatial resolution better captured the scale of heterogeneity in this landscape, whereas at 1 km, multiple vegetation covers are contributing, resulting in similar ET patterns for all the sites at this scale.

In the grassland area (Figure 5.7a), the STARFM 30 m ET decreases more rapidly in the spring than the MODIS-DisALEXI 1 km ET. This decrease corresponds to the drying of the herbaceous stratum, and thus the reduction in the available pasture for forage. Because there are no trees in the STARFM extraction area, transpiration flux is not appreciable during the summer months. The MODIS estimates include contributions from surrounding trees and therefore, maintain significant ET rates during the dry seasons. In each year, the pasture drying process started in May and ended in early to mid-July.

In contrast to zone A, in zone B the late spring decrease in ET is more gradual due to the high soil moisture conditions. The behavior during this season was accurately reproduced by the 30 m resolution model data. In this case, the 30 m and 1 km ET timeseries are more similar to the wet grassland (absent moisture limitations), mimics the transpiration curve of the surrounding trees. The main differences are during springtime peaks, where STARFM reaches values around 4.5–5 mm d^{-1}, and about 4 mm d^{-1} with MODIS.

In zone C, the differences between DisALEXI/MODIS and STARFM were not pronounced due to the homogeneity of the surrounding landscape. This type of landscape is representative of the most common structure of the *dehesa* ecosystem, following a behavior similar to that described in Section 5.3.2.

Finally, in zone D we see that the 1 km MODIS information is not able to resolve the higher ET focused in this riparian forested area. ET estimates at 30 m suggest the use of groundwater (even shallow water from the creek) by the vegetation during summer, where the ET was maintained over 1.5 mm d^{-1}, while MODIS ET incorporating surrounding grasslands drops to near 0. A more stable ET trend is seen over this river/scrub zone, where the ET reached similar maximums during the 3 years. These scrub species may have a high

nutritional interest both for the domestic livestock, as well as for game species (Hajer et al., 2004).

Cumulative annual water use curves, relevant for water resources management purposes, at 30 m and 1 km resolution are contrasted between relatively wet and dry hydrological years (2013/14 and 2014/2015, respectively) over the zones A and D in Figure 5.8. These two areas were chosen because they showed higher scale-dependent differences (Figure 5.7). Total precipitation measured at the flux site was 704 mm in 2013/14 and 511 mm in 2014/15.

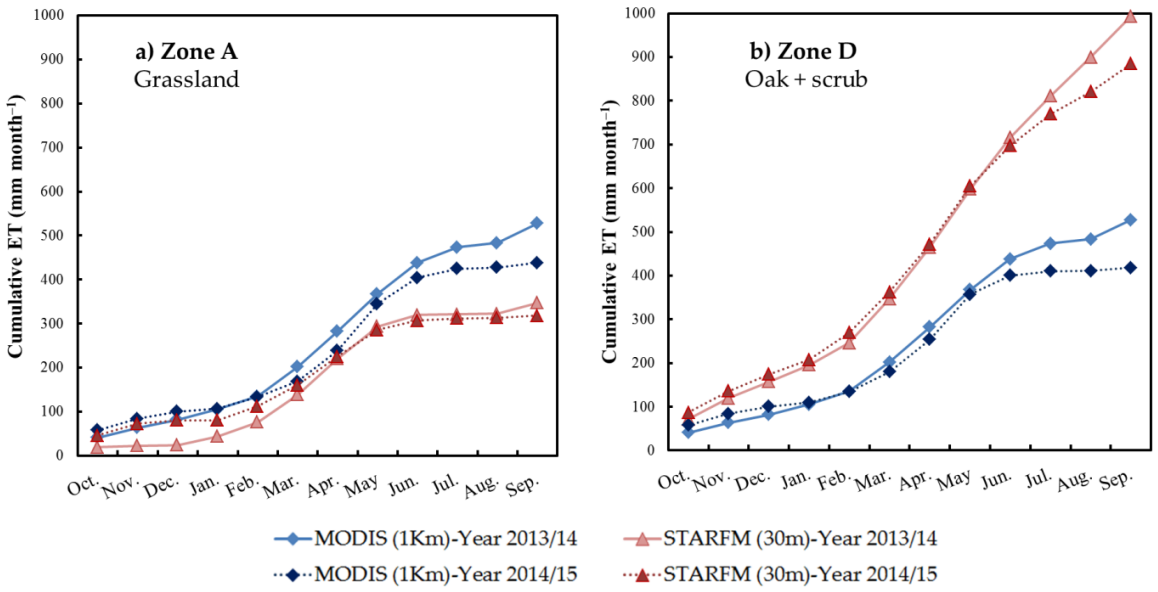

Figure 5.8. Evolution of cumulative monthly ET estimated by DisALEXI/MODIS and STARFM approaches for the hydrological year 2013/14 and 2014/15, over a) zone A and b) zone D.

At both resolutions, cumulative ET is higher in the wet year (2013/14) as expected. While cumulative ET at 1 km resolution was similar between zones (around 450-500 mm/year), the 30 m resolution data showed substantial variations between sites, with values ranging between 350 and 900 mm/year.

In the open grassland area, zone A (Figure 5.8a), the DisALEXI/MODIS approach produced an overestimation of the annual ET in the order of 120-180 mm when compared with the fusion model. Differences were more pronounced during the dry season when the STARFM curve remained stable from May on due to grass senescence. In zone D (Figure 5.8b), with transpiring vegetation throughout the year, the cumulative ET continuously increased at 30 m resolution. Neither intra- nor inter-annual significant variations in water consumption were observed with STARFM in this area close to a stream, probably due to higher use of groundwater by trees and scrubs and a lesser coupling of water consumption

with rainfall events. MODIS cumulative ET showed a slight plateau during the months of July and August, capturing the behavior of the surrounding grassland area in the analysis. An underestimation of approximately 450 mm/year was quantified in this area using 1 km resolution data.

In addition, spatially distributed maps of ET over the *Martin Gonzalo* watershed and *Santa Clotilde dehesa* farm (Figure 5.1c) on three days, representative of different seasons of the period 2013-2015 are presented in Figure 5.9, highlighting the area with a *dehesa* ecosystem. They were produced by the ALEXI model (5 km), the DisALEXI/MODIS application (1 km) and the STARFM technique (30 m).

At the watershed scale, the more detailed representation of ET at a fine resolution provides a better understanding of the variability of the *dehesa* vegetation water consumption. At 30 m the variations in topography and soils, affecting the vegetation species composition and abundance, can be observed and are largely lost at the 1 km resolution and not existent at the 5 km scale. At the farm scale, the STARFM model allowed for the observation of ET variability in the different vegetation patches previously described, highlighting the existence of micro-ecosystems and climates at the local scale.

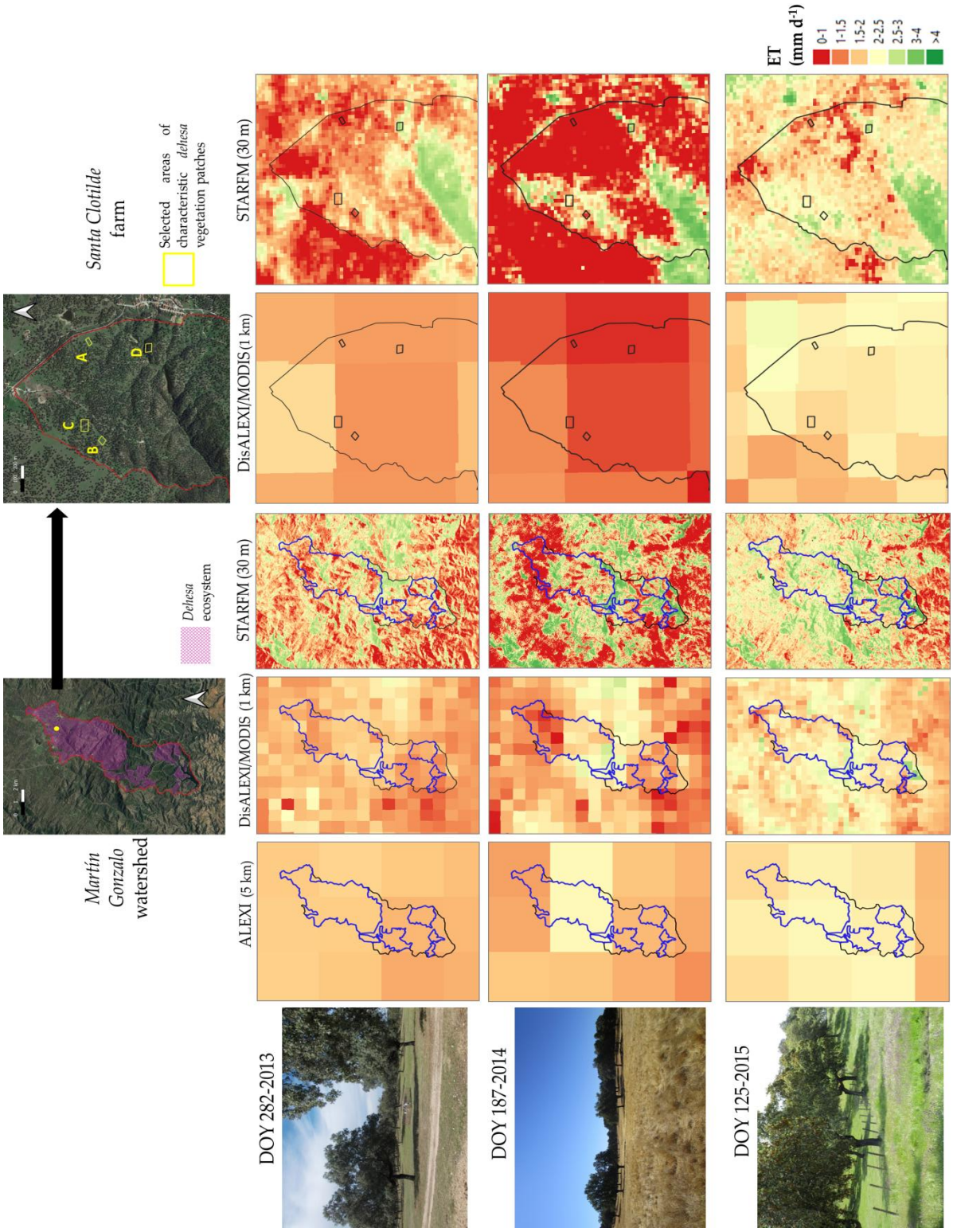

Figure 5.9. Distributed ET maps over the *Martin Gonzalo* watershed and *Santa Clotilde dehesa* farm derived from ALEXI (5 km), the DisALEXI/MODIS application (1 km) and the STARFM approach (30 m) on three representative dates of spring, summer, and autumn seasons. Blue lines show the *dehesa* ecosystem areas.

5.4. Discussion

5.4.1. DisALEXI Model Validation

The estimation of Rn flux presented an error (RMSE = 1.15 MJ m^{-2} d^{-1}) slightly higher compared to other applications over agricultural areas (Anderson et al., 2012; Cammalleri et al., 2013, 2014), but it was aligned with the errors over sparse vegetation cover crops, such as grapevines (Semmens et al., 2016; Knipper et al., 2019) and forested/mosaic areas (Yang et al., 2017; Anderson et al., 2018). Ideally, future filtering of insolation inputs needs to be avoided in order to build an automated application, which should include a proxy to account for the quality of the input data. An alternative could be to migrate to an MSG Land-SAF satellite insolation product. Anderson et al. (2019) tested different satellite insolation products generated by geostationary satellites, which significantly improved insolation performance over CFSR, although it did not translate into comparable improvement in the ET retrieval accuracy.

Likewise, the errors in H flux (RMSE value of 1.99 MJ m^{-2} d^{-1} when using MODIS data and 2.18 MJ m^{-2} d^{-1} with Landsat) were higher than other applications over agricultural areas (in the range of 1.2-1.7 MJ m^{-2} d^{-1} observed by Cammalleri et al. (2013, 2014) and Semmens et al. (2016), but in the same range as those obtained in more complex vegetation (Yang et al., 2017; Knipper et al., 2019).

In relation to LE flux modeled by DisALEXI, a similar behavior over another *dehesa* site (fluxnet code ES-LMA) using LST data measured in the field and MODIS images, was observed by Andreu et al. (2018a, 2018b). These authors used a lower Priestley-Taylor coefficient and stated that even integrating the green fraction and reducing the coefficient, during the dry season the flux was so low as to approach zero. Furthermore, the same trend had been previously observed by Carpintero et al. (2014, 2016) in the study area, where the scheme was applied using a different meteorological dataset source and study period. In this regard, Burchard-Levine et al. (2020) implemented the TSEB model over a *dehesa* area with modifications, considering phenological dynamics of this tree-grass ecosystem and assuming a dominant vegetation structure and cover for different seasons, and different seasonal vegetation parameters. This new adaptation improved the model performance, decreasing the overestimation of LE flux and RMSD errors compared to the application of TSEB assuming a single vegetation source.

5.4.2. Temporal Patterns in ET Curves

The ET time series estimated for the hydrological years 2013/2014 and 2014/2015 reflected the evolution of the vegetation water consumption, depending on water availability. Both hydrological years have similar ET rates, despite the lower precipitation rates in the second one. In 2014/15 water use exceeded the rainfall, suggesting that the vegetation tapped water from other sources to sustain transpiration rates within a threshold

that plants could survive. It is known that oak tree roots are able to explore a large volume of soil, with a high dependence on deep water reserves (Moreno et al., 2005; Cubera and Moreno, 2007). Moreover, oaks form both arbuscular and ectotrophic mycorrhizae, and create mycorrhizal symbioses with partners, adapting to different conditions and accessing many different resources (Allen, 2015).

The similarity of water consumption in spring 2015 with respect to 2014 (with a significantly lower rainfall but an unusually high rainfall in the previous autumn) highlighted the importance of significant antecedent rainfall events to recharge the subsurface layers. In this sense, Fernández (1993) found a significant correlation between grassland species abundance in the *dehesa* and autumn rainfall.

The ET values observed during the summers (Figure 5.5; minima values of 0.7 mm d^{-1} at the end of the dry season) were comparable with David et al.'s results (2007), who found that oak trees maintained transpiration rates above 0.7 mm d^{-1} during the dry season with more than 70% of the transpired water being taken from groundwater sources. In seasons with low LE values (summers and winters), the uncertainty in the data observed by the eddy covariance system (Burba and Anderson, 2010), added to the fact that LE flux was obtained by closing the balance with the residual method must be considered in the error assessment.

The accuracy of the different modeled daily ET series, shown in Table 5.2, is below the target error of 0.8 mm d^{-1} suggested by Seguin et al. (1999). The errors (RMSE = 0.67 mm d^{-1} with STARFM approach) were close to those found by other authors for woody sparse semiarid crops (Padilla et al., 2011; Mateos et al., 2013; Andreu et al., 2018b), and slightly higher than the RMSE value (~0.5 mm d^{-1}) found by Campos et al. (2013) and Carpintero et al. (2020) in a *dehesa* ecosystem using a locally calibrated remote sensing-based soil water balance.

5.4.3. Performance of MOD16A2 ET

Sriwongsitanon et al. (2020) showed a strong agreement of MOD16A2 values with the bulk ET computed using a water balance framework in the forested humid tropics of Thailand, on a monthly and annual scale. The estimations from that study were consistent with the soil moisture conditions and land use classes. An acceptable accuracy of this product was also found by Aguilar et al. (2018) and Niyogi et al. (2020) for water consumption monitoring over agricultural areas in Northwestern Mexico and Indiana (Midwestern United States). Comparisons of this product with in-situ measurements at 15 flux tower sites with different climates and biome types ranging from croplands, grasslands, shrublands, savannas, to forests over Europe were evaluated by Hu et al. (2015). The global ET was consistent over most of Europe, with the best results over crops and meadows located in a temperate and humid climate. However, the seasonal performance of

MOD16A2 was worse over vegetation under a semiarid climate, with RMSE equal to 1.17 mm d^{-1}, comparable to the error found in this work (Figure 5.6; RMSE = 1.02 mm d^{-1}). Global product ET was always underestimated for a *dehesa* ecosystem in Spain (similar study area and results to those of this work), demonstrating the weakness of this algorithm over limited water availability conditions (Hu et al., 2015). The same behavior of ET underestimation was observed over a semiarid region in Iran (Jamshidi et al., 2019), highlighting the high dependence of MOD16A2 performance with the climate type.

As shown in Figure 5.6, through the STARFM framework application we were capable of estimating with higher accuracy the temporal trend of ET (mm $8d^{-1}$) for this semiarid ecosystem, when compared with the MOD16A2 product.

5.4.4. Variability of *Dehesa* Vegetation Water Use at Field Scale

Dehesa landscape structure features, with variations in the distribution of vegetation strata, are associated with the creation of different microclimates, directly influencing ecological processes, such as plant regeneration and growth, soil respiration, nutrient cycling, and wildlife habitats (Chen et al., 1996).

The trends observed in the grassland area (zone A; Figure 5.7a), where the pasture drying process started in May and ended in early to mid-July, were consistent with the pasture production cycle observed in a similar *dehesa* farm in Spain (Las Majadas). The maximum production was obtained in the spring (around 60–70%) and autumn (15–20%), while the pasture growth was at a minimum in winter (5–15%) and zero in the summer (Moreno and Cáceres, 2016). Information about the pasture drying date at Landsat-scale, for which a high temporal frequency is crucial, can benefit the assessment of the nutritional quality for livestock feed (Moreno and Cáceres, 2016). The ET behavior in zone B (Figure 5.7b), where high humidity conditions existed, demonstrates the greater transpiration and production capacity of these moist grasslands, important for managing grazing rotations.

Due to the great expansion of the zone C vegetation structure (Figure 5.7c; a mixture of grass and trees with a low coverage fraction), previous applications of models for estimating water consumption at a low spatial resolution (from 1 km to 5 km) generally have worked well over this ecosystem. These models have provided very useful information at the basin or regional scale (Andreu et al., 2018a, 2018b; González-Dugo et al., 2021). In zone D, the high spatial resolution ET reflects the presence of dense evergreen vegetation transpiring throughout the year. These areas provide essential ecosystem services, such as shelter for livestock and wildlife (rabbits, Iberian Lynx, etc.), or the creation of specific conditions under the canopy, with different radiation interception, and soils with increased fertility and water retention (Joffre et al., 1993).

The spatial variability in the ET maps is represented in Figure 5.9 over the *Martin Gonzalo* watershed (left) and *Santa Clotilde* farm (right). From a hydrological modeling

viewpoint, the 30 m resolution ET product may be very useful to identify and delineate hydrological zones with different water storage capacities and runoff processes within the basin. Nevertheless, the coarse resolution may be enough for regional managing purposes, such as drought monitoring. At the field scale, regular availability of this type of map can lead to developing better agricultural management decisions related to grazing rotations, delineating areas containing fragile ecosystems and important ecological riparian areas with higher water holding capacity and vegetation cover that can sustain a wide diversity of plant and animal species.

5.5. Conclusions

The ALEXI/DisALEXI model and the STARFM data fusion technique adequately estimated the ET dynamics of a Mediterranean oak savanna at fine spatial and temporal resolution (30 m, daily) for the period 2013–2015. The energy fluxes provided by DisALEXI using MODIS images (1 km, daily) and Landsat images (60–100 m, 16 days) were compared with in-situ measurements from an eddy covariance flux tower system. The modeled fluxes compared reasonably well to field observations, with RMSE values ranging between 0.60 and 2.18 MJ m^{-2} d^{-1} depending on the sensor resolution and the flux component, a similar range to those obtained by other authors over complex landscapes. In addition, the daily 30 m ET series from STARFM model obtained a RMSE value of 0.67 mm d^{-1}, which is considered an acceptable error for *dehesa* management purposes.

The ET time series generated by both approaches, DisALEXI and STARFM with different resolutions, showed an annual bimodal behavior of the vegetation water consumption over the *dehesa* structure (grass and trees, with a tree cover fraction of 25%), with two marked peaks of different magnitudes (around 4-5 mm d^{-1} during the spring, and between 1.5 and 2.5 mm d^{-1} in the autumn). Modeled ET accurately reproduced the temporal dynamics of the water consumed by the vegetation, clearly linked to the distribution of the annual rainfall and the energy availability. Nevertheless, some difficulties of the model to reproduce certain abrupt changes in the ET behavior were identified, showing some limitations of the modeling scheme without more frequent observations and the importance of high-quality input data.

The results showed that when the data fusion model was applied, a slight improvement of RMSE, compared to using MODIS or simpler linear interpolations with Landsat data, was observed. This can be due to the combination of daily temporal frequency capturing the changes in ET and the high spatial resolution providing a better representation of the footprint of the flux tower. Modeled annual ET, close to 600 mm for both hydrological years despite their different rainfall regimes, provides an indicative value of current vegetation water needs and how the system adapts to meet these needs under the different water availability conditions. Holm oak’s ability to explore a large volume of soil and

access groundwater resources under higher than typical water-limited conditions can explain a lack of a difference in ET between years and the minimum modeled values of transpiration of 0.7 mm d^{-1} at the end of the dry season. However, for periods of long-term and sustained drought, the ecosystem is likely to have a different response.

The major advantage of the data fusion technique and the high spatio-temporal resolution was found in the analysis of ET dynamics over different vegetation microbiomes, characteristics of the *dehesa* landscape. The results showed that high-resolution ET maps (daily, 30 m) can provide key information to better understand the hydrological functioning of different vegetation distributions difficult to detect at a 1 km pixel resolution and assist in decision making at the farm or local level. However, 1-5 km resolution ET information may suffice for regional monitoring and water planning purposes, such as regional drought detection and impacts on water resources of different biomes.

5.6. Acknowledgements

This research was funded by the FPU program - University Teachers Training - from the Department of Education, Culture and Sport. Dr. Andreu's work was funded by the European Union's Horizon 2020 Research and Innovation program under the Marie Skłodowska-Curie grant agreement No 703978. Additional support was provided by the project PP.PEI.IDF2019.004, co-funded at 80% by the European Regional Development Fund (ERDF), as part of the Andalusian operational program 2014-2020, and the project PID2019-107693RR-C22 (MCIU/AEI/FEDER, UE). This research was supported in part by the U.S. Department of Agriculture, Agricultural Research Service. USDA is an equal opportunity provider and employer. The authors would like to thank M. Ramos, J. Alfieri, J. Prueger and L. McKee for their help with field instrumentation installation as well as the maintenance, and measurements. We also would like to thank the collaboration of Santa Clotilde managers.

5.7. References

Aguilar, A., Flores, H., Crespo, G., Marín, M.I., Campos, I., Calera, A., 2018. Performance Assessment of MOD16 in Evapotranspiration Evaluation in Northwestern Mexico. Water 10, 901. https://doi.org/10.3390/w10070901.

Allen, M.F., 2015. How Oaks Respond to Water Limitation, in: Standiford, Richard B.; Purcell, Kathryn L., tech. cords. Proceedings of the seventh California oak symposium: managing oak woodlands in a dynamic world. Gen. Tech. Rep. PSW-GTR-251, Berkeley, CA, pp-13–21.

Anderson, M.C., Allen, R.G., Morse, A., Kustas, W.P., 2012. Use of Landsat thermal imagery in monitoring evapotranspiration and managing water resources. Remote Sens. Environ. 122, 50–65. https://doi.org/10.1016/j.rse.2011.08.025.

Anderson, M., Diak, G., Gao, F., Knipper, K., Hain, C., Eichelmann, E., Hemes, K.S., Baldocchi, D., Kustas, W., Yang, Y., 2019. Impact of insolation data source on remote sensing retrievals of evapotranspiration over the California delta. Remote Sens. 11. https://doi.org/10.3390/rs11030216.

Anderson, M., Gao, F., Knipper, K., Hain, C., Dulaney, W., Baldocchi, D., Eichelmann, E., Hemes, K., Yang, Y., Medellin-Azuara, J., Kustas, W.P., 2018. Field-scale assessment of land and water use change over the California delta using remote sensing. Remote Sens. 10. https://doi.org/10.3390/rs10060889.

Anderson, M.C., Kustas, W.P., Norman, J.M., Hain, C.R., Mecikalski, J.R., Schultz, L., González-Dugo, M.P., Cammalleri, C., d'Urso, G., Pimstein, A., Gao, F., 2010. Mapping daily evapotranspiration at field to global scales using geostationary and polar orbiting satellite imagery. Hydrol. Earth Syst. Sci. Discuss. 7, 5957–5990. https://doi.org/10.5194/hessd-7-5957-2010.

Anderson, M.C., Norman, J.M., Diak, G.R., Kustas, W.P., Mecikalski, J.R., 1997. A two-source time-integrated model for estimating surface fluxes using thermal infrared remote sensing. Remote Sens. Environ. 60, 195–216. https://doi.org/10.1016/S0034-4257(96)00215-5.

Anderson, M.C., Norman, J.M., Mecikalski, J.R., Otkin, J.A., Kustas, W.P., 2007. A climatological study of evapotranspiration and moisture stress across the continental United States based on thermal remote sensing: 2. Surface moisture climatology. J. Geophys. Res. Atmos. 112, 1–13. https://doi.org/10.1029/2006JD007507.

Anderson, M.C., Norman, J.M., Mecikalski, J.R., Torn, R.D., Kustas, W.P., Basara, J.B., 2004. A multiscale remote sensing model for disaggregating regional fluxes to micrometeorological scales. J. Hydrometeorol. 5, 343–363. https://doi.org/10.1175/1525-7541(2004)005<0343:AMRSMF>2.0.CO;2

Andreu, A., Kustas, W.P., Polo, M.J., Carrara, A., González-Dugo, M.P., 2018a. Modeling surface energy fluxes over a dehesa (oak savanna) ecosystem using a thermal based two-source energy balance model (TSEB) I. Remote Sens. 10, 1–27. https://doi.org/10.3390/rs10040567.

Andreu, A., Kustas, W.P., Polo, M.J., Carrara, A., González-Dugo, M.P., 2018b. Modeling surface energy fluxes over a dehesa (oak savanna) ecosystem using a thermal based two source energy balance model (TSEB) II-Integration of remote sensing medium and low spatial resolution satellite images. Remote Sens. 10, 1–19. https://doi.org/10.3390/rs10040558.

Baldocchi, D.D., Xu, L., 2007. What limits evaporation from Mediterranean oak woodlands - The supply of moisture in the soil, physiological control by plants or the demand by the atmosphere? Adv. Water Resour. 30, 2113–2122. https://doi.org/10.1016/j.advwatres.2006.06.013.

Baldocchi, D.D., Xu, L., Kiang, N., 2004. How plant functional-type, weather, seasonal drought, and soil physical properties alter water and energy fluxes of an oak-grass savanna and an annual grassland. Agric. For. Meteorol. 123, 13–39. https://doi.org/10.1016/j.agrformet.2003.11.006

Bastiaanssen, W.G.M., Menenti, M., Feddes, R.A., Holtslag, A. A. M., 1998. A remote sensing surface energy balance algorithm for land (SEBAL). 1 Formulation. J. Hydrol. 212–213, 198–212. https://doi.org/10.1016/S0022-1694(98)00254-6.

Berk, A., Bernstein, L.S., Robertson, D.C., 1987. MODTRAN: A Moderate Resolution Model for LOWTRAN 7. GL-TR-89-0122, Air Force Geophysics Lab, Bedford, MA.

Burba, G., Anderson, D., 2010. A Brief Practical Guide to Eddy Covariance Flux Measurements: Principles and Workflow Examples for Scientific and Industrial Applications. https://doi.org/10.13140/RG.2.1.1626.4161.

Burchard-Levine, V., Nieto, H., Riaño, D., Migliavacca, M., El-Madany, T.S., Perez-Priego, O., Carrara, A., Martín, M.P., 2020. Seasonal adaptation of the thermal-based two-source energy balance model for

estimating evapotranspiration in a semiarid tree-grass ecosystem. Remote Sens. 12. https://doi.org/10.3390/rs12060904.

Cammalleri, C., Agnese, C., Ciraolo, G., Minacapilli, M., Provenzano, G., Rallo, G., 2010. Actual evapotranspiration assessment by means of a coupled energy/hydrologic balance model: Validation over an olive grove by means of scintillometry and measurements of soil water contents. J. Hydrol. 392, 70–82. https://doi.org/10.1016/j.jhydrol.2010.07.046.

Cammalleri, C., Anderson, M.C., Gao, F., Hain, C.R., Kustas, W.P., 2013. A data fusion approach for mapping daily evapotranspiration at field scale. Water Resour. Res. 49, 4672–4686. https://doi.org/10.1002/wrcr.20349.

Cammalleri, C., Anderson, M.C., Gao, F., Hain, C.R., Kustas, W.P., 2014. Mapping daily evapotranspiration at field scales over rainfed and irrigated agricultural areas using remote sensing data fusion. Agric. For. Meteorol. 186, 1–11. https://doi.org/10.1016/j.agrformet.2013.11.001.

Campos, P., Huntsinger, L., Oviedo, J., Díaz, M., Starrs, P., Standiford, R., Montero, G., 2013. Mediterranean Oak Woodland Working Landscapes: Dehesas of Spain and Ranchlands of California, Springer: Dordrecht, The Netherlands.

Campos, I., Villodre, J., Carrara, A., Calera, A., 2013. Remote sensing-based soil water balance to estimate Mediterranean holm oak savanna (dehesa) evapotranspiration under water stress conditions. J. Hydrol. 494, 1–9. https://doi.org/10.1016/j.jhydrol.2013.04.033.

Carpintero, E., Andreu, A., Gómez-Giráldez, P.J., Blázquez, Á., González-Dugo, M.P., 2020. Remote-sensing-basedwater balance for monitoring of evapotranspiration and water stress of a mediterranean Oak-Grass Savanna. Water (Switzerland) 12. https://doi.org/10.3390/w12051418.

Carpintero, E., González-Dugo, M.P., Hain, C., Nieto, H., Gao, F., Andreu, A., Kustas, W.P., Anderson, M.C., 2016. Continuous evapotranspiration monitoring and water stress at watershed scale in a Mediterranean oak savanna, in: Remote Sensing for Agriculture, Ecosystems, and Hydrology XVIII, 9998, Proceeding of SPIE, SPIE: Bellingham, WA, USA.

Carpintero, E., Semmens, K., Anderson, M.C., Andreu, A., Gao, F., Kustas, W.P., González-Dugo, M.P., 2014. Use of remote sensing data fusion for daily evapotranspiration monitoring at watershed scale over a *dehesa* ecosystem, in: Sobrino, J.A. (Eds.), Proceedings of Fourth International Symposium on Recent Advances in Quantitative Remote Sensing, Valencia, Spain, 22-26th September 2014, pp. 310–314.

Chen, J., Saunders, S.C., Crow, T.R., Naiman, R.J., Brosofske, K.D., Mroz, G.D., Brookshire, B.L., Franklin, J.F., 1996. Microclimate in Forest Ecosystem the effects of different management regimes. Bioscience *49*, 288–297.

Coelho, C.; Ferreira, A.J.D., Laouina, A., Hamza, A., Chaker, M., Naafa, R., Regaya, K., Boulet, A. K., Keizer, J.J., Carvalho, T.M.M., 2004. Changes in Land Use and Land Management Practices Affecting Land Degradation within Forest and Grazing Ecosystems in the Western Mediterranean, in: Schnabel, S., Ferreira, A. (Eds.), Sustainability of Agrosylvopastoral Systems, Dehesas, Montados, Schweizerbart Science Publishers: Stuttgart, Germany, pp. 137–154.

Cramer, W., Guiot, J., Fader, M., Garrabou, J., Gattuso, J.P., Iglesias, A., Lange, M.A., Lionello, P., Llasat, M.C., Paz, S., Peñuelas, J., Snoussi, M., Toreti, A., Tsimplis, M.N., Xoplaki, E., 2018. Climate change and interconnected risks to sustainable development in the Mediterranean. Nat. Clim. Chang. 8, 972–980. https://doi.org/10.1038/s41558-018-0299-2.

Cramer, W., Guiot, J., Marini, K, 2020. Climate and Environmental Change in the Mediterranean Basin – Current Situation and Risks for the Future. First Mediterranean Assessment Report. MedECC

(Mediterranean Experts on Climate and Environmental Change). Union for the Mediterranean, Plan Bleu, UNEP/MAP, Marseille, France.

Cubera, E., Moreno, G., 2007. Effect of single Quercus ilex trees upon spatial and seasonal changes in soil water content in dehesas of central western Spain. Ann. For. Sci. 64, 355–364. https://doi.org/10.1051/forest:2007012.

David, T.S., Henriques, M.O., Kurz-Besson, C., Nunes, J., Valente, F., Vaz, M., Pereira, J.S., Siegwolf, R., Chaves, M.M., Gazarini, L.C., David, J.S., 2007. Water-use strategies in two co-occurring Mediterranean evergreen oaks: Surviving the summer drought. Tree Physiol. 27, 793–803. https://doi.org/10.1093/treephys/27.6.793.

Diak, G.R., Whipple, M.S., 1995. Note on estimating surface sensible heat fluxes using surface temperatures measured from a geostationary satellite during FIFE 1989. J. Geophys. Res. 100. https://doi.org/10.1029/95jd00729

Díaz, M., Tietje, W.D., Barrett, R.H., 2013. Effects of Management on Biological Diversity and Endangered Species, in: Campos, P., Huntsinger. L., Oviedo, J.L., Starrs, P.F., Díaz, M., Standiford, R.B, Montero, G. (Eds.), Mediterranean Oak Woodland Working Landscapes. Landscape Series, 16, Springer, Dordrecht, The Netherlands, pp. 213-243.

Fernández-Alés, R., 1993. Response of Mediterranean grassland species to changing rainfall. A reply to Figueroa and Davy. Orsis 8, 121-126.

Gao, F., Anderson, M.C., Kustas, W.P., Wang, Y., 2012a. Simple method for retrieving leaf area index from Landsat using MODIS leaf area index products as reference. J. Appl. Remote Sens. 6, 063554. https://doi.org/10.1117/1.JRS.6.063554.

Gao, F., Kustas, W.P., Anderson, M.C., 2012b. A data mining approach for sharpening thermal satellite imagery over land. Remote Sens. 4, 3287–3319. https://doi.org/10.3390/rs4113287.

Gao, F., Masek, J., Schwaller, M., Hall, F., 2006. On the blending of the landsat and MODIS surface reflectance: Predicting daily landsat surface reflectance. IEEE Trans. Geosci. Remote Sens. 44, 2207–2218. https://doi.org/10.1109/TGRS.2006.872081.

García-Ruiz, J.M., López-Moreno, I.I., Vicente-Serrano, S.M., Lasanta-Martínez, T., Beguería, S., 2011. Mediterranean water resources in a global change scenario. Earth-Science Rev. 105, 121–139. https://doi.org/10.1016/j.earscirev.2011.01.006.

Gauquelin, T., Michon, G., Joffre, R., Duponnois, R., Génin, D., Fady, B., Bou Dagher-Kharrat, M., Derridj, A., Slimani, S., Badri, W., Alifriqui, M., Auclair, L., Simenel, R., Aderghal, M., Baudoin, E., Galiana, A., Prin, Y., Sanguin, H., Fernandez, C., Baldy, V., 2016. Mediterranean forests, land use and climate change: a social-ecological perspective. Reg. Environ. Chang. 18, 623–636. https://doi.org/10.1007/s10113-016-0994-3.

González-Dugo, M., Chen, X., Andreu, A., Carpintero, E., Gómez-Giraldez, P., Carrara, A., Su, Z., 2021. Long-term water stress and drought monitoring of Mediterranean oak savanna vegetation using thermal remote sensing. Hydrol. Earth Syst. Sci. 25, 755–768. https://doi.org/10.5194/hess-25-755-2021.

Gonzalez-Dugo, M.P., Neale, C.M.U., Mateos, L., Kustas, W.P., Prueger, J.H., Anderson, M.C., Li, F., 2009. A comparison of operational remote sensing-based models for estimating crop evapotranspiration. Agric. For. Meteorol. 149, 1843–1853. https://doi.org/10.1016/j.agrformet.2009.06.012.

Hain, C.R., Anderson, M.C., 2017. Estimating morning changes in land surface temperature from MODIS day/night observations: Applications for surface energy balance modeling. Geophys. Res. Lett. 44, 9723-9733. https://doi.org/10.1002/2017GL074952.

Hajer, A., López, S., González, J.S., Ranilla, M.J., 2004. Chemical composition and in vitro digestibility of some Spanish browse plant species. J. Sci. Food Agric. 84, 197-204. https://doi.org/10.1002/jsfa.1635.

Hsieh, C.I., Katul, G., Chi, T.W., 2000. An approximate analytical model for footprint estimation of scalar fluxes in thermally stratified atmospheric flows. Adv. Water Resour. 23, 765–772. https://doi.org/ 10.1016/S0309-1708(99)00042-1.

Hu, G., Jia, L., Menenti, M., 2015. Comparison of MOD16 and LSA-SAF MSG evapotranspiration products over Europe for 2011. Remote Sens. Environ. 156, 510–526. https://doi.org/10.1016/j.rse.2014.10.017.

Jamshidi, S., Zand-Parsa, S., Pakparvar, M., Niyogi, D., 2019. Evaluation of Evapotranspiration over a Semiarid Region Using Multiresolution Data Sources. J. Hydrometeorol. 20, 947-964. https://doi.org/10.1175/JHM-D-18-0082.1.

Joffre, R., Rambal, S., 1993. How tree cover influences the water balance of Mediterranean rangelands. Ecology 74, 570–582. https://doi.org/10.2307/1939317.

Joffre, R., Rambal, S., Damesin, C., 2008. Functional attributes in Mediterranean-type ecosystems, in: Pugnaire, F.I., Valladares, F. (Eds.), Handbook of functional plant ecology, 2nd edn. CRC Press Books, Boca Raton.

Johnston, M.R., Andreu, A., Verfaillie, J., Baldocchi, D., González-Dugo, M.P., Moorcroft, P.R., 2021. Measuring surface temperatures in a woodland savanna: Opportunities and challenges of thermal imaging in an open-canopy ecosystem. Agric. For. Meteorol. 310, 108484. https://doi.org/10.1016/j.agrformet.2021.108484.

Jönsson, P., Eklundh, L., 2004. TIMESAT - A program for analyzing time-series of satellite sensor data. Comput. Geosci. 30, 833–845. https://doi.org/10.1016/j.cageo.2004.05.006.

Knipper, K.R., Kustas, W.P., Anderson, M.C., Alfieri, J.G., Prueger, J.H., Hain, C.R., Gao, F., Yang, Y., McKee, L.G., Nieto, H., Hipps, L.E., Alsina, M.M., Sanchez, L., 2019. Evapotranspiration estimates derived using thermal-based satellite remote sensing and data fusion for irrigation management in California vineyards. Irrig. Sci. 37, 431–449. https://doi.org/10.1007/s00271-018-0591-y.

Kustas, W.P., Alfieri, J.G., Evett, S., Agam, N., 2015. Quantifying variability in field-scale evapotranspiration measurements in an irrigated agricultural region under advection. Irrig. Sci. 33, 325–338. https://doi.org/10.1007/s00271-015-0469-1

Kustas, W.P., Norman, J.M., 1999. Evaluation of soil and vegetation heat flux predictions using a simple two-source model with radiometric temperatures for partial canopy cover. Agric. For. Meteorol. 94, 13–29. https://doi.org/10.1016/S0168-1923(99)00005-2.

Liang, S., 2000. Narrowband to broadband conversions of land surface albedo: I. Algorithms. Remote Sens. Environ. 76, 213–238. https://doi.org/ 10.1016/S0034-4257(00)00205-4.

Lionello, P., Scarascia, L., 2018. The relation between climate change in the Mediterranean region and global warming. Reg. Environ. Chang. 18, 1481–1493. https://doi.org/10.1007/s10113-018-1290-1.

Mateos, L., González-Dugo, M.P., Testi, L., Villalobos, F.J., 2013. Monitoring evapotranspiration of irrigated crops using crop coefficients derived from time series of satellite images. I. Method validation. Agric. Water Manag. 125, 81-91. https://doi.org/10.1016/j.agwat.2012.11.005.

Milano, M., Ruelland, D., Fernandez, S., Dezetter, A., Fabre, J., Servat, E., Fritsch, J.M., Ardoin-Bardin, S., Thivet, G., 2013. Current state of Mediterranean water resources and future trends under climatic and anthropogenic changes. Hydrol. Sci. J. 58, 498–518. https://doi.org/10.1080/02626667.2013.774458.

Moreno, G., Cáceres, Y., 2016. System report: Iberian Dehesas, Spain. AGFORWARD. Agroforestry for

Europe, Plasencia.

Moreno, G., Obrador, J.J., Cubera, E., Dupraz, C., 2005. Fine root distribution in Dehesas of Central-Western Spain. Plant Soil 277, 153–162. https://doi.org/10.1007/s11104-005-6805-0.

Moreno G., Pulido F.J., 2009. The Functioning, Management and Persistence of Dehesas, in: Rigueiro-Rodríguez A., McAdam J., Mosquera-Losada M.R. (Eds.), Agroforestry in Europe. Advances in Agroforestry, vol 6, Springer, Dordrecht.

Mu, Q., Zhao, M., Running, S.W., 2011. Improvements to a MODIS global terrestrial evapotranspiration algorithm. Remote Sens. Environ. 115, 1781–1800. https://doi.org/10.1016/j.rse.2011.02.019.

Niyogi, D., Jamshidi, S., Smith, D., Kellner, O., 2020. Evapotranspiration Climatology of Indiana, USA Using In Situ and Remotely Sensed Products. J. Appl. Meteorol. Climatol. 12, 1-52. https://doi.org/10.1175/JAMC-D-20-0024.1.

Norman, J.M., Anderson, M.C., Kustas, W.P., French, A.N., Mecikalski, J., Torn, R., Diak, G.R., Schmugge, T.J., Tanner, B.C.W., 2003. Remote sensing of surface energy fluxes at 101-m pixel resolutions. Water Resour. Res. 39. https://doi.org/10.1029/2002WR001775.

Norman, J.M., Kustas, W.P., Humes, K.S., 1995. Source approach for estimating soil and vegetation energy fluxes in observations of directional radiometric surface temperature. Agric. For. Meteorol. 77, 263–293. https://doi.org/10.1016/0168-1923(95)02265-Y.

Padilla, F.L.M., González-Dugo, M.P., Gavilán, P., Domínguez, J., 2011. Integration of vegetation indices into a water balance model to estimate evapotranspiration of wheat and corn. Hydrol. Earth Syst. Sci. 15, 1213–1225. https://doi.org/10.5194/hess-15-1213-2011.

Plieninger, T., Rolo, V., Moreno, G., 2010. Large-scale patterns of Quercus ilex, Quercus suber, and Quercus pyrenaica regeneration in central-western Spain. Ecosystems 13, 644–660. https://doi.org/10.1007/s10021-010-9345-2.

Rodriguez-Iturbe, I., Porporato, A., Laio, F., Ridolfi, L., 2001. Plants in water-controlled ecosystems: Active role in hydrologic processes and responce to water stress I. Scope and general outline. Adv. Water Resour. 24, 695–705. https://doi.org/10.1016/S0309-1708(01)00004-5.

Rundel, P.W., Arroyo, M.T.K., Cowling, R.M., Keeley, J.E., Lamont, B.B., Vargas, P., 2016. Mediterranean Biomes: Evolution of Their Vegetation, Floras, and Climate. Annu. Rev. Ecol. Evol. Syst. 47, 383–407. https://doi.org/10.1146/annurev-ecolsys-121415-032330.

Saha, S., Moorthi, S., Pan, H.L., Wu, X., Wang, Jiande, Nadiga, S., Tripp, P., Kistler, R., Woollen, J., Behringer, D., Liu, H., Stokes, D., Grumbine, R., Gayno, G., Wang, Jun, Hou, Y.T., Chuang, H.Y., Juang, H.M.H., Sela, J., Iredell, M., Treadon, R., Kleist, D., Van Delst, P., Keyser, D., Derber, J., Ek, M., Meng, J., Wei, H., Yang, R., Lord, S., Van Den Dool, H., Kumar, A., Wang, W., Long, C., Chelliah, M., Xue, Y., Huang, B., Schemm, J.K., Ebisuzaki, W., Lin, R., Xie, P., Chen, M., Zhou, S., Higgins, W., Zou, C.Z., Liu, Q., Chen, Y., Han, Y., Cucurull, L., Reynolds, R.W., Rutledge, G., Goldberg, M., 2010. The NCEP climate forecast system reanalysis. Bull. Am. Meteorol. Soc. 91, 1015–1057. https://doi.org/10.1175/2010BAMS3001.1.

Seguin, B., Becker, F., Phulpin, T., Gu, X.F., Guyot, G., Kerr, Y., King, C., Lagouarde, J.P., Ottlé, C., Stoll, M.P., Tabbagh, A., Vidal, A., 1999. IRSUTE: A minisatellite project for land surface heat flux estimation from field to regional scale. Remote Sens. Environ. 68, 357–369. https://doi.org/10.1016/S0034-4257(98)00122-9.

Semmens, K.A., Anderson, M.C., Kustas, W.P., Gao, F., Alfieri, J.G., McKee, L., Prueger, J.H., Hain, C.R., Cammalleri, C., Yang, Y., Xia, T., Sanchez, L., Alsina, M.M., Vélez, M., 2016. Monitoring daily

evapotranspiration over two California vineyards using Landsat 8 in a multi-sensor data fusion approach. Remote Sens. Environ. 185, 155–170. https://doi.org/10.1016/j.rse.2015.10.025.

Sriwongsitanon, N., Suwawong, T., Thianpopirug, S., Williams, J., Jia, L., Bastiaanssen, W., 2020. Validation of seven global remotely sensed ET products across Thailand using water balance measurements and land use classifications. J. Hydrol. Reg. Stud. 30, 100709. https://doi.org/10.1016/j.ejrh.2020.100709.

Su, Z., 2002. The Surface Energy Balance System (SEBS) for estimation of turbulent heat fluxes. Hydrol. Earth Syst. Sci. 6, 85–100. https://doi.org/10.5194/hess-6-85-2002.

Sun, L., Anderson, M.C., Gao, F., Hain, C.R., Alfieri, J.G., Sharifi, A., McCarty, G., Yang, Y., 2017. Investigating water use over the Choptank River Watershed using a multi-satellite data fusion approach. Water Resources Res. 53, 5298-5319. https://doi.org/10.1002/2017WR020700

Thiébault, S., Moatti, J., Ducrocq, V., Gaume, E., Dulac, F., Hamonou, E., Shin, Y., Joel, G., Boulet, G., Guégan, J., et al., 2016. The Mediterranean Region Under Climate Change: A Scientific Update, IRD Éditions, Marseille, France.

Timmermans, W.J., Kustas, W.P., Anderson, M.C., French, A.N., 2007. An intercomparison of the Surface Energy Balance Algorithm for Land (SEBAL) and the Two-Source Energy Balance (TSEB) modeling schemes. Remote Sens. Environ. 108, 369–384. https://doi.org/10.1016/j.rse.2006.11.028.

Turco, M., Llasat, M.C., von Hardenberg, J., Provenzale, A., 2014. Climate change impacts on wildfires in a Mediterranean environment. Clim. Change 125, 369–380. https://doi.org/10.1007/s10584-014-1183-3.

Walker, J.J., De Beurs, K.M., Wynne, R.H., Gao, F., 2012. Evaluation of Landsat and MODIS data fusion products for analysis of dryland forest phenology. Remote Sens. Environ. 117, 381–393. https://doi.org/10.1016/j.rse.2011.10.014.

Webb, E.K., Pearman, G.I., Leuning, R., 1980. Correction of flux measurements for density effects due to heat and water vapour transfer. Q. J. R. Meteorol. Soc. 106, 85–100. https://doi.org/10.1002/qj.49710644707.

Yang, Y., Anderson, M.C., Gao, F., Hain, C.R., Semmens, K.A., Kustas, W.P., Noormets, A., Wynne, R.H., Thomas, V.A., Sun, G., 2017. Daily Landsat-scale evapotranspiration estimation over a forested landscape in North Carolina, USA, using multi-satellite data fusion. Hydrol. Earth Syst. Sci. 21, 1017–1037. https://doi.org/10.5194/hess-21-1017-2017.

Yang, Y., Anderson, M.C., Gao, F., Wood, J.D., Gu, L., Hain, C., 2021. Studying drought-induced forest mortality using high spatiotemporal resolution evapotranspiration data from thermal satellite imaging. Remote Sens. Environ. 265, 112640. https://doi.org/10.1016/j.rse.2021.112640.

Zhu, X., Chen, J., Gao, F., Chen, X., Masek, J.G., 2010. An enhanced spatial and temporal adaptive reflectance fusion model for complex heterogeneous regions. Remote Sens. Environ. 114, 2610–2623. https://doi.org/10.1016/j.rse.2010.05.032.

Chapter 6

General conclusions and future research lines

Evapotranspiration plays a crucial role in controlling the water balance of a catchment. This dissertation has advanced the available knowledge about the estimation of evapotranspiration and its dynamics over Mediterranean heterogeneous ecosystems. We demonstrated the utility of SWB and SEB approximations, integrating different sources of remotely sensed data and based on different approaches, to estimate the water consumed by Mediterranean landscapes. The strengths and weaknesses of each methodology have been analyzed. Recommendations to improve management at the local and regional scale, based on technical, distributed, and high-quality information has been provided and may contribute to reducing these ecosystems' vulnerability. Although our research has been focused on *dehesa* landscapes, a typical man-made system widely spread in the southern areas of the Iberian Peninsula, the variability of the region has been represented, addressing the study of other Mediterranean landscapes.

In chapter two, one of the parameters needed as input by the VI-ETo method (SAVI index of pure vegetation, $SAVI_{max}$) proved to be different in holm oaks and olive trees when compared to other Mediterranean tree crops, as a consequence of the differential spectral response of these species. Specific values of this parameter were recommended for both vegetation covers ($SAVI_{max}$=0.51 for oak trees and $SAVI_{max}$=0.57 for olive trees), which share some morphological features to cope with the recurrent dry periods in the Mediterranean climate. The use of appropriate values had notable implications in the computation of ET and water stress, as opposed to using a generic value for Mediterranean crops ($SAVI_{max}$= 0.75). These results highlighted the importance of including these species' spectral properties in ET modeling, which could affect irrigation recommendations and the precise estimation of water resources.

In chapter three, the VI-ETo method accurately reproduced the temporal dynamics and the annual bimodal behavior of *dehesa* water consumption, evaluated in an oak-grass savanna farm and an open grassland area, both located in Southern Spain and with eddy covariance flux tower equipment (RMSE = 0.47 mm day^{-1}). The errors obtained were similar to those collected in the literature for more homogeneous systems using similar approaches. Due to the images' temporal frequency and the modeling scheme (applying a soil water daily balance), fast and isolated ET pulses were properly reproduced, key for understanding the hydrological behavior of the system. Over grasslands, the use of Sentinel images (5-day time step) allowed us to identify the starting dates of grass greening and drying, as well as the date when ET maximum rates were reached. This can be useful for management purposes and could help to decide the livestock grazing periods, without compromising the ecosystem conservation.

To improve the modeling of ET over the complex canopy structure of *dehesas* using the VI-ETo scheme, some effective layer-specific model parameters were provided (maximum basal canopy coefficient, $K_{cb\ full}$, and depletion fraction, p), which were tested in the study

area. A calibration process was followed to determine the optimal values for the best model performance. These values took into account the heterogeneity of the oak-grass savanna system and were proposed for the whole system and for the grassland separately.

An analysis of the effect of the non-photosynthetic grass layer on the vegetation cover fraction estimation from remotely sensed data has been performed in this work. A slight deviation was observed in the estimation of tree ground cover during the summer, although it was not significant enough to require more precise spectral mixing modelling.

Regarding the evaluation of the VI-ETo model's ability to quantify water consumption over other typical Mediterranean vegetation covers (chapter four), daily water requirements of two small high-altitude watersheds in *Sierra Nevada* mountains were computed. The predominant canopies of these areas are natural vegetation formations of shrubs, holm oaks and grasslands, coniferous plantations, and irrigated horticultural crops. The annual discharge flows of both watersheds were determined from the modeled ET data, and also with a simple surface water balance application. They were very similar to those obtained with the HBV (Hydrologiska Byråns Vattenbalansavdelning) hydrological model and to the values measured at the outlet of one of the basins. Thus, the usefulness of the VI-ETo methodology to model ET dynamics on these vegetation types was demonstrated, and the model can be extrapolated to other Mediterranean basins. In addition, the coupled use of the VI-ETo and HBV models opens the possibility that in the future, hydrological models that require calibration can be validated with real information about the vegetation behavior when there are no gauging stations.

On the other hand, in chapter five, the evolution of ET was monitored over the oak savanna vegetation using a remote sensing-based energy balance model (ALEXI/DisALEXI approach), providing different temporal and spatial resolutions estimations, integrating Landsat and MODIS as thermal data. Modeled energy components compared reasonably well to *in-situ* flux measurements acquired by the eddy covariance system, with RMSE values ranging between 0.6 and 2.18 MJ m^{-2} d^{-1} depending on the sensor and the analyzed flux. Thus, we demonstrated the feasibility of using a modeling scheme based on a dual-source energy balance model on this complex landscape. The temporal and spatial resolution of this application might be insufficient for continuous monitoring of the different vegetation layers that shape *dehesa*.

Thus, a remote data fusion algorithm (the STARFM technique) was used to increase the spatio-temporal resolution of the ET maps previously generated with the SEB approach (1 km, daily, and 60-100 m, every 15 days). The resulting ET series (30 m, daily) provided an RMSE value of 0.67 mm d^{-1}, which was considered an acceptable error for management purposes. This error was slightly lower compared to using MODIS resolution (1 km) or simpler interpolation methods for Landsat images due to the high temporal frequency and better spatial representation of the flux tower footprint. The analysis of ET patterns over

small heterogeneous vegetated patches that form the *dehesa* structure revealed the importance of having fine resolution information at the field scale to distinguish the water consumed by the different vegetation components. For example, it was key for identifying phenology dates of grasslands or understanding the hydrological functioning of riverside dense evergreen vegetation with high ET rates, important for the provision of many ecosystem services. Accurately modeling the different behavior of *dehesa* microclimates is useful to support farmers' management.

Finally, the water stress monitoring over the whole system (oak + grass) and the grassland derived from the VI-ETo approach highlighted the usefulness of the ratio ET/ET_o to identify periods of water stress, which was confirmed for the grassland by the soil water content measured.

These results have also highlighted the need for further research about certain aspects. In particular, the following points were identified for future work in this area:

- Tentative values for some layer-specific parameters of the oak trees for mapping ET with the VI-ETo approach, such as the maximum basal canopy coefficient ($K_{cb\ full}$) and depletion fraction (p), have been suggested in this work. However, these values require further validation and refinement in order to improve the application and extrapolation of this approach to other *dehesa* areas with different densities and distributions of tree canopy, and to other Mediterranean landscapes with an abundance of holm oak trees.

- Our research has revealed clear differences in annual ET behavior between several vegetation patches that compose the *dehesa* landscape at the field scale and which are associated with the creation of different microclimates. A better knowledge of the relationships between these ET dynamics and other variables, such as grassland communities and richness, topography and soil properties, species phenology, biodiversity hotspots, or livestock comfortability should be explored in the future and may lead to interesting findings to promote the conservation of the system

A preliminary analysis performed in this work had shown a reduced influence of non-photosynthetic vegetation in the estimation of tree ground cover during the summer. However, this analysis also pointed out the difficulties to separate the soil from the dead grass spectra. The abundance of non-photosynthetic grass during part of the year and its influence on the radiation balance and evaporation from the soil, conditioning both the energy and water balances, deserve further attention.